INVESTIGATION OF NONLINEAR TRANSFORMATION OF IMPULSES IN
IMPACT UNITS FOR IMPROVEMENT OF HAMMER DRILL PERFORMANCE

by

SALLY ANN (KEMBER) SOUNDRANAYAGAM

Doctoral Thesis
Submitted in partial fulfilment of the requirements
for the award of

Doctor of Philosophy of Loughborough University
1999

ABSTRACT

Hammer drills are known to cause vibration induced injury. One method of alleviating this problem is to reduce the level of vibration generated by the hammer drill impact unit, so that less vibration is felt by the operator. The objective of this study was to increase the understanding of impact unit behaviour and develop theoretical models to assist the design process.

The impact unit was initially simplified to a two degree of freedom vibro-impact system with impact excitation. The periodic Green's function method was used to study the system analytically. The equations of motion were solved for the initial two degree of freedom system for both sinusoidal and impulse excitation cases, without recourse to numerical methods. This is the first purely analytical solution that has been obtained for such a two degree of freedom system with impact excitation. Two solutions to the equation of motion were found but a stability analysis showed that only one was stable.

The analytical solution provides a reliable basis for the development of more detailed numerical models of the impact unit. A Simulink model achieved a good agreement with the analytical solution for both sinusoidal and impulse excitation. It was found that the use of compliance in the impact surfaces was essential to avoid the accumulation of integration errors due to infinite acceleration at impact. A more complex model with a loose mass was also simulated.

A two mass test rig was developed to provide data to support the development of the simplified models. Two resonances and an antiresonance were identified, confirming the modelling results.

The first experimental rig to be based on an actual hammer drill was also developed, to support the development of more complex models. A laser vibrometer was used to measure the velocities of the internal parts. By varying the hammer drill speed a general understanding of its behaviour was obtained. The hammer drill showed periodic behaviour with the same period as the excitation but with some variation from cycle to cycle.

ACKNOWLEDGEMENTS

CONTENTS

NOMENCLATURE

A	amplitude of response to sinusoidal excitation	m
A_1, A_2	see page 42	
b	$= \Omega\varsigma = c/2m$	rad/s
B	$= e^{-bT}$	
c	damping coefficient	Ns/m
F	impulse amplitude of impact excitation	Ns
F_0	force amplitude of sinusoidal excitation	N
J	impulse	Ns
k	stiffness	N/m
$L(i\omega)$	receptance (dynamic compliance)	m/N
m	mass	kg
M	$= m_1 m_2/(m_1+m_2)$ mass ratio	kg
r	$= 1 - \cos\Omega_1 T$	
R	coefficient of restitution	
t	time	s
T	period between impacts	s
x	displacement	m
$\dot{x}$	velocity	m/s
$\ddot{x}$	acceleration	m/s^2
δ	Dirac delta function	
Δ	distance between two masses at rest	m
ς	damping ratio	
λ	damped natural frequency	rad/s
τ	time lead	s
φ	phase angle	rad
χ	periodic Green's function	s/kg
$\dot{\chi}$	periodic Green's fuction differentiated with respect to time	1/kg
ω	excitation frequency	rad/s
Ω	natural frequency	rad/s

Subscripts

1	excited system
2	passive system
-	before impact
+	after impact

1 INTRODUCTION

1.1 Hammer drills and their sources of vibration

Hammer drills and related equipment, such as rock drills and paving breakers, use repetitive impact to drill or break up hard brittle materials such as rock and concrete. The use of repetitive impact rather than a constant feed force allows much higher penetration rates to be achieved.

These devices may be hand or machine held, and may be driven by electrical, hydraulic or pneumatic means. The subject of this study is the widely used hand held hammer drill driven by an electric motor. These drills are manufactured in a variety of sizes from small domestic drills to large industrial drills such as the Hilti TE74 used in the experimental part of this study.

Hand held vibrating equipment can cause damage to nerves, joints, muscles and the blood supply if used regularly over a long period of time. Vibration induced white finger is a common condition caused by damage to the blood supply to the fingers, and recently led to a £500 million compensation settlement by British Coal.

There are several methods of reducing the incidence and severity of vibration induced injury. Duration of exposure to vibration can be reduced by rotating personnel. Regular health checks can be made and affected personnel can be redeployed so that their condition is not worsened. Heated handles can help in the case of vibration white finger because a cold working environment for the hands increases the risk. Manufacturers can also improve their designs to increase the damping within the device, and remove or reposition other features such as gas exhaust ports which are also believed to increase the risk of vibration induced injury. A more fundamental approach is to reduce the vibration levels of the mechanism itself. [Gemne et al 1993, Griffin 1990].

The main source of vibration in a hammer drill is the impact unit. A typical electrically driven impact unit is shown in Figure 1.1. The electric motor drives a piston via a gearbox and a crank, which in turn drives the striker via an air cushion. The striker strikes the intermediate piston, which then strikes the drill bit which in

turn cuts into the material (such as concrete). The intermediate piston has a buffer that prevents it from returning too far into the drill mechanism. The buffer may also be involved in the stability of the motion of the drill. These parts are all contained within a tube which is rotated when a drilling action is required, or is held stationary if only the chisel action is required.
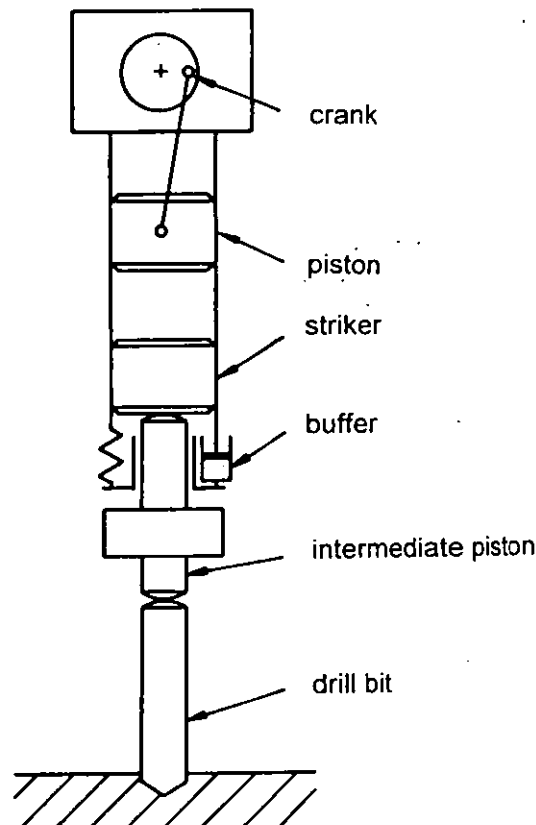
Figure 1.1 Impact unit of a typical industrial hammer drill
[after Kember and Babitsky 1999a]

The main sources of vibration for this type of impact unit are:

1. the pressure spike generated as the air between the piston and the striker is compressed
2. the motion of the various masses
3. the impact between the intermediate piston and the buffer

The pressure spike shape and amplitude could be modified so that it is less damaging to the user. The vibration from the motion of the masses could also be reduced by making the masses smaller or out of lighter materials (but with less

effective impacts) or by increasing the mass of the drill body (which may be unpopular with the user).

The aim of the current study is to obtain a better understanding of the dynamics of the impacting parts of the impact unit, to allow the drill to be designed for reduced impact levels between the intermediate piston and the buffer.

The impact unit of a hammer drill is a typical example of a vibro-impact system. The next section introduces vibro-impact processes and their terminology.

1.2 Vibro-impact processes
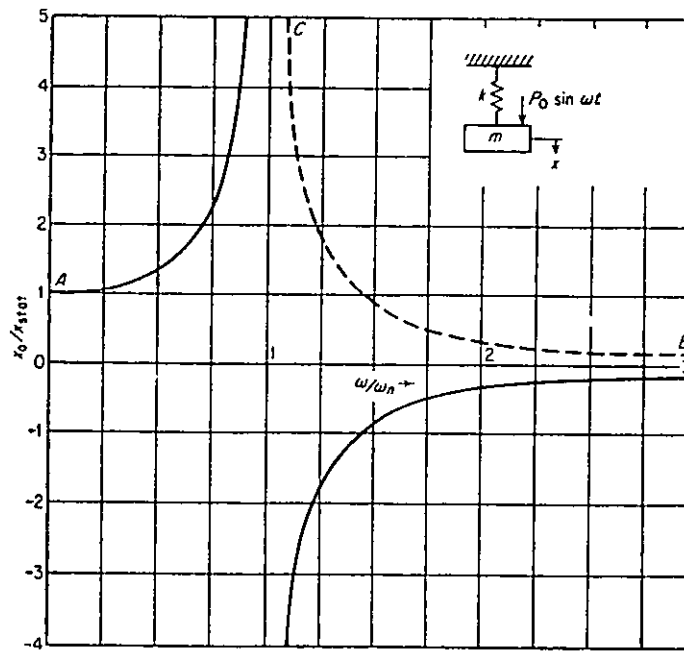
Figure 1.2 Frequency response of a linear system [Den Hartog 1956]

A vibro-impact system consists of one or more interacting processes that involve systematically repeated impacts. These impacts cannot be analysed individually if the frequency of impact is of the same order of magnitude as the natural frequency of the system without impact. In this case the system will still be responding to a previous impact when the next impact occurs [Babitsky 1998]. Such vibro-impact processes can be found in several areas of engineering and include impacts that occur at joints in mechanisms, repeated impacts within machines and the use of repeated impacts to attenuate unwanted vibratory motion. There are also the largely

theoretical problems of impact oscillators and of a ball repeatedly striking a vibrating table. These processes will be explained briefly in this section and the next, and methods of analysis will be described in sections 2.1 to 2.4.
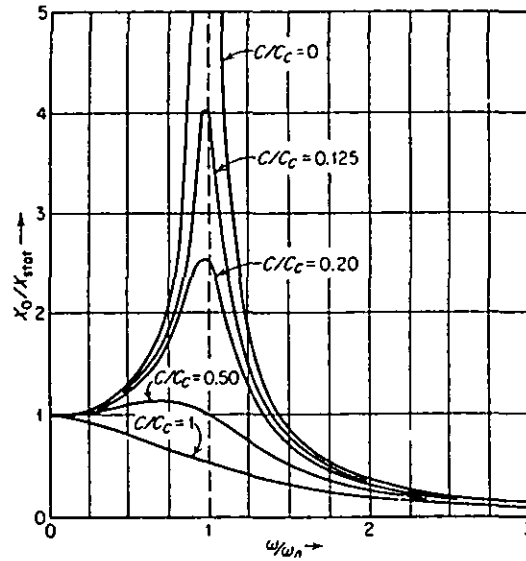
Figure 1.3 Frequency response of a damped linear system [Den Hartog 1956]

A vibro-impact process is an example of nonlinear vibration and will therefore exhibit characteristics that identify it as nonlinear. A clear indicator of a system with nonlinearity is the shape of its frequency response curve. An undamped linear single degree of freedom system has the frequency response shown in Figure 1.2, with a resonance (where the magnitude of the amplitude tends to infinity) when the frequency of excitation ω is equal to the natural frequency ω_n of the system. It should be noted that the phase change at resonance requires the amplitude values to become negative. If the system is damped then the resonant frequency is lower than the natural frequency of the undamped system, and the amplitude at resonance is less than infinity (Figure 1.3). The resonant frequency of a linear system is independent of the amplitude of the forcing function and has the same value whether the excitation frequency is swept up through the resonance or swept down through the resonance. This is not the case with a nonlinear system.

The frequency response of a nonlinear system has a different shape and there are a variety of methods of deriving the frequency response. The method described here

is an approximate one [Den Hartog 1956]. Other methods include perturbation methods [Nayfeh 1981] and harmonic linearisation [Magnus 1965, Kolovsky 1966].
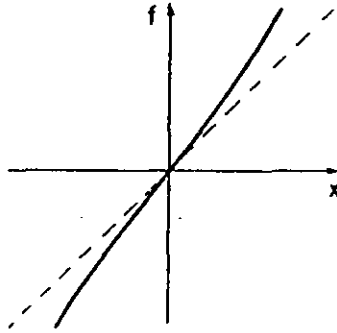
Figure 1.4 A nonlinear spring stiffness characteristic [Stoker 1950]
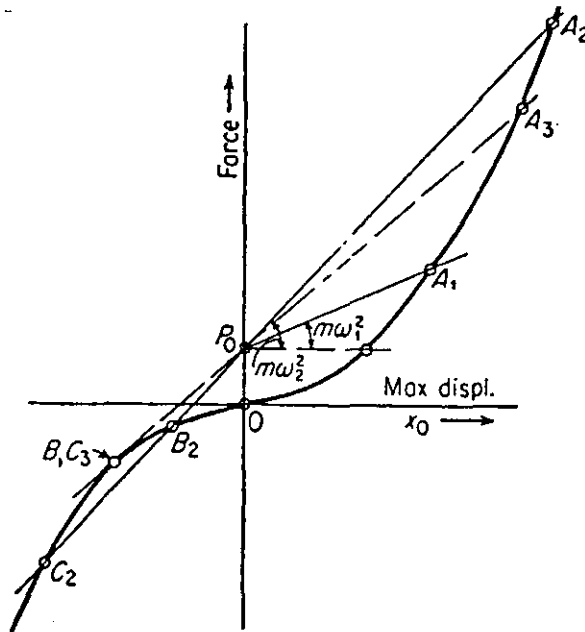
Figure 1.5 Graphical means of calculating the frequency response of a nonlinear spring
[Den Hartog 1956]

If the nonlinear system is undamped and has nonlinear springs then its equation of motion is

$$m\ddot{x} + f(x) = P_0 \cos \omega t \qquad (1.1)$$

An approximate solution can be found by assuming that the response is sinusoidal and has the same frequency as the excitation so

$$x = x_0 \cos \omega t \qquad \text{and} \qquad \ddot{x} = -x_0 \omega^2 \cos \omega t$$

The inertia force will then have its maximum value $-mx_0\omega^2$ when the forcing function has its maximum value P_0. Equation (1.1) is a condition of equilibrium for the forces at any time and so, for a given value of x_0, equation (1.1) becomes:

$$f(x_0) = P_0 + m\omega^2 x_0 \qquad (1.2)$$
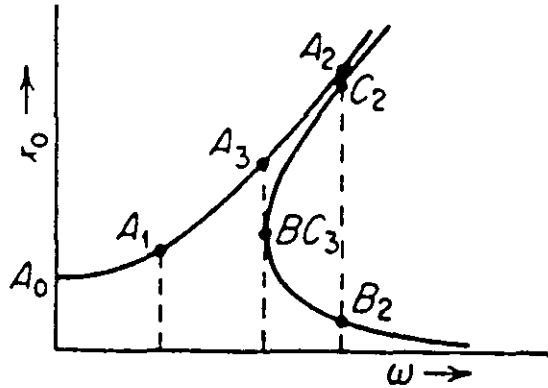
Figure 1.6 Frequency response of an undamped nonlinear system [Den Hartog 1956]

If $f(x_0)$ represents a nonlinear spring then equation (1.1) is not satisfied at all points. However a graphical solution may be used to analyse the system. The spring characteristic can be plotted on a force/displacement diagram, shown in Figure 1.4 as a stiffening spring. If various values of ω are inserted into the right hand side of equation (1.2), then a series of straight lines representing $P_0 + m\omega^2 x_0$ can be drawn on the same diagram (Figure 1.5). Where such a straight line intersects the spring characteristic, a point of equilibrium is found. When $\omega = 0$, a horizontal line from P_0 on the F axis meets the spring characteristic at point A_0. The displacement at this point can then be plotted on the amplitude frequency graph (Figure 1.6). When ω is increased to ω_1, the straight line intersects the spring characteristic at point A_1. When ω is increased to ω_2, the line now intersects the characteristic at three points A_2, B_2 and C_2. This process is repeated to produce the frequency response. It is

seen that region B-C of the response is $180°$ out of phase with region A and so would actually be negative. However, the graph in Figure 1.6 shows the magnitude of the amplitude. Using this procedure, P_0 can be varied. When P_0 is zero (free vibration) the backbone curve is obtained. As P_0 is increased, a family of curves can be drawn (Figure 1.7, the curve marked 1 has the lowest value of P_0). These curves asymptotically approach the backbone curve when the system is undamped.
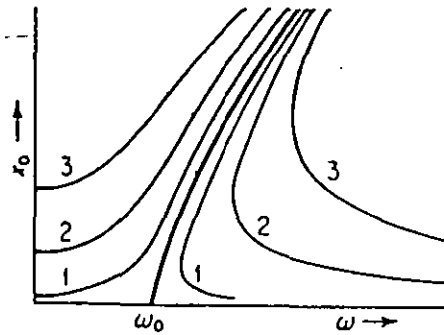
Figure 1.7 Variation of the frequency response with P_0 [Den Hartog 1956]
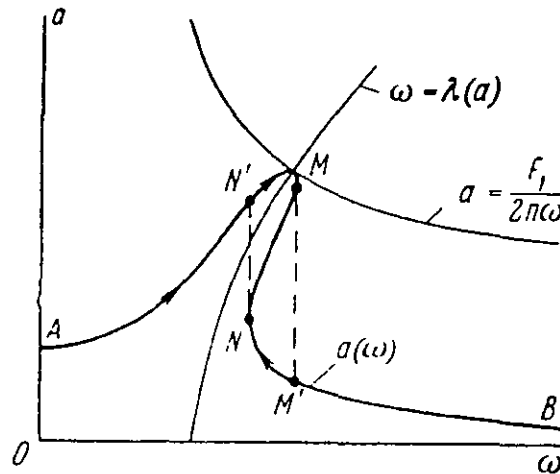
Figure 1.8 Frequency response of a damped nonlinear system [Kolovsky 1966]

An equation for the amplitude a of a damped system under sinusoidal excitation $F\cos\omega t$ may be obtained by using harmonic linearisation (see harmonic balance method, section 2.2.4) [Kolovsky 1966]:

$$a = \frac{F_1}{\sqrt{\left(\lambda^2 - \omega^2\right)^2 + 4n^2\omega^2}}$$

where $F_1 = F/m$, $n = c/2m$, $\lambda^2 = k(a_0,a)/m$, (m is the mass, c is the damping coefficient and $k(a_0,a)$ is the linearised form of the nonlinear stiffness). If the

excitation frequency equals the linearised natural frequency, $\lambda = \omega$, the damping line $a = F_1/2n\omega$ will limit the amplitude at resonance. The damping line therefore intersects the backbone curve at the point where the frequency response curve is rounded off (Figure 1.8).
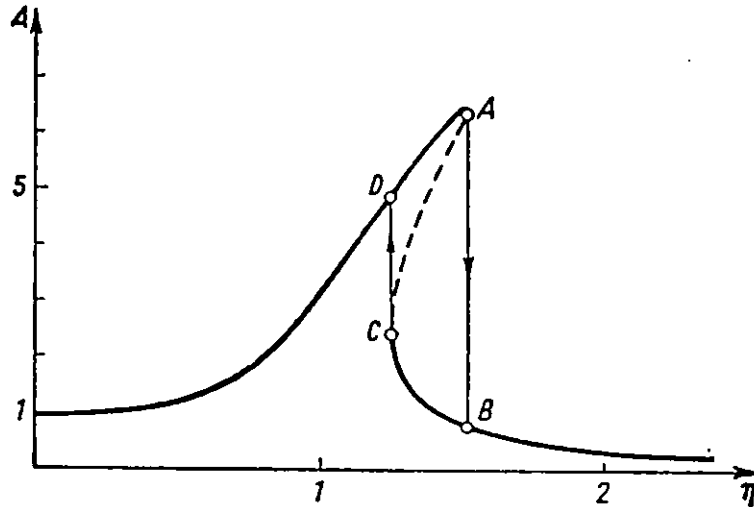
Figure 1.9 The jump phenomenon [Magnus 1965]

As operation in region C of the response in Figure 1.6 cannot be achieved in practice, the system will jump to avoid that portion of the curve (Figure 1.9). If the excitation frequency is slowly increased from zero, the amplitude will reach a peak at A and then, with a small increase in frequency, the amplitude will dramatically reduce (B) and then steadily decline. If the excitation frequency is now decreased, the amplitude will gradually increase until C when there will be a small jump in amplitude (D) and thereafter there will be a steady decline in amplitude to a value of 1. This behaviour is known as the jump phenomenon and demonstrates that the resonant frequency depends on the direction of frequency sweep. If the amplitude of the excitation (P_0) is varied, this will have an effect on the frequencies at which the jumps occur because the position of the damping curve (Figure 1.8) will be affected. When the excitation amplitude is small, the two jump frequencies will be close together and the system behaviour is almost linear (Figure 1.10a). When the amplitude is large, the jump frequencies will be further apart (Figure 1.10b).

Other nonlinear processes exhibit similar behaviour. A system with a softening spring is shown in Figure 1.11. Some nonlinear processes have more complex

responses, for example that shown in Figure 1.12. A typical response of a vibro-impact system will be shown in the next section.
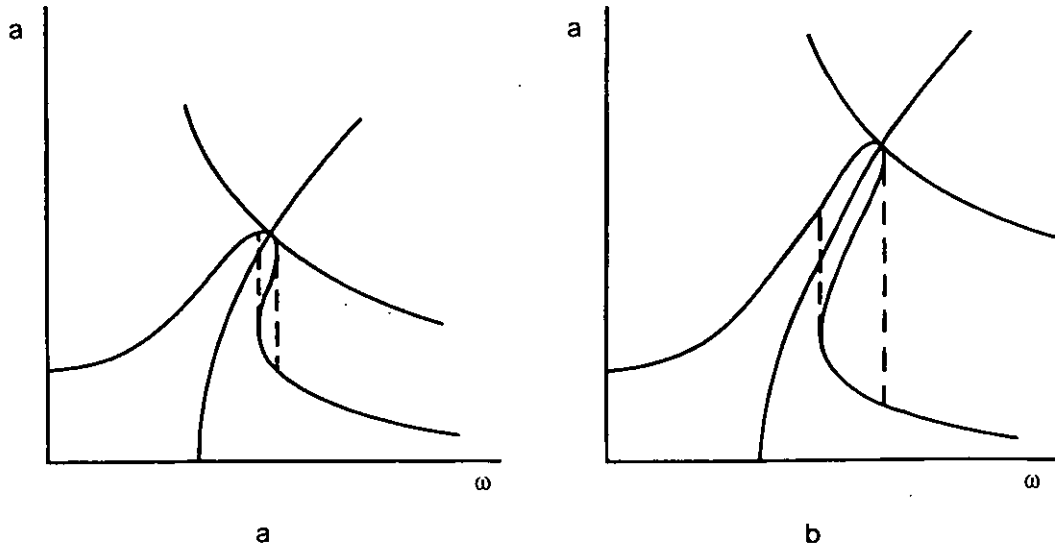
Figure 1.10 The effect of excitation amplitude on the jump phenomenon
a small amplitude   *b* large amplitude
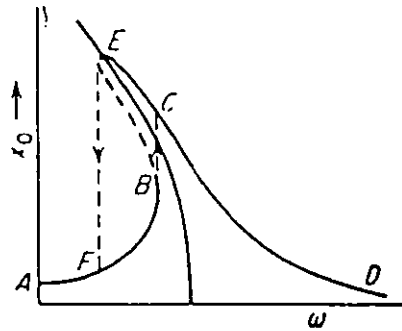
Figure 1.11 Frequency response of a system with a softening spring [Den Hartog 1956]

Chaos is a very active area in nonlinear vibration research. When a nonlinear system behaves in an apparently random manner, without the presence of a random excitation, then its motion may be chaotic. A clear indicator of chaos is the trajectory in state (or phase) space.
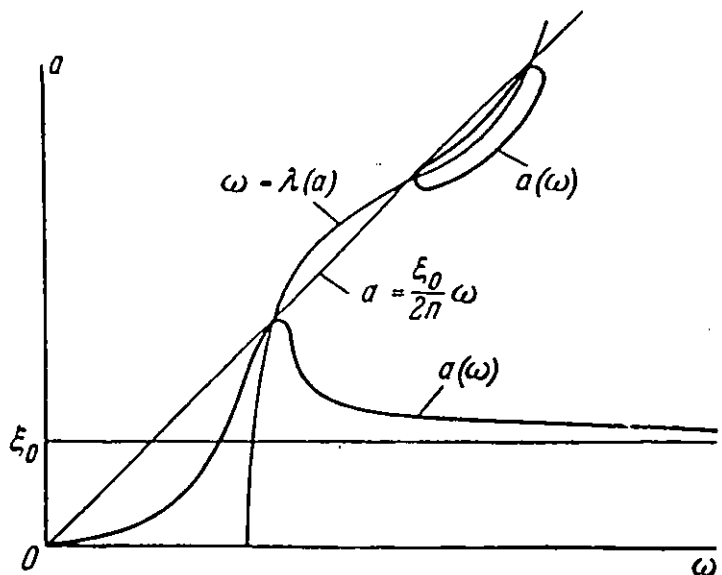
Figure 1.12 A more complicated frequency response [Kolovsky 1966]

(a) Node
(b) Saddle
(c) Focus
(d) Saddle-focus
(e) Center

Figure 1.13 State space trajectories [Hayashi 1964]

The equations of motion of such a system can be written in terms of simultaneous first order differential equations. These are known as the state equations and they contain the minimum number of variables that completely define the system. The

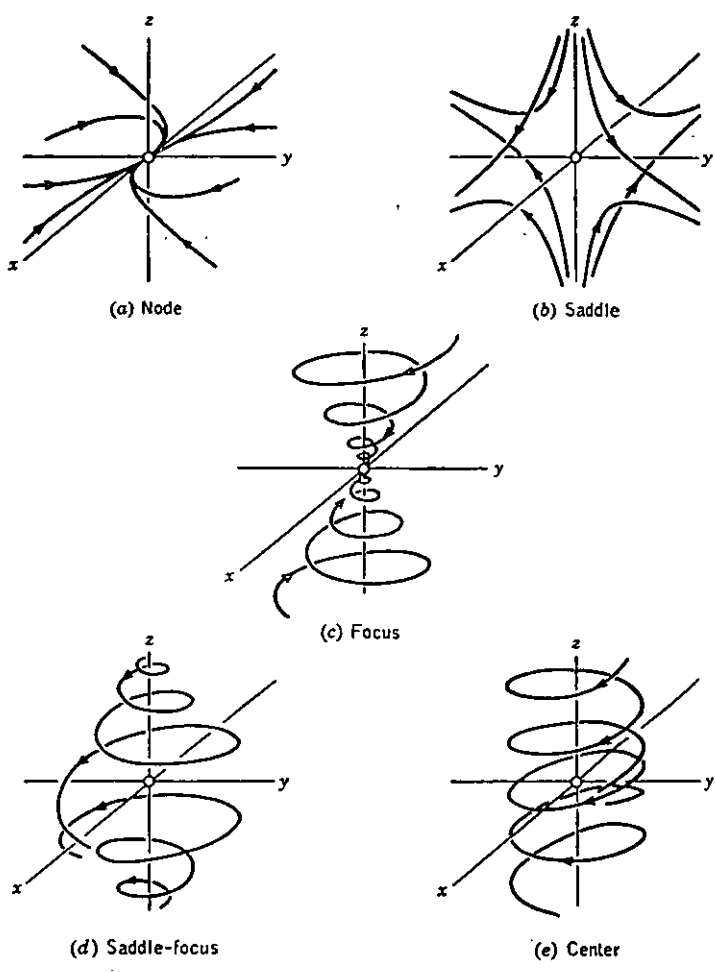variables, which are usually displacement and velocity, are known as the state variables. Sometimes a third state variable is required, and often this is time. The state space consists of axes representing the state variables, for example displacement and velocity. (If the system has only two variables, then the resulting state space may be described as the phase plane.) When the system behaviour is plotted in state space the shape of the trajectory often takes particular forms (Figure 1.13). The trajectories can converge at a point, either by spiralling towards it (a focus *c*) or by moving towards it along a line or curve (a node *a*), or they can converge to a loop (or centre *e*) known as a Poincaré limit cycle [Minorsky 1962]. If the trajectories converge to these shapes then these shapes represent a stable solution to the equation of motion, and are then called attractors. If the trajectories diverge from them, the shapes represent unstable solutions which generally cannot be achieved in practice due to their unstable nature. Stability is discussed further in sections 2.2.2 and 2.2.3. Chaotic behaviour has a stable trajectory with a complex shape that is usually spread over a wide area of the state space. This type of trajectory is known as a strange attractor. A well known strange attractor is the Lorenz attractor shown in Figure 1.14 [Nise 1995, Cook 1986, Hilborn 1994, Moon 1987]. A hammer drill operating in a chaotic manner would have low efficiency since it has been shown that the most efficient regime is periodic with one impact per cycle [Zevin 1976]. Chaotic behaviour is therefore not relevant to this study.

Nonlinear systems can be readily identified experimentally since the amplitude of their response is not linearly related to the excitation amplitude. It is also likely that the resonant frequencies will be shifted due to the jump phenomenon. This shift effect can clearly be seen if the excitation frequency is slowly swept up and down. The jump phenomenon can also cause distorted and asymmetric frequency responses. If the excitation is a single frequency sinewave then the presence of subharmonic and superharmonic responses (responses that are at some multiple of the excitation frequency) as well as the response at the frequency of excitation, indicates that the system is nonlinear (a linear system has just one response which is at the frequency of excitation). Other indications are poor repeatability, low

coherence or random (chaotic) response to a nonrandom excitation (high levels of noise can also cause these effects) [Ewins 1984, McConnell 1995].
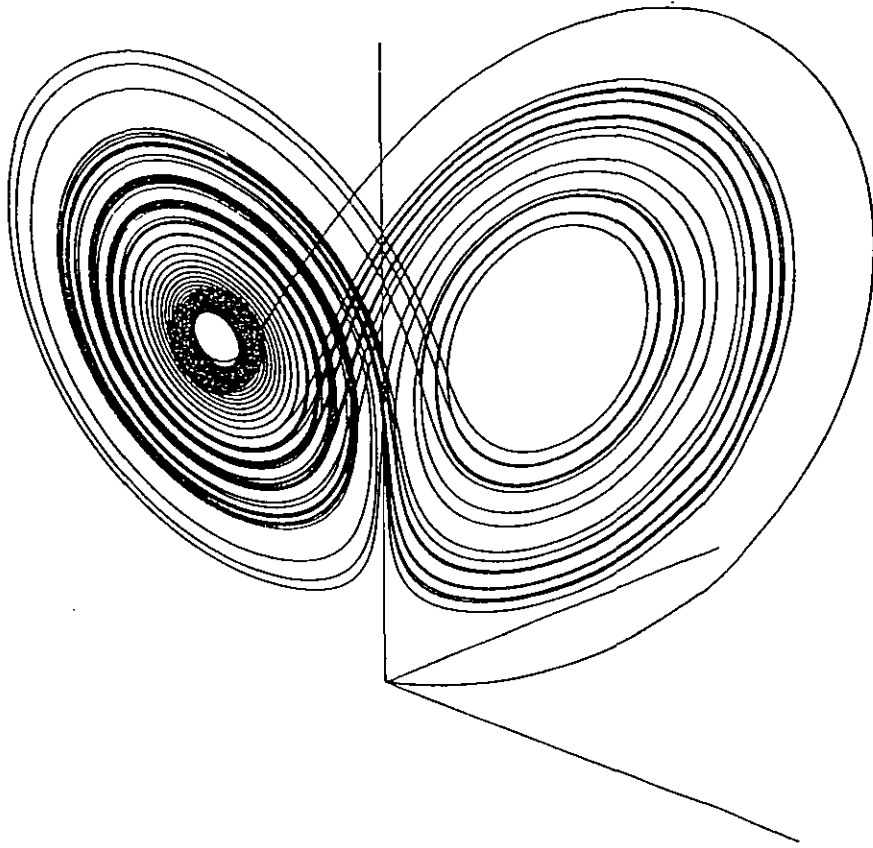
Figure 1.14 Lorenz attractor [Moon 1987]

1.3 Types of vibro-impact system

1.3.1 Impact oscillator
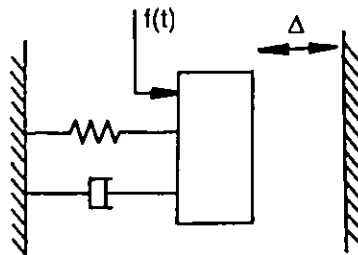
Figure 1.15 Impact oscillator.

The simplest and most studied vibro-impact system is the impact oscillator (Figure 1.15). It shows the jump phenomenon as described in the previous section but with a slight difference due to the change in behaviour when impacts start. The frequency response is shown in Figure 1.16.
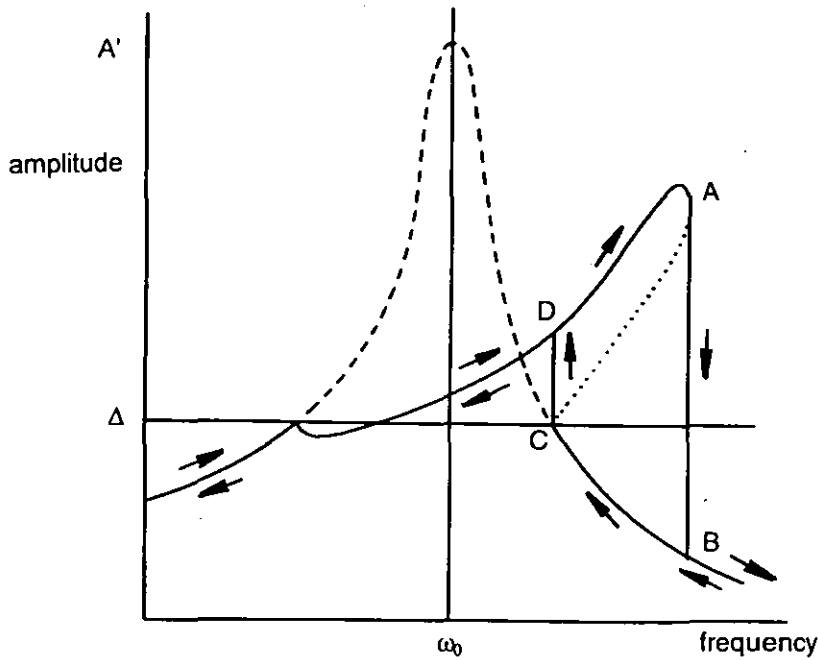
Figure 1.16 Impact oscillator amplitude-frequency characteristic [after Babitsky 1992].

The difference between the impact oscillator and the single degree of freedom system with stiffening spring described in section 1.2 is that the impact oscillator is a linear system with a stop. If the stop were not present, the frequency response would be a linear response. At low frequencies the system therefore oscillates about its equilibrium position, the response is linear and no impacts occur. However if the frequency of excitation is increased, so that the amplitude increases to Δ, the mass will come into contact with the stop, and the response will now deviate from the linear frequency response shown by the dashed line. At this frequency chaotic behaviour is common. As the frequency is increased further, the impact oscillator repeatedly hits the stop in a periodic manner. The mass no longer oscillates around its equilibrium position and so the "amplitude" A' is defined as half the peak-to-peak displacement. (In the nonlinear literature there is no separate term for this form of amplitude.) As the frequency is increased, the value of A' increases until the peak A is reached. A jump then occurs to B, contact with the stop ceases and the impact oscillator returns to being a linear oscillator again. If the frequency of excitation is now decreased, the system will behave in a linear manner until the mass just begins

to contact the stop at C when the jump to D occurs and impacts start. The dotted section of the curve is unstable, as in the examples given in section 1.2. An interesting feature of the impact oscillator is that the system can be behaving like a linear system between B and C but, if it receives a shock force, it can then jump to the resonant impacting region between D and A.
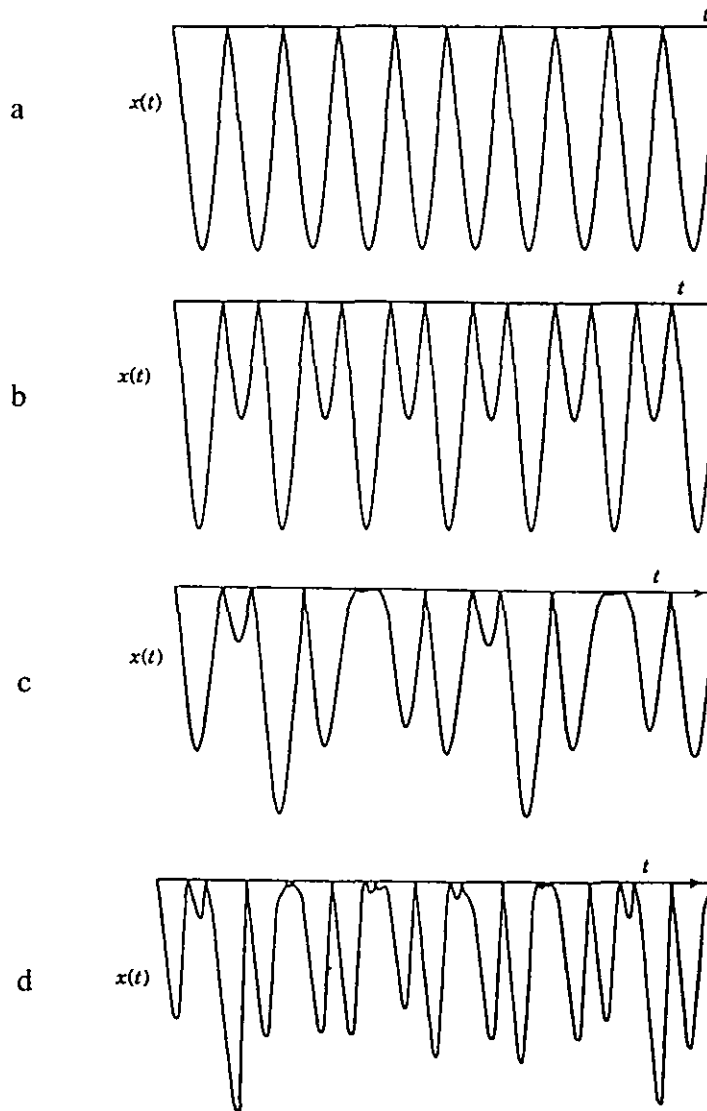
Figure 1.17 Displacement traces for a variety of impact oscillator behaviour achieved by adjustment of system parameters [Budd et al 1995]. a. and b. - regular periodic behaviour, c. - periodic behaviour with chatter, d. - irregular or chaotic behaviour.

The type and pattern of contact in the impact phase of the oscillator can vary with the values of the system parameters. Figure 1.17 shows examples of typical behaviour. The behaviour seen in Figure 1.17*d* is irregular and apparently random and so could be chaos, while Figure 1.17*c* shows chatter.

There have been several studies of the impact oscillator, many of them including chaos or chatter in their analysis. The largest energy transfer occurs with one impact per cycle of excitation [Zevin 1976].

A system closely related to the impact oscillator is a flexible beam striking a stop or snubber (Figure 1.18). It is an important area of study since heat exchanger and boiler tubes can repeatedly strike their supporting framework due to flow induced vibration caused by vortex shedding [Den Hartog 1956].
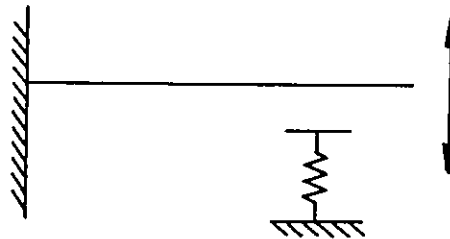
Figure 1.18 Beam striking a stop

1.3.2 Impact pair
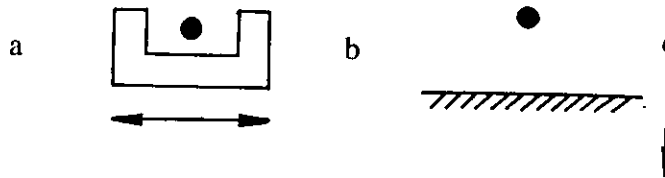
Figure 1.19 a. Impact pair **b.** Ball bouncing on a vibrating table.

Impacts within mechanical joints are caused by the presence of clearances between the elements of the joint. These impacts result in noise and increased wear and so methods of detecting such behaviour, along with ways of removing or controlling it, are required. Theoretical studies are usually based on a generalisation known as the impact pair (Figure 1.19*a*) [Kobrinskii 1969]. A ball bouncing on a table can be

used as a model for the impact pair (Figure 1.19*b*). Kobrinskii [1969] studied this system to solve its equations of motion and this has become an area of specialist study in a similar way to the impact oscillator.

1.3.3 Impact vibration absorbers

The technique of using impact to attenuate unwanted motion has been known since the 1930's [Paget 1937]. The earliest devices were known as acceleration dampers and are now more commonly known as impact dampers or impact vibration absorbers. The term impact vibration absorber is perhaps more accurate because the displacement of the secondary mass is limited but undamped [Hunt 1979]. By contrast, in the Lanchester damper, the secondary masses rotate against friction and are therefore damped but have unlimited displacement [Thomson 1993]. The impact vibration absorber usually consists of a small mass which oscillates and strikes a pair of stops in response to the motion of the main mass (Figure 1.21). There are also similar devices with additional masses and different configurations.
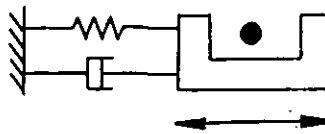
Figure 1.20 Impact vibration absorber.

1.3.4 Vibro-impact machines

Vibro-impact machines, sometimes known as percussion machines, make use of repeated impacts to carry out a task. They are routinely used for drilling or breaking up rock, concrete and masonry. Hand held devices include the hammer drill, the paving breaker and the rock drill (often supported on a stand). Larger machines are used in drilling deep holes for explosives in quarries or for oil and water extraction [MacGregor 1967] or for pile driving [Gutman 1968]. Vibro-impact machines are used for the vibratory transport of materials and small components, and for other processes. All these vibro-impact devices consist of a sequence of one or more masses which impact upon one another and upon the material or object to be

drilled or vibrated. Some of these machines, and methods of studying them, will be considered in more detail later.

1.4 Research approach

The impact unit described in section 1.1 is complex and it was therefore decided to start from a simplified model. A simplified model allows a greater choice of analysis methods and can provide a better understanding of the underlying physical mechanisms. Further complexity can be added at a later stage. Figure 1.21 shows the simplified model of the impact unit.
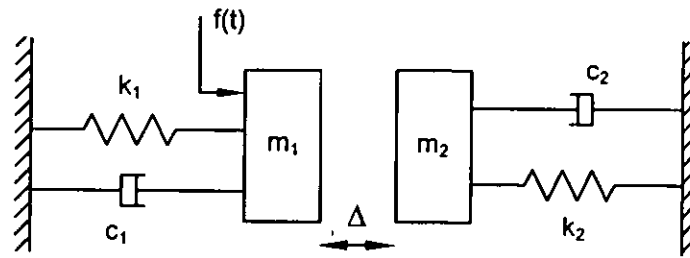
Figure 1.21 The two degree of freedom model of an impact unit.

The simplified model chosen was a two degree of freedom system consisting of: a linear spring-damper combination representing the buffer, two masses representing the intermediate piston and the drill bit, and a second linear spring-damper combination representing the material being worked, for example concrete. The two masses are assumed to be rigid bodies so that stress waves can be ignored, and are also assumed to be continuously in contact with the springs and dampers. The striker is replaced by impact excitation applied to the intermediate piston. Later models could be made more realistic by allowing the masses to float freely, by using nonlinear springs, by adding dry friction (particularly for masonry), and by considering stress waves (especially for the drill bit).

It was decided to first develop an analytical model to provide an understanding of the physical mechanisms involved. It was also decided to develop a numerical model to allow models of greater complexity to be developed. The numerical

method employed was required to produce similar results to the analytical method for simple models.

It is helpful to be able to use experimental data to check that the solutions given by both the analytical method and the numerical method are realistic. It was therefore decided to develop a two mass test rig and a hammer drill test rig.

2 LITERATURE REVIEW

Nonlinear vibration problems generally require specialist techniques. Most commonly used methods of vibration analysis require the assumption that the system is linear. For example, the principle of superposition, which applies to linear systems, does not apply to a nonlinear process. If the nonlinearity is small then a perturbation method can be used [Meirovitch 1997]. A vibro-impact process is strongly nonlinear and so such techniques are usually unsuitable. As a consequence a variety of methods have been developed for vibro-impact systems. Some were developed specifically for vibro-impact systems while others are adapted versions of techniques used for other types of nonlinearity. Most of these methods can be applied to all vibro-impact systems.

Vibro-impact research methods are classified here as: analytical methods, numerical simulations and experimental studies. The analytical methods include work where there was only limited use of numerical methods, mostly to solve simultaneous equations or to find the eigenvalues of a matrix, after extensive manipulation of the equations of motion. Numerical simulations denote work where there was little or no manipulation of the equations of motion. A final section describes studies where experimental work was carried out.

2.1 Modelling the impact process

An important step in the analysis of a vibro-impact system is the choice of impact interaction. If the impact is elastic (there is no permanent deformation or damage) then the impact can be modelled by the equations of classical mechanics or by Herzian contact or by a combination of springs and dampers. Impacts that cause damage, as in rock drilling, are usually modelled with springs and dampers (friction is also included in some cases).

2.1.1 Classical impact theory

This is based on the impulse-momentum form of Newton's second law of motion which can be written as:

$$\int_{t_i}^{t_f} F dt = \int_i^f d(mv) = mv_f - mv_i = \Delta(mv)$$

where $\int_{t_i}^{t_f} F dt$ is the impulse, and i refers to the initial value (before impact) and f refers to the final value (after impact).

When two bodies collide, the impact force between them can be considered to be an internal force within the system so that the system's total momentum remains constant, provided no external forces act. This is the law of conservation of momentum:

$$m_1 v_{1i} + m_2 v_{2i} = m_1 v_{1f} + m_2 v_{2f}$$

In practice this equation can be used when external forces are applied, such as the effect of gravity, provided these forces are small (and can be neglected) in comparison to the forces caused by impact.

When calculating the velocities after an impact, another equation is required since there are two unknown velocities. This second equation is based on the loss of kinetic energy which is expressed by the coefficient of restitution:

$$R(v_{1i} - v_{2i}) = v_{2f} - v_{1f}$$

The coefficient of restitution R is dependent upon the materials and contact geometries of the two bodies and, to some extent, the relative velocity [Hunt and Crossley 1975].

The classical theory of impact is a relationship between the initial and final states of the bodies and the impulse due to impact. It is inherently unable to provide details of events during impact such as deformations or stresses, even though it can be shown that deformation must occur. For example a ball striking a wall must deform otherwise it would have to undergo infinite acceleration as it changes direction.

In vibro-impact studies, the classical theory is often used in analytical studies due to its simplicity. One drawback is that the object would have to be perfectly rigid. However the classical theory can still be used provided only minimal deformation occurs, and there are only small losses of energy in the transmission of stress waves through the body (many reflections of the waves can occur during the time duration

of impact). The classical theory thus is a reasonable approximation for small compact objects such as spheres, but much less useful for bodies with high surface to volume ratios such as rods. Another difficulty is the choice of the value of the coefficient of restitution. [Den Hartog 1961, Goldsmith 1960, Johnson 1976, Kibble 1985]

2.1.2 Herzian contact

One of the disadvantages of the classical theory of impact is that deformations which occur at impact cannot be calculated. However Herz's law of contact can be used to find these deformations and also to calculate the forces involved and contact durations.

The quasi-static version of Herz's law applies to frictionless elastic bodies with non-conforming surfaces and requires that the effect of stress waves should be negligible. Johnson [1985] explains the applicability of this law through the analogy of two rigid railway trucks with light spring buffers, where all the deformation at impact occurs in the buffers and the trucks move as rigid bodies.

The relationship between force and deformation is taken from the relationship for static elastic contact and can be written as follows:

$$P = k\delta^{\frac{3}{2}}$$

where k is dependent on the surface geometries, their Young's moduli and their Poisson's ratios, P is the force due to contact and δ is the relative indentation distance.

As with the classical law of impact, Herz's law of contact will give good predictions of behaviour when the bodies are compact but will not apply to slender bodies like rods [Johnson 1985, Goldsmith 1960]. It is also possible to add terms to the basic Herzian equation to account for hysteresis and plastic deformation [Lankarani and Nikravesh 1994].

Some studies of vibro-impact devices have used the Herzian contact equation to add stiffness and damping to the equations of motion, thereby including surface

compliance on impact. A linearised form of the Herzian contact equation has been used to calculate stiffness and damping for the impact surfaces of an impact pair [Dubowsky and Freudenstein 1971a]. Veluswami et al [1975] also used the same equation to calculate stiffness and damping but they also used a coefficient of restitution as well, to help define the surface damping which incorporated hysteresis. Fujita and Hattori [1980] used the Herzian contact force directly as a resistive force in the impact surface without calculating stiffness or damping. They also simplified the resistive force to an exponential function and found good agreement between both versions and experimental measurements.

2.1.3 Other forms of surface compliance

Many studies have included springs and dampers in the impact surfaces, treating the impact as a backlash or dead zone problem. There are several reasons for using such compliance models: to make numerical simulation and the use of some approximation methods easier, to model a snubber or stop with viscoelastic or hysteretic behaviour, to calculate the forces and stresses at impact, or to model an interaction more accurately especially where one solid is being broken down.

Comparin and Singh [1989] studied surface stresses in an impact pair. Chatterjee et al [1996] and Lin and Bapat [1992] preferred to use compliance rather than classical impact because compliance made numerical integration easier. Both studies used the Harmonic Balance Method (section 2.2.4). Other studies have also used compliance to model beam/stop systems but without giving reasons for the use of compliance [Galhoud et al 1987, Bapat and Sankar 1985]. Neilson et al [1995] used dry friction combined with a variety of springs and dampers to model vibro-impact pile drivers acting against soil. The dry friction element allowed the pile driver model to penetrate the 'soil'. Hunt and Crossley [1975] chose to use a spring and damper to obtain the Kelvin-Voigt model of a viscoelastic material and combined it with a nonlinear contact equation rather like Herzian contact. Babitsky and Veprik [1998] also used a viscoelastic impact model derived from experimental measurements. Fu [1969] used a resisting force related to penetration depth of a paving breaker into the ground.

Care must be taken with the compliance equations to avoid physically impossible force directions, for instance, a spring force that might also act to draw the two impact surfaces together as well as forcing them apart. Luo and Hanagud [1998] noted that this is likely to happen if separation distance, or duration of contact, are used solely as the definition of contact.

2.1.4 Stress waves

The assumptions used for classical impact, that the entire body undergoes a change in velocity instantaneously, may not be acceptable if, for example, if the body is not small and compact, or if it is undergoing many rapidly occuring changes. In these situations the transmission of stress waves will have to be considered.

There are three types of stress waves that can occur in a bounded elastic medium (such as a long rod): longitudinal (or extensional) waves, torsional waves and bending (or flexural) waves. In a long rod it is possible to reduce the stress waves to just one type, the longitudinal wave, but the Poisson's ratio must be set to zero. Despite this, the one dimensional theory (or non-dispersional theory) provides predictions that are close to reality, except in the immediate vicinity of sudden changes in section.

The equation of motion for the longitudinal wave is

$$\frac{\partial^2 u}{\partial t^2} = c^2 \frac{\partial^2 u}{\partial x^2}$$

where $c = \sqrt{E/\rho}$ is the wave propagation velocity, E is Young's modulus, ρ is the density and u is the displacement in the x direction (along the rod).

A stress wave is transmitted through a rod, when a force is applied to one end for a short time duration. This force compresses and displaces a small zone of material at the end. This material gains a velocity which moves it away from the end so compressing and displacing the next zone of material. The material at the end is slowed down by this process and so ceases to be compressed. This mechanism is repeated along the length of the rod and appears as a compressive wave. This continues until the wave reaches a discontinuity. If the discontinuity is a change in

section, a change in material properties, or two bodies touching, then two stress waves are produced, one is reflected back while the second travels on beyond the discontinuity. If the discontinuity is a free end then the wave is reflected back with the stress having opposite sign (a compressive wave becomes a tensile wave). Stress waves can also superimpose on each other when two waves meet. [Kolsky 1963, Timoshenko and Goodier 1982, Donnell 1930]

One dimensional stress wave theory has been used to calculate an equivalent coefficient of restitution [Fu and Paul 1969] though the authors do not explain how to calculate it, nor does their reference, Donnell [1930]. However Donnell does give the loss of kinetic energy due to impact for some systems based on stress wave theory and Goldsmith [1960] gives the loss of kinetic energy due to impact based on the classical theory of impact. If these two equations are equated, they can be rearranged to obtain the coefficient of restitution. This may be the technique that Fu and Paul used. The alternative to calculating the coefficient of restitution is to measure it experimentally.
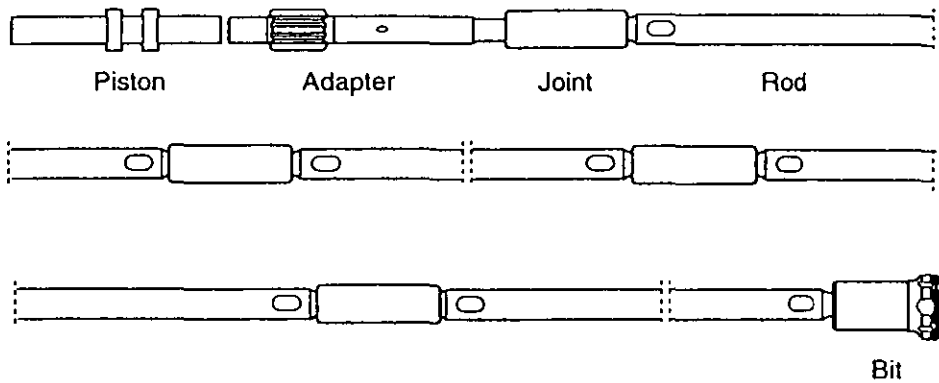
Figure 2.1 Percussive rock drilling system [Beccu 1996].

Some types of vibro-impact machine such as the rock drill have long rods with joints, as shown in Figure 2.1. Stress waves are the means of energy transfer from the exciter to the drill bit. Due to the length of the rods, classical impact theory is inapplicable. The stress waves are liable to be dissipated by the rods and joint pieces and reflected at joint surfaces, and therefore correct selection of materials and joint types is vital for efficient drilling. Most studies consider only the transmission of stress waves from single impacts and so the methods used are not

suitable for vibro-impact studies without modification. Typical methods use the fast Fourier transform or the Laplace transform or time stepping to simulate stress wave transmission [Lundberg 1973a, 1973b, Doyle 1989, Beccu 1996, Lundberg 1982, Nygren 1995, Wu and Lundberg 1994].

Stress waves can be measured experimentally. Doyle [1989] discusses some methods while Borg [1977] used optical measurement and Lundberg at al [1990] used strain gauges.

2.2 Analytical methods

2.2.1 Early methods

Two early methods used to study vibro-impact processes were subsequently abandoned. One considered the energy used over one cycle but with fully elastic collisions [Lieber and Jensen 1945]. The other method involved solving the equations of motion with initial conditions, then resetting the equations after an impact and solving again. This process was repeated until a steady state was achieved [Grubin 1956]. A slight variation of the method allowed for phases of the motion to be skipped if necessary [Kaper 1961]. Park [1967] also used Grubin's method to study a two degree of freedom model of a vibratory transport system and Park described the method as being tedious.

2.2.2 The stitching method

This is an improvement on the work of Grubin suggested by Warburton [1957]. It is assumed that a steady state has been achieved with periodic impacts. The conditions at impact give periodicity and continuity and so require the equations of motion to be solved just once. The method is sometimes known as the stitching method. This method has been the preferred choice of most of the recent research into vibro-impact processes. It is often referred to by researchers as Warburton's method or Kobrinskii's method (as Brunshtein and Kobrinskii used it [Kobrinskii 1969]). The technique was actually first used in vibro-impact by Rusakov and

Kharkevich [1942] following previous developments in this technique for control problems [Andronov 1945].

During the 1960's several studies using the stitching method were published, all devoted to the impact damper. All these studies used a fixed number of impacts for each excitation cycle. With the exception of Sadek [1965-6], all the studies also considered stability of the solutions. However, these studies were not in agreement regarding impact patterns, experimental results and stability analyses. [Egle 1967a, 1967b, Masri 1967, Masri and Caughey 1966, Sadek and Mills 1967]

Masri [1970] generalised the solution to any desired pattern and number of impacts within an excitation cycle. These solutions were checked for stability by a perturbation method used by Kobrinskii [1969] and Masri and Caughey [1966] which will be explained below. This solution method was improved by Bapat [1982] and applied to both the impact damper and the impact pair [Bapat et al 1983, Popplewell et al 1983a, Bapat and Bapat 1988]. It has also been used for vibro-impact machines, including models of a paving breaker [Fu 1969, Fu and Paul 1968, 1969, Sikarskie and Paul 1969] and a one degree of freedom model of a vibratory soil plough [Senator 1970]. There have also been studies of a pile driver modelled as two perfectly symmetrical single degree of freedom systems [Peterka and Szollos [1996, 1997] and of a two degree of freedom model of a pipe snubber [Galhoud et al 1987, Luo and Hanagud 1998].

In the stitching method the equations of motion and the continuity and periodicity equations are solved simultaneously (this often requires numerical solution) to produce several solutions. Stability methods are used to identify the stable solutions. Unstable solutions are not physically possible and are opposed to the hypothesis that the system has stable periodic motion. Therefore stability is equivalent to a condition for existence of solutions. A common stability method makes use of the periodic nature of vibro-impact devices. It has two forms, a geometrical form and a more mathematical form known as difference equations.

If the relationship between velocity and displacement is plotted in phase space (explained in section 1.2) and the resulting trajectory is a closed loop, the system's

oscillations are stable and stationary, and the loop is known as a Poincaré limit cycle [Minorsky 1962]. To check the orbital stability following a small perturbation, a cross section of the trajectory is taken at the point where the cycle starts and finishes. This cross section is known as a Poincaré section (Figure 2.2). The difference between the start point and end point is used to determine the stability of the system; the trajectory in the phase plane should converge to the limit cycle of a stable system. If it does not converge, the system is unstable.

These differences, after several cycles provide a series of difference equations or Poincaré maps [Moon 1987] which also means that a mathematical version can be set up without the need to produce graphs. This technique was developed, for automatic control problems, by Andronov [1945] and his colleagues Bautin and Maier. Later it was used by Masri and Caughey [1966], Kobrinskii [1969] and Brunshtein, Bapat [1982] and others for vibro-impact problems.
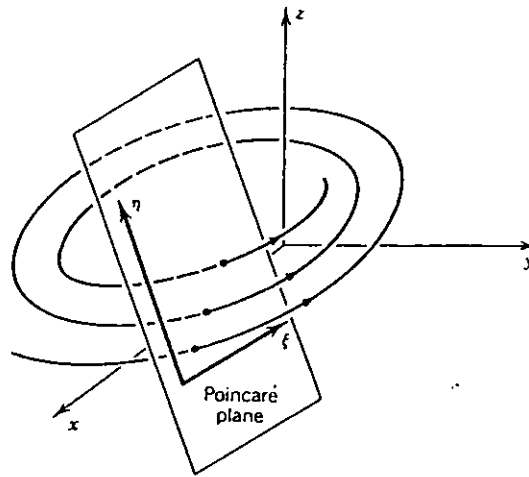
Figure 2.2 Phase plane showing a Poincaré section through a trajectory [Moon 1987]

A small perturbation is applied to the solution of the equations of motion which will cause small changes to certain variables such as the velocity and displacement (depending upon the system under study). If only first order terms are included, then the changes or differences after one cycle can be related to the changes after several cycles by a matrix. For a stable solution, the moduli of all the eigenvalues of that matrix must be less than unity.

This stability method may require numerical calculation to form the matrix and to find the eigenvalues, especially when the system is complicated. The calculations can then develop errors due to rounding. Bapat [1982] noted that these rounding errors might be the source of disagreements between his results and the results of others, particularly when the eigenvalues are close to unity.

The main disadvantage with the stitching method is the need for numerical solutions for all but the simplest systems. However it remains the most popular method, especially for the impact oscillator.

2.2.3 Solution by using periodic Green's functions

An alternative approach was developed in the Soviet Union using a type of non-smooth function known as the periodic Green's function (PGF). Babitsky [1998] demonstrated that this method could produce exactly the same results as the method explained in section 2.2.2 for simple systems. In addition he showed that the PGF method could also provide results for more complicated systems without resorting to numerical methods. A more mathematical treatment of this method appears in Babitsky and Krupenin [1985] and this has been used in studies of heat exchanger tubes [Veprik and Krupenin 1985].

Originally the PGF was known as the Impulse Frequency Characteristic but it was later renamed in honour of Green. The PGF is not to be confused with the Green's function which was developed by Green [Roach 1970]. The Green's function is often used to convert a differential equation into an integral equation, and it is formulated by the use of the Dirac delta function (which is also used to form a PGF). One use of the Green's function in vibration is in the formulation of the convolution integral which gives the response of a linear system to an arbitrary excitation constructed from impulses [Thomson 1993, Meirovitch 1986]. The difference between a PGF and a convolution integral is that the PGF gives the steady state solution immediately without calculating a transient, and without integration or differentiation. The convolution integral could produce the same

result as the PGF but it would require integration over an infinite time interval and the transients would need to be removed by damping.

The PGF is formed by combining a series of Dirac delta functions with the dynamic compliance of the system under consideration. The application of a PGF to a one degree of freedom system is given in section 3.1 .
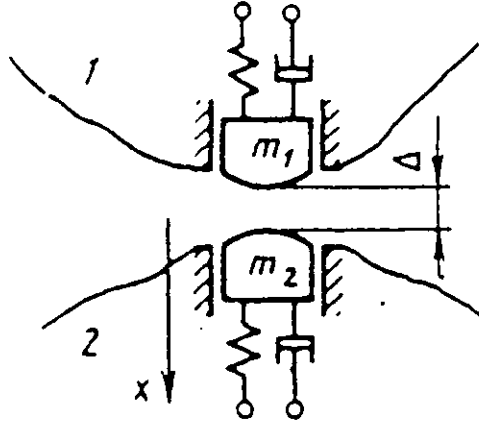
Figure 2.3 A vibro-impact device – [Babitsky et al 1995].

Once the PGF is formulated, it can be inserted into the equation of motion to represent impulsive excitation or impact. For example Figure 2.3 shows a simple vibro-impact system. The equation of motion for this system is :

$$x(t) = a\cos(\omega t + \phi) - J\chi(t)$$

where $x(t)$ is the relative displacement, $\chi(t)$ is the PGF and J is the impulse due to impact.

By considering the classical impact equations and boundary conditions the equation of motion can be solved for the two unknowns J and ϕ to determine x. For this system J is given by [Babitsky 1998, Babitsky et al 1995]:

$$J = \frac{-\Delta\chi(0) \pm \sqrt{a^2\chi^2(0) - \frac{1}{\omega^2}\left[\dot{\chi}(0) + \frac{1}{(1+R)M}\right]^2 (\Delta^2 - a^2)}}{\chi^2(0) + \frac{1}{\omega^2}\left[\dot{\chi}(0) + \frac{1}{(1+R)M}\right]^2} \qquad (2.1)$$

where Δ is the distance between the two masses, R is the coefficient of restitution and M is $(m_1 m_2)/(m_1 + m_2)$. Vibro-impact motion can only occur if J is real but since there are two solutions stability must be considered to find the correct solution. Instead of using a perturbation method with the PGF method, it is simpler to use the principle of balance of energy.
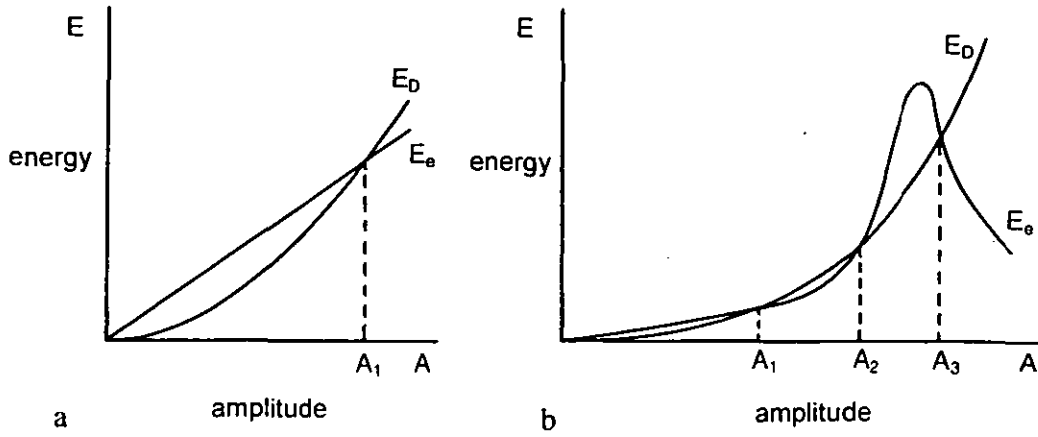
Figure 2.4 Energy balance: *a* Linear system, *b* Nonlinear system [after Magnus 1965].

E_D energy dissipated by damping, E_e energy gained from excitation

A periodic system has several forms of energy (for example potential energy and kinetic energy) which vary in value during one period of motion. Each of these will generally sum to zero over a whole period. However, two forms of energy that do not sum to zero are the energy gained from the source of excitation and the energy lost by dissipation through damping and impact. If the oscillation is stable and stationary, then these two energies will be equal and opposite. For example Figure 2.4*a* shows the excitation energy and dissipation energy for a linear system. If the system is disturbed such that the amplitude A is less than A_1 then the excitation energy E_e is greater than the dissipation energy E_D and so the amplitude will tend to increase towards A_1. Likewise if A is greater than A_1 then E_D is greater than E_e and so A will tend to decrease towards A_1. The system is stable and stationary when the amplitude is A_1 and the two energies are balanced (this is an alternative definition for the terms stable and stationary compared to the limit cycle definition mentioned in the previous section).

Nonlinear systems also show the same behaviour except that the curves often have more than one crossing point, and some crossing points may not be stable. For example, in Figure 2.4*b* A_2 is an unstable point. [Magnus 1965]

This principle of energy balance can be used to check for stability. To be stable the energy terms must be arranged so that the system will return to a stable state after a perturbation. If the system is not stable, the energy terms will be arranged so as to increase the instability. [Babitsky et al 1995, Magnus 1965] Babitsky [1998] has

shown, by using this principle of energy balance, that the stable solution for equation (2.1) corresponds to the positive root while the value of J corresponding to the negative root is the unstable solution.

2.2.4 Solution by the harmonic balance method

This approximate method is used in control problems and has recently been used in vibro-impact studies, mainly with the impact oscillator. The harmonic balance method (HBM) is also referred to as describing functions or equivalent linearisation. This method was used by Babitsky and Kolovsky [1967], Babitsky [1998], Blankenship and Kahraman [1995], Lin and Bapat [1992], Dubowsky and Freudenstein [1971b], Tomlinson and Lam [1984], Comparin and Singh [1989], and Chatterjee et al [1995]. The HBM is used to obtain either a linear equation of motion or a linear transfer function (for control systems).

A nonlinear equation of motion can take the form:

$$m\ddot{x} + f(x, \dot{x}) = 0$$

If we assume that the solution is an approximately harmonic oscillation:

$$x \approx A \cos \omega t$$

then the nonlinear term can be written as a Fourier series:

$$f(x, \dot{x}) \approx a_0 + a_1 \cos \omega t + b_1 \sin \omega t + \ldots\ldots$$

Usually the series is truncated to the first order terms only and the describing function (known in control theory as the linearised transfer function) is called a single input describing function (SIDF). This enables the equation of motion to be rewritten in linear form:

$$m\ddot{x} + c^* \dot{x} + k^* x = 0$$

where c^* and k^* are calculated from the coefficients of the Fourier series.

Sometimes it is necessary to assume the following oscillation:

$$x \approx A_0 + A_1 \cos \omega t$$

especially if a_0 in the Fourier series is not zero. This leads to a dual input describing function (DIDF), and if the Fourier series is extended to more terms, the

result is known as a multiple input describing function (MIDF) [Magnus, 1965, Cook, 1986].

A difficulty with this technique is the correct choice of A_0, A_1 and ω. In some cases it is possible to make a good estimate of these values, in other cases it may be necessary to find these values experimentally by deriving the transfer function from the results of a frequency response analysis [Lin and Bapat 1992, Nise 1995]. However the HBM, or an alternative the incremental HBM, only works well with systems with smooth nonlinearities because several harmonics must often be added to obtain convergence when there are discontinuities [Chatterjee et al 1996, Cook 1986]. The HBM also has difficulties finding reliable solutions for systems where there is chaos.

2.2.5 Alternative methods

The Dirac delta function in its Fourier series form has been used in a very similar manner to the PGF method [Palej and Niziol 1986]. The technique appears cumbersome in comparison with the PGF method since matrix algebra is required. In a similar way the Dirac delta function has been used to study a multiple damper [Cempel 1974]. An averaging technique has also been based on the Dirac delta function [Mitropolsky and Samoilenko 1985]. An improved averaging technique based on the Periodic Green's Function has been developed [Babitsky et al 1982]. Another method combined a saw tooth function with a smooth function to study vibro-impact problems [Zhuravlyov and Klimov 1988].

Methods are available for determining the size of clearances and/or system health from measurements taken during operation of a device containing impact pairs [Lin and Bapat 1992, Cempel 1978] while others consider the effect of random vibrations and therefore employ statistical techniques [Wood and Byrne 1981, 1982, Lee and Byrne 1987, Lin and Bapat, 1993]. Fourier analysis has been used to study an impact pair under periodic loading [Bapat and Bapat 1988] and to study combined impact and sliding [Whiston 1983].

2.3 Numerical methods

Early computational work was usually carried out using analogue computers partly because of the limitations of early digital computers. Several studies mention the use of analogue computation but only a few describe in detail the method used [Mansour and Teixeira Filho 1974, Veluswami et al 1975, Comparin and Singh 1989]. Two studies were based on vibro-impact machines: a sonic riveter [Gladwell and Mansour 1971] and a vibratory transport system [Park 1967]. One study combined an analogue computer with a mechanical impacting device [Masri and Ibrahim 1972]. Studies using digital computation often did not provide details of the numerical simulation technique used. The most common method appears to be a simple integration of the equation of motion using a small time step until the body strikes a surface or another body. The motion of the body is then modified and the process is repeated until a steady state is reached [Mansour and Teixeira Filho 1974, Masri and Ibrahim 1973, Dalrymple 1989, Semercigil et al 1992, Neilson et al 1995]. A complex percussion machine model consisting of two rotating cam disks combined with a hand/arm model has been examined using numerical simulation [Glocker and Pfeiffer 1992].

There are now several simulation packages available which can be used to simulate vibro-impact systems. Simulink (part of the Matlab suite of software) allows systems to be built up out of standard or customised blocks. The resulting circuit is similar to a control block diagram or an analogue computer circuit. Simulink is able to accept discontinuities and nonlinear elements directly and is therefore more convenient than programming in a standard language such as Fortran or C. [Moscinski and Ogonowski 1995, Matlab and Simulink Manuals]. Simulink has been applied to vibro-impact systems [Awrejcewicz et al 1996, Babitsky and Veprik 1999].

2.4 Experimental studies

Most experimental measurements have been devoted to the simpler vibro-impact devices such as the impact oscillator, the impact pair and the impact vibration

absorber. These measurements were carried out principally to support analytical or numerical studies and were normally focussed on impact patterns and regions of stability.

The impact oscillator has been studied as a beam impacting a stop [Lin and Bapat 1992, Fang and Wickert 1994, Sin and Wiercigroch 1999]. The impact pair has been studied as a mass on a string (simple pendulum) in a vibrating slot [Bapat et al 1983, Veluswami and Crossley 1975] or as a mass in a vibrating container [Dalrymple 1989]. The commonly studied impact vibration absorber has been a ball on a string vibrating in a slot [Egle 1967a, Popplewell et al 1983, Semercigil et al 1992]. The ball has also been in a container [Bapat and Sankar 1985, Yasuda and Toyoda 1978]. Alternatively the absorber has been in the form of a beam rattling between two stops [Kato et al 1976, Nigm and Shabana 1983].

The most commonly used transducers have been the accelerometer and the force gauge or impedance head and, in the case of beams, strain gauges. The behaviour of the masses on strings or in containers has not been measured except by Veluswami and Crossley [1975] who used an accelerometer inside a ball.

Some non-contacting methods of displacement measurement used include: optical displacement measurement [Yasuda and Toyoda 1978], high speed photography [Bapat 1982], eddy current displacement probe [Fang and Wickert 1994] and a Wayne-Kerr capacitance probe [Popplewell et al 1983]. Often contacting and non-contacting methods were used together.

There have also been some studies of two degree of freedom systems similar to Figure 1.21. A vertical two mass experiment was carried out where the masses slid on linear bearings and the springs were helical springs rather than beams [Park 1967]. Usually two degree of freedom experimental rigs have used two beams [Kobrinskii 1969, Galhoud et al 1987, Luo and Hanagud 1998]. Other vibro-impact experimental studies have been of a pair of gears [Blankenship and Kahraman 1995], high speed photography of a paving breaker with part of the casing cut away [Sikarskie and Paul 1969] and studies of a pile driver operating on sand [Neilson et al 1995].

Most of the experimental studies mentioned in this section used electrodynamic shakers to excite the structures. One recent study used piezo ceramic actuators attached to the surface of a beam [Luo and Hanagud 1998].

2.5 Discussion

A wide variety of papers have been published on vibro-impact devices. Much of the early work was aimed at obtaining a better understanding of practical devices, mainly impact vibration absorbers, with a few studies of other types of vibro-impact machines. However, in later studies the emphasis turned to problems that were generally of theoretical interest only.

Relatively few studies have been devoted to two degree of freedom vibro-impact systems, which have included analytical, numerical and experimental methods. However, none of these studies have modelled a two degree of freedom system with impact excitation. It should also be stated that, in the open literature, no details of design methodology or modelling techniques for hammer drills have been published.

The current study involves the use of an impact model. The classical impact equations are the best choice for the development of an analytical model because the equations are simple. Both compliance and Herzian contact impact models are well suited to numerical simulation since they avoid instantaneous changes of direction and infinite acceleration. A compliance model made up of springs and dampers is the most straightforward to set up. Stress waves add extra complexity to the models and so will be assumed to be of negligible effect, although in future studies it is likely that stress waves would be included for a closer match between the models and the actual hammer drill.

Analytical methods generally provide a better physical understanding of model behaviour than numerical methods. The most commonly used analytical method for vibro-impact systems has been the stitching method. However this requires the solution of differential equations and much manipulation of simultaneous equations. These simultaneous equations invariably require numerical solution, for

all but the simplest cases. An alternative method, the HBM, does not work well with discontinuities such as impact.

The PGF method by contrast is particularly well suited to modelling systems involving impact since it is based on the Dirac delta function. This feature also makes it ideal for use with impact excitation. The equations of motion may be formulated directly as displacement equations, avoiding any requirement to solve differential equations. There are also fewer simultaneous equations to solve, thus making the need for numerical solution less likely. However, the PGF method is limited to linear systems and therefore nonlinear systems require to be linearised by a method like the HBM before this method can be applied.

The other analytical methods mentioned in section 2.2.5 are complex, and the literature on them is sparse and with limited explanation. Of the known analytical methods for the study of vibro-impact systems, the PGF method was selected as the best suited to this study.

The advantage of a numerical method over an analytical method is that more complex models can be solved and their behaviour studied. However, it is important to have first obtained a thorough understanding of simpler versions of a given system from analytical methods. These simpler systems, when solved numerically, should give results that are in close agreement with the results from an analytical method. The simple numerical models can then be built up into more complex models. Spurious results from the numerical method will thus be largely avoided.

Many of the papers on analytical solutions to the various vibro-impact devices have also used numerical methods but seldom provide detailed explanations of the methods used. Early studies used analogue computers but analysis of vibro-impact systems by digital computer replaced these earlier studies as computer power increased. Generally programs were written in a language such as Fortran and some papers mention the use of Runge-Kutta methods of solving differential equations but with few other details. More recently computer packages consisting of basic model building blocks have become available and these allow more rapid

development of reliable models than through writing a program in Fortran. One such package, Simulink, was available to the current project and was therefore chosen for the numerical simulation work.

Experimental studies of simple vibro-impact devices are useful for comparison with results from analytical or numerical models and they can also aid understanding of physical behaviour. Several experimental studies have been carried out on vibro-impact devices. However the types of system studied did not match the basic two degree of freedom system chosen for this study. The measurement methods used were commonly of the contacting type such as accelerometers and strain gauges. A few studies used optical methods but did not include the use of laser vibrometers. The equipment available for this project included force gauges, accelerometers, a laser vibrometer, electrodynamic shakers and a signal analyser. It was decided to develop a two mass rig based on the simplified model, with beams as springs in a similar manner to several previous studies.

The more complex vibro-impact machines have rarely been studied experimentally and specifically there is a lack of data on the behaviour of the parts within a hammer drill impact unit. Eventually the models developed in this project and subsequent projects will need to be compared to an actual hammer drill. As a consequence an experimental rig based on a hammer drill would provide very useful data.

This study will thus consider a simplified model of a hammer drill impact unit consisting of two single degree of freedom systems, one with impact excitation, where the masses will be permitted to impact upon one another. The model will be studied analytically using the PGF method and numerically using Simulink. These results will be compared with measurements from a simple two mass test rig. Development of more complex numerical models will be undertaken as well as the development of an experimental test rig based on a hammer drill.

3 ANALYTICAL METHOD

The equations of motion for the model described in section 1.4 may be solved analytically by the use of periodic Green's functions (PGF's). A PGF for a single degree of freedom system is first derived, and this is then applied to the model to solve the equations. The stability of the solution is then discussed. The solution can be simplified to a single degree of freedom system to demonstrate the general behaviour of a two degree of freedom system. Both sinusoidal and impulse excitations are considered.

3.1 Formation of a periodic Green's function

A periodic Green's function for the system shown in Figure 1.21 may be developed using the technique of Rosenwasser [1969]. Initially this function was referred to as an impulse-frequency characteristic but in Babitsky and Krupenin [1985], and more recently, the function is described as the periodic Green's function.
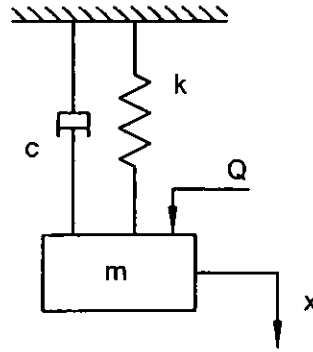
Figure 3.1. Single degree of freedom system

The equation of motion for the vibration of a single degree of freedom system (Figure 3.1) with viscous damping is

$$m\ddot{x} + c\dot{x} + kx = f(t). \tag{3.1}$$

If the excitation is $f(t) = Fe^{i\omega t}$ and, assuming a periodic solution of the form $x(t) = X(i\omega)e^{i\omega t}$ (where $X(i\omega)$ is the complex amplitude), the equation of motion becomes:

$$\left(m(i\omega)^2 + ci\omega + k\right)X(i\omega)e^{i\omega t} = Fe^{i\omega t} . \tag{3.2}$$

The receptance or dynamic compliance (the ratio between the complex amplitudes of the steady state displacement and excitation force) is then:

$$L(i\omega) = \frac{1}{(k - \omega^2 m) + i(\omega c)} = \frac{X(i\omega)}{F} \qquad . \qquad (3.3)$$

The receptance gives a measure of the response of the system to a sinusoidal excitation and it can be rewritten in the following form:

$$L(i\omega) = \frac{1}{m(\Omega^2 + (i\omega)^2 + 2bi\omega)} \qquad , \qquad (3.4)$$

where $\Omega^2 = \dfrac{k}{m}$, $2b = 2\Omega\zeta = \dfrac{c}{m}$, Ω is the undamped natural frequency of the fundamental mode and ζ is the damping ratio [Ewins 1984, Meirovitch 1986].

A periodic impulse excitation can be represented by a periodic series of Dirac δ functions:

$$f(t) = \sum_{q=-\infty}^{\infty} \delta(t - qT) \qquad (3.5)$$

where T is the time between pulses.

The excitation $f(t)$ can also be written as a Fourier series [Lighthill 1964, Rosenwasser, 1969]:

$$f(t) = \frac{1}{T} \sum_{q=-\infty}^{\infty} e^{iq\omega t} \qquad \text{where} \qquad \omega = 2\pi/T \qquad (3.6)$$

The steady-state response due to the series of impulses can then be written as the product of the force and the receptance:

$$\chi(t) = \frac{1}{T} \sum_{q=-\infty}^{\infty} L(iq\omega) e^{iq\omega t} \qquad (3.7)$$

which is the periodic Green's function.

Substituting equation (3.4) into equation (3.7) gives:

$$\chi(t) = \frac{1}{Tm} \sum_{q=-\infty}^{\infty} \frac{1}{\Omega^2 + (iq\omega)^2 + 2b(iq\omega)} e^{iq\omega t} \qquad (3.8)$$

Series (3.8) gives the steady-state response of the system to a series of impulses at $t = ...-3T, -2T, -T, 0, T, 2T, 3T...$ Equation (3.8) can be transformed to a finite expression to cover a single period as follows [Rosenwasser 1969].

A generalised PGF may be written:

$$\chi(t) = \frac{1}{T} \sum_{q=-\infty}^{\infty} L(iq\omega) e^{iq\omega t} \qquad (3.9)$$

If the polynomial $L(iq\omega)$ has the rational-fractional structure:

$$L(p) = \frac{m(p)}{d(p)} = \frac{m_0 p^{2k-2} + m_1 p^{2k-3} + \ldots + m_{2k-2}}{d_0 p^{2k} + d_1 p^{2k-1} + \ldots + d_{2k}} \qquad (3.10)$$

and the roots of the equation $d(iq\omega)=0$ are simple (all different), then equation (3.9) can be expressed as:

$$\chi(t) = \sum_{\rho=1}^{n} \frac{m(p_\rho)}{d'(p_\rho)} \frac{e^{p_\rho t}}{1 - e^{p_\rho T}} \qquad (0<t<T) \qquad (3.11)$$

where p_ρ are the roots of the equation $d(ni\omega)=0$ and $'$ indicates a differentiated variable. The proof of this transformation is given in Rosenwasser [1969]. Equation (3.8) may then be written:

$$\chi(t) = \frac{1}{m} \sum_{\rho=1}^{n} \frac{1}{2p_\rho + 2b} \frac{e^{p_\rho t}}{1 - e^{p_\rho T}} \qquad (0<t<T) \qquad (3.12)$$

The roots of the equation $d(iq\omega)=0$ are: $p_{1,2} = -b \pm i\sqrt{\Omega^2 - b^2}$.

Substituting these two roots into (3.12) gives:

$$\chi(t) = \frac{1}{m} \left(\frac{1}{2(-b+i\lambda)+2b} \frac{e^{-bt} e^{i\lambda t}}{1 - e^{-bT} e^{i\lambda T}} \right) + \frac{1}{m} \left(\frac{1}{2(-b-i\lambda)+2b} \frac{e^{-bt} e^{-i\lambda t}}{1 - e^{-bT} e^{-i\lambda T}} \right)$$

where $\lambda = \sqrt{\Omega^2 - b^2}$. Rearranging we have:

$$\chi(t) = \frac{e^{-bt}}{2im\lambda} \left(\frac{e^{i\lambda t}}{1 - e^{-bT} e^{i\lambda T}} - \frac{e^{-i\lambda t}}{1 - e^{-bT} e^{-i\lambda T}} \right) \qquad (0<t<T) \qquad (3.13)$$

Since $e^{i\theta} = \cos\theta + i\sin\theta$, equation (3.13) becomes:

$$\chi(t) = \frac{e^{-bt}}{m\lambda} \left(\frac{\sin\lambda t + e^{-bT} \sin\lambda(T-t)}{1 + e^{-2bT} - 2e^{-bT} \cos\lambda T} \right) \qquad (0<t<T) \qquad (3.14)$$

Equation (3.14) represents the periodic Green's function (PGF) over one period (used here to denote T, the time between impacts) for a single degree of freedom system. Note that this PGF reflects the steady state periodic behaviour of the

system with one impact per period occuring at $t=0$ (impact also occurs at $t=T$ which is the beginning of the next period).

If there is a time lead τ, where $0<\tau<T$ (impact does not occur at $t=0$), it is possible to write the PGF as:

$$\chi(t+\tau) = \frac{1}{T} \sum_{k=-\infty}^{\infty} \frac{m(ki\omega)}{d(ki\omega)} e^{ki\omega(t+\tau)} \qquad (3.15)$$

In Rosenwasser [1969], a transformation is given for a PGF with a time lag where the result is not one equation but two, so that the term $t-\tau$ is kept within the range of one period as long as τ is less than one period T. By analogy, a similar pair of equations can be set up for a PGF with a time lead as follows:

$$\chi(t+\tau) = \begin{cases} \sum_{p=1}^{n} \dfrac{m(p_\rho)}{d'(p_\rho)} \dfrac{e^{p_\rho(t+\tau-T)}}{1-e^{p_\rho T}} & 0<t<T \text{ and } T<t+\tau<2T \\[4mm] \sum_{p=1}^{n} \dfrac{m(p_\rho)}{d'(p_\rho)} \dfrac{e^{p_\rho(t+\tau)}}{1-e^{p_\rho T}} & 0<t<T \text{ and } 0<t+\tau<T \end{cases} \qquad (3.16)$$

Converting to one period gives:

$$\chi(t+\tau) = \begin{cases} \dfrac{e^{-b(t+\tau-T)}}{m\lambda} \left(\dfrac{\sin\lambda t + e^{-bT}\sin\lambda(2T-t-\tau)}{1+e^{-2bT}-2e^{-bT}\cos\lambda T} \right) & 0<t<T \text{ and } T<t+\tau<2T \\[4mm] \dfrac{e^{-b(t+\tau)}}{m\lambda} \left(\dfrac{\sin\lambda t + e^{-bT}\sin\lambda(T-t-\tau)}{1+e^{-2bT}-2e^{-bT}\cos\lambda T} \right) & 0<t<T \text{ and } 0<t+\tau<T \end{cases}$$

$$(3.17)$$

Other PGFs can be calculated for more complicated systems and systems with more than one impact per cycle. A nonlinear oscillator may require linearising before creating a PGF. Also a PGF can be developed for a system from a receptance (dynamic compliance) which has been measured experimentally.

3.2 Solution for the initial model

The formation of the conventional PGF for a single degree of freedom system has been described above. It is now necessary to derive a specific solution for the two degree of freedom system with sinusoidal excitation and then with impact excitation.

The model appears in Figure 3.2. The formulation of this model was described in section 1.4 . The system with subscript 1 will be referred to as the excited system while the system with subscript 2 will be referred to as the passive system.
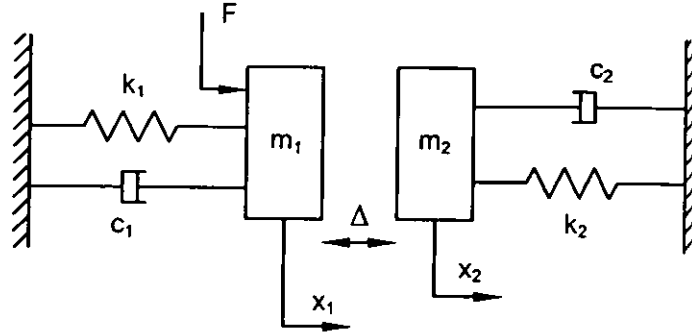
Figure 3.2 The initial model of a two degree of freedom system

3.2.1 Sinusoidal excitation

The displacement x_1 of mass m_1 can be represented as the sum of two components: the response to the sinusoidal excitation, and the response to the impact interaction with mass m_2. The steady state response to the impact with mass m_2 is the PGF given in equation (3.14) multiplied by the unknown impulse of interaction J between the two masses. An impact between the two masses occurs at $t = 0$ and at $t = T$ where T is the period of the excitation. The response is $J_1 \chi_1(t)$ where χ_1 is the PGF of the single degree of freedom system containing m_1 and J_1 is the impulse acting on m_1.

The sinusoidal excitation will not be in phase with the impacts between the two masses. There will be a time difference τ between the respective zero positions. The phase between the excitation $F_0 \cos(\omega t + \varphi_1)$ and the impact between the two

masses will be $\varphi_1 = \omega\tau$ where τ is unknown. Now the response of the system to the excitation is

$$A\cos(\omega t + \varphi)$$

where $A = F_0 / \sqrt{(k_1 - m_1\omega^2)^2 + (c_1\omega)^2}$, $\varphi = \varphi_1 - \varphi_2$ and φ_2 represents the phase difference between the excitation and the response if there were no impacts. This phase difference can be shown to be [Thomson 1993]:

$$\varphi_2 = \tan^{-1}\left(\frac{c\omega}{k - m\omega^2}\right)$$

As the mass-spring-damper system is linear, the two responses can be added to give the equation of motion of m_1:

$$x_1(t) = A\cos(\omega t + \varphi) - J_1\chi_1 \qquad (3.18)$$

In a similar way the equation of motion for m_2 is:

$$x_2(t) = J_2\chi_2(t) \qquad (3.19)$$

where the PGFs are given by

$$\chi_1(t) = \frac{e^{-b_1 t}}{m_1\lambda_1}\left(\frac{\sin\lambda_1 t + e^{-b_1 T}\sin\lambda_1(T - t)}{1 + e^{-2b_1 T} - 2e^{-b_1 T}\cos\lambda_1 T}\right)$$

and

$$\chi_2(t) = \frac{e^{-b_2 t}}{m_2\lambda_2}\left(\frac{\sin\lambda_2 t + e^{-b_2 T}\sin\lambda_2(T - t)}{1 + e^{-2b_2 T} - 2e^{-b_2 T}\cos\lambda_2 T}\right)$$

and where the following relationships apply to both systems (with appropriate subscripts):

$$2b = 2\Omega\zeta = \frac{c}{m}, \quad \lambda = \sqrt{\Omega^2 - b^2}, \quad \Omega^2 = \frac{k}{m}, \quad \zeta = \frac{c}{2\sqrt{km}}.$$

(Ω is the undamped natural frequency of the first mode and ζ is the damping ratio.) The PGFs can be simplified. Let $B_1 = e^{-b_1 T}$ and $B_2 = e^{-b_2 T}$. We then have

$$A_1 = 1/m_1\lambda_1(1 + B_1^2 - 2B_1\cos\lambda_1 T) \text{ and } A_2 = 1/m_2\lambda_2(1 + B_2^2 - 2B_2\cos\lambda_2 T).$$

If we assume that the motion of the system has reached a steady state with all displacements having the same period T, and that at $t = 0$ impact between m_1 and m_2 occurs, the two displacements at $t = 0$ can be related by:

$$x_1(0) - x_2(0) = \Delta .$$

(3.20)

There is another relationship at $t = 0$ which is the equation relating J to velocity. At this instant when impact occurs, the impact forces in a typical vibro-impact device are much greater than any other forces that may be acting on the system (such as spring forces or gravity) and which may therefore be neglected. It is therefore permitted to use the following three equations:

the equation for conservation of momentum:

$$m_1 \dot{x}_{1+} + m_2 \dot{x}_{2+} = m_1 \dot{x}_{1-} + m_2 \dot{x}_{2-}$$

(3.21)

(where subscript + indicates the velocity after impact and subscript - the velocity before impact),

the definition of the coefficient of restitution R:

$$R = \frac{\dot{x}_{2+} - \dot{x}_{1+}}{\dot{x}_{1-} - \dot{x}_{2-}}$$

(3.22)

and the impulse-momentum relationship:

$$J = J_2 = \left(m_2 \dot{x}_{2+} - m_2 \dot{x}_{2-} \right) = -J_1$$

(3.23)

Here J_1 is the impact impulse on m_1 and J_2 is the impact impulse on m_2 and where the positive direction is defined in Figure 3.2, which implies that $J \geq 0$.

The relationships (3.21), (3.22) and (3.23) can be arranged to give:

$$J = M(1 + R)(\dot{x}_{1-} - \dot{x}_{2-})$$

(3.24)

where $M = \dfrac{m_1 m_2}{m_1 + m_2}$.

Therefore the displacement of the active system at $t = 0$ is:

$$x_1(0) = A \cos\varphi - J\chi_1(0)$$

(3.25)

and the displacement of the passive system is:

$$x_2(0) = J\chi_2(0)$$

(3.26)

where $\chi_1(0) = A_1 B_1 \sin\lambda_1 T$ and $\chi_2(0) = A_2 B_2 \sin\lambda_2 T$.

Hence substituting equations (3.25) and (3.26) into equation (3.19):

$$\Delta = A\cos\varphi - J\chi \qquad (3.27)$$

where $\chi = \chi_1(0) + \chi_2(0)$.

At $t=0$, the velocities are:

$$\dot{x}_{1-}(0) = -A\omega\sin\varphi - J\dot{\chi}_{1-}(0) \qquad (3.28)$$

and

$$\dot{x}_{2-}(0) = J\dot{\chi}_{2-}(0) \qquad (3.29)$$

where $\dot{\chi}_{1-}(0) = \dot{\chi}_1(T) = A_1 B_1\left(\lambda_1 \cos\lambda_1 T - b_1 \sin\lambda_1 T\right) - A_1 B_1^2 \lambda_1$

and $\dot{\chi}_{2-}(0) = \dot{\chi}_2(T) = A_2 B_2\left(\lambda_2 \cos\lambda_2 T - b_2 \sin\lambda_2 T\right) - A_2 B_2^2 \lambda_2$.

Substituting equations (3.28) and (3.29) into equation (3.24) gives:

$$J = -M(1+R)A\omega\sin\varphi - M(1+R)J\dot{\chi} \qquad (3.30)$$

where $\dot{\chi} = \dot{\chi}_1(T) + \dot{\chi}_2(T)$.

The two simultaneous equations (3.27) and (3.30) contain two unknowns, J and φ which need to be determined. Rearranging equations (3.27) and (3.30):

$$\frac{\Delta + J\chi}{A} = \cos\varphi \qquad (3.31)$$

and

$$\frac{-J\left(\frac{1}{M(1+R)} + \dot{\chi}\right)}{A\omega} = \sin\varphi. \qquad (3.32)$$

If equations (3.31) and (3.32) are squared and added, the terms with φ are removed:

$$J^2\left[\left(\frac{1}{M(1+R)} + \dot{\chi}\right)^2 + \omega^2\chi^2\right] + J\left[2\Delta\chi\omega^2\right] + \omega^2\Delta^2 = \omega^2 A^2$$

Solving for J we have:

$$J = \frac{\chi\Delta\omega^2}{\left(\frac{1}{M(1+R)} + \dot{\chi}\right)^2 + \omega^2\chi^2}\left(-1 \pm \sqrt{1 - \frac{\left(\left(\frac{1}{M(1+R)} + \dot{\chi}\right)^2 + \omega^2\chi^2\right)\left(\Delta^2 - A^2\right)}{\chi^2\Delta^2\omega^2}}\right) \qquad (3.33)$$

The unknown φ can be found from (3.31) and (3.32).

The solution given by equation (3.33) is for the system with sinusoidal excitation considered here. However this equation is identical to that derived for a generalised system with sinusoidal excitation referenced in section 2.2.3.

.

3.2.2 Impulse excitation

The steady state response to the impulse excitation is similarly formed from the impulse F and a PGF. As the impact from the excitation does not occur at the same time as the impact between the two masses, a PGF with a time lead is used. This is developed using the transformation in equation (3.17). The response is $F\chi_1(t+\tau)$. The total response of the active system is then:

$$x_1(t) = F\chi_1(t+\tau) + J_1\chi_1(t)$$

where

$$\chi_1(t+\tau) = \frac{e^{-b_1(t+\tau-T)}}{m_1\lambda_1}\left(\frac{\sin\lambda_1(t+\tau-T) + e^{-b_1T}\sin\lambda_1(2T-t-\tau)}{1+e^{-2b_1T}-2e^{-b_1T}\cos\lambda_1 T}\right)$$

for $0 < t < T$ and $T < t+\tau < 2T$

or

$$\chi_1(t+\tau) = \frac{e^{-b_1(t+\tau)}}{m_1\lambda_1}\left(\frac{\sin\lambda_1(t+\tau) + e^{-b_1T}\sin\lambda_1(T-t-\tau)}{1+e^{-2b_1T}-2e^{-b_1T}\cos\lambda_1 T}\right)$$

for $0 < t < T$ and $0 < t+\tau < T$

The response of the passive system is the same as that with sinusoidal excitation:

$$x_2(t) = J_2\chi_2(t)$$

Thus at $t=0$, the displacement of the active system is:

$$x_1(0) = FA_1 e^{-b_1\tau}\left(\sin\lambda_1\tau + B_1\sin\lambda_1(T-\tau)\right) - J\chi_1(0) \qquad (3.34)$$

and the displacement of the passive system is:

$$x_2(0) = J\chi_2(0) \qquad (3.35)$$

where $\chi_1(0) = A_1 B_1\sin\lambda_1 T$ and $\chi_2(0) = A_2 B_2\sin\lambda_2 T$ as before.

Using the same two equations at impact (3.20) and (3.23), and substituting equations (3.34) and (3.35) into equation (3.20):

$$\Delta = FA_1 e^{-b_1\tau}\left(\sin\lambda_1\tau + B_1\sin\lambda_1(T-\tau)\right) - J\chi \qquad (3.36)$$

where $\chi = \chi_1(0) + \chi_2(0)$.

At $t=0$, the velocities are:

$$\dot{x}_{1-}(0) = FA_1 e^{-b_1\tau}\left(\lambda_1\cos\lambda_1\tau - b_1\sin\lambda_1\tau\right)$$
$$-FA_1 B_1 e^{-b_1\tau}\left(\lambda_1\cos\lambda_1(T-\tau) + b_1\sin\lambda_1(T-\tau)\right) - J\dot{\chi}_{1-}(0) \qquad (3.37)$$

and

$$\dot{x}_{2-}(0) = J\dot{\chi}_{2-}(0) \qquad (3.38)$$

where $\dot{\chi}_{1-}(0) = \dot{\chi}_1(T) = A_1 B_1 \left(\lambda_1 \cos\lambda_1 T - b_1 \sin\lambda_1 T\right) - A_1 B_1^2 \lambda_1$

and $\dot{\chi}_{2-}(0) = \dot{\chi}_2(T) = A_2 B_2 \left(\lambda_2 \cos\lambda_2 T - b_2 \sin\lambda_2 T\right) - A_2 B_2^2 \lambda_2$.

Inserting equations (3.37) and (3.38) into equation (3.23) gives:

$$
\begin{aligned}
J &= M(1+R)FA_1 e^{-b_1\tau}\left(\lambda_1 \cos\lambda_1\tau - b_1\sin\lambda_1\tau\right) \\
&\quad -M(1+R)FA_1 B_1 e^{-b_1(\tau)}\left(\lambda_1 \cos\lambda_1(T-\tau) + b_1\sin\lambda_1(T-\tau)\right) - M(1+R)J\dot{\chi}
\end{aligned}
\qquad (3.39)
$$

where $\dot{\chi} = \dot{\chi}_1(T) + \dot{\chi}_2(T)$.

The two simultaneous equations (3.36) and (3.39) contain two unknowns, J and τ, which need to be determined. As the two equations are very complex, they can be simplified if it is assumed that the damping coefficient c_1 is small, and the energy losses due to damping are small in comparison with the loss of kinetic energy due to impact (which is usual in real mechanical systems). Since b_1 is calculated by dividing c_1 by $2m_1$, b_1 will be close to zero. Thus the following simplifications can be made:

$$e^{-b_1\tau} \approx 1, \quad \lambda_1 = \sqrt{\Omega_1^2 - b_1^2} \approx \Omega_1, \quad B_1 = e^{-b_1 T} \approx 1$$

and $A_1 = 1/\left(m_1\lambda_1\left(1 + B_1^2 - 2B_1\cos\lambda_1 T\right)\right) \approx 1/\left(m_1\Omega_1\left(2 - 2\cos\Omega_1 T\right)\right)$

hence equations (3.36) and (3.39) become:

$$\frac{\Delta + J\dot{\chi}}{FA_1} = \sin\Omega_1\tau + \sin\Omega_1\left(T-\tau\right) \qquad (3.40)$$

and

$$\frac{J\left(\frac{1}{M(1+R)} + \dot{\chi}\right)}{FA_1\Omega_1} = \cos\Omega_1\tau - \cos\Omega_1\left(T-\tau\right). \qquad (3.41)$$

If equations (3.40) and (3.41) are squared and added, the terms with the time lead τ are removed:

$$J^2\left[\left(\frac{1}{M(1+R)} + \dot{\chi}\right)^2 + \Omega_1^2\dot{\chi}^2\right] + J\left[2\Delta\dot{\chi}\Omega_1^2\right] + \Omega_1^2\Delta^2 = 2\Omega_1^2 F^2 A_1^2\left(1 - \cos\Omega_1 T\right)$$

Solving for J gives:

$$J = \frac{\chi \Delta \Omega_1^2}{\left(\frac{1}{M(1+R)} + \dot{\chi}\right)^2 + \Omega_1^2 \chi^2} \left(-1 \pm \sqrt{1 - \frac{\left(\left(\frac{1}{M(1+R)} + \dot{\chi}\right)^2 + \Omega_1^2 \chi^2\right)\left(\Delta^2 - 2rF^2A_1^2\right)}{\chi^2 \Delta^2 \Omega_1^2}} \right) \quad (3.42)$$

where $r = 1 - \cos\Omega_1 T$.

The time lead τ can be found by solving equations (3.40) and (3.41) for $\sin\Omega_1\tau$ and $\cos\Omega_1\tau$ to give the following:

$$\sin\Omega_1\tau = \frac{r\Omega_1(\Delta + J\chi) - J\left(\frac{1}{M(1+R)} + \dot{\chi}\right)\sin\Omega_1 T}{2rFA_1\Omega_1} \quad (3.43)$$

$$\cos\Omega_1\tau = \frac{\Omega_1(\Delta + J\chi)\sin\Omega_1 T + rJ\left(\frac{1}{M(1+R)} + \dot{\chi}\right)}{2rFA_1\Omega_1}. \quad (3.44)$$

This solution can also be found in Kember and Babitsky [1999b].

3.3 Stability

For both sinusoidal and impact excitation, solutions (3.33) and (3.42), two solutions for J are obtained, one with a positive square root and one with a negative square root. To identify the stable solution the energy balance principle may be employed, as explained in Babitsky [1998] and Babitsky and Krupenin [1985] for general sinusoidally excited vibro-impact systems. See section 2.2.3. This has been extended here to the case of impact excitation for the system being analysed.

Based on these previous studies with sinusoidally excited systems, it is proposed that equations (3.32) and (3.43) represent the energy balance of the systems with $\sin\varphi$ proportional to the energy from the excitation. This is shown to be valid in the next section.

For sinusoidal excitation, equations (3.31) and (3.32) can be rewritten:

$$\sin\varphi = -(a + qJ) \quad (3.46)$$

and

$$\cos\varphi = h + dJ. \quad (3.47)$$

where a, q, h, and d are defined as follows:

$$a = 0$$

$$q = \frac{\frac{1}{M(1+R)} + \dot{\chi}}{A\omega}$$ (3.45)

$$h = \frac{\Delta}{A}$$

$$d = \frac{\chi}{A}$$

It is proposed that after a small perturbation the motion becomes:

$$\tilde{x}_1(t) = A\cos(\omega t + \tilde{\varphi}(t)) - \tilde{J}(t)\chi_1(t)$$

where $\tilde{\varphi}(t)$ and $\tilde{J}(t)$ are arbitrary slowly varying variables. Since equation (3.46) represents the energy balance and $\sin\varphi$ is proportional to the energy of excitation, the system is stable if the following condition is true:

$$\frac{d}{d\tilde{J}}\left[a + h\tilde{J} + \sin\tilde{\varphi}\right]_{\tilde{J}=J} > 0 \quad .$$ (3.48)

Thus the balance of energies changes in such a manner as to compensate the perturbation.

Differentiating equation (3.48) gives

$$\left\{q + \cos\tilde{\varphi}\frac{d\tilde{\varphi}}{d\tilde{J}}\right\}_{\tilde{J}=J} > 0.$$ (3.49)

where $\tilde{\varphi}$ and $\tilde{J}$ are two arbitrary functions which can be related by an additional condition. In this case it is convenient to take this additional condition to be equation (3.47). Inserting the two arbitrary functions into equation (3.47) and differentiating gives:

$$-\sin\tilde{\varphi}\frac{d\tilde{\varphi}}{d\tilde{J}} = d.$$ (3.50)

Using equation (3.50) to substitute for $\frac{d\tilde{\varphi}}{d\tilde{J}}$, equation (3.49) becomes:

$$\{q - d\cot\tilde{\varphi}\}_{\tilde{J}=J} > 0$$ (3.51)

when $\tilde{J} = J$ and $\tilde{\varphi} = \varphi$. If equation (3.47) is divided by equation (3.46) to give $\cot \varphi$, then equation (3.51) may be written:

$$\frac{hd + d^2 J}{a + qJ} + b > 0.$$

(3.52)

Multiplying equation (3.52) by $a+qJ$ and rearranging

$$J > \frac{-(aq + hd)}{q^2 + d^2}.$$

(3.53)

Substituting for a, q, h and d from equation (3.45) we have:

$$J > -\frac{\chi \Delta \omega}{\left(\frac{1}{M(1+R)} + \dot{\chi}\right)^2 + \omega \chi^2}$$

(3.54)

Therefore the positive root of equation (3.33) corresponds to the stable solution. This agrees with stability results for other vibro-impact systems [Babitsky 1998, Babitsky and Krupenin 1985].

For the case of impulse excitation, a, q, h, and d are defined as follows:

$$a = -\frac{r\Omega_1 \Delta}{2rFA_1\Omega_1}$$

$$q = \frac{-\left(r\Omega_1\chi - \left(\frac{1}{M(1+R)} + \dot{\chi}\right)\sin\Omega_1 T\right)}{2rFA_1\Omega_1}$$

$$h = \frac{\Omega_1 \Delta \sin\Omega_1 T}{2rFA_1\Omega_1}$$

(3.55)

$$d = \frac{\Omega_1\chi\sin\Omega_1 T + r\left(\frac{1}{M(1+R)} + \dot{\chi}\right)}{2rFA_1\Omega_1}$$

so that equations (3.43) and (3.44) can be rewritten:

$$\sin\Omega_1\tau = \sin\varphi = -(a + qJ)$$

(3.56)

and

$$\cos\Omega_1\tau = \cos\varphi = c + hJ.$$

(3.57)

It is proposed that after a small perturbation the motion becomes:

$$\tilde{x}_1(t) = F\chi_1(t + \tilde{\tau}(t)) - \tilde{J}(t)\chi_1(t)$$

where in a similar way to the sinusoidal case $\tilde{\varphi}(t) = \Omega_1 \tilde{r}(t)$ and $\tilde{\varphi}(t)$ and $\tilde{J}(t)$ are arbitrary slowly varying variables. The remainder of the derivation is identical to the sinusoidal case so that substituting for a, q, h and d in equation (3.53) gives:

$$J > -\frac{\chi \Delta \Omega_1^2}{\left(\frac{1}{M(1+R)} + \dot{\chi}\right)^2 + \Omega_1^2 \chi^2}$$

which again means that by comparison with equation 3.42 the positive root gives the correct solution.

3.4 Substantiation of the stability method

The explanation that the equation for $\sin \varphi$ is proportional to the energy supplied by the excitation is complex [Babitsky et al 1995] and this is summarised here. The energy due to the excitation over one period is defined as [Magnus 1965]:

$$E = \int_0^T P(t)\dot{x}(t)dt \tag{3.61}$$

where $P(t)$ is the excitation force.

Babitsky et al [1995] calculate the energy of excitation for a generalised system with sinusoidal excitation where the equation of motion has been simplified to:

$$x(t) \approx -J\chi(t) \quad \text{where} \quad \chi(t) = \sum_{q=-\infty}^{\infty} L(qi\omega)e^{qi\omega t}$$

and where $L(qi\omega)$ is the receptance or dynamic compliance.

Thus the excitation energy in equation (3.61) becomes:

$$E = -\int_0^T JP\cos(\omega t + \varphi)\sum L(qi\omega)\frac{d}{dt}\left(e^{qi\omega t}\right)dt \tag{3.62}$$

We also have

$$\frac{d}{dt}\left(e^{qi\omega t}\right) = qi\omega e^{qi\omega t} = \begin{cases} |q|i\omega\cos|q|\omega t - |q|\omega\sin|q|\omega t & q > 0 \\ -|q|i\omega\cos|q|\omega t - |q|\omega\sin|q|\omega t & q < 0 \end{cases}$$

therefore $\quad \sum \dfrac{d}{dt}\left(e^{qi\omega t}\right) = -\sum q\omega\sin q\omega t$

Since $\cos(\omega t + \varphi) = \cos\omega t \cos\varphi - \sin\omega t \sin\varphi$ the excitation energy becomes

$$E = \int_0^T JP(\cos\omega t \cos\varphi - \sin\omega t \sin\varphi)\sum L(qi\omega)qi\omega\sin q\omega t \ dt$$

Since

$$\int_0^{2\pi}\cos\theta\sin\theta d\theta = 0 \quad \text{and} \quad \int_0^{2\pi}\sin^2\theta \ d\theta = \pi$$

and if $\theta = \omega t$ and $dt = d\theta/\omega$

equation (3.62) reduces to:

$$E \propto \pi\sin\varphi$$

3.5 Reduction to a single degree of freedom system

The stable solutions for J for both sinusoidal and impact excitation, (3.33) and (3.42), can be simplified to show the underlying nonlinear structure of the system. If c_1 and c_2 are made very small and R almost 1 so that there are no energy losses, then $\frac{1}{M(1+R)} + \dot{\chi} = 0$ and so equation (3.33) simplifies to:

$$J = \frac{-\Delta + A}{\chi}. \tag{3.63}$$

and equation (3.42) for the impulse excitation simplifies to:

$$J = \frac{-\Delta + FA_1\sqrt{2r}}{\chi} \tag{3.64}$$

If m_2 is very large so that the system is effectively a single degree of freedom system (an impact oscillator) then

$$\chi = A_1\sin\Omega_1 T = \frac{1}{2m_1\Omega_1\tan\left(\dfrac{\Omega_1 T}{2}\right)}$$

As $r = 1 - \cos\Omega_1 T = 2\sin^2\left(\dfrac{\Omega_1 T}{2}\right)$ and $\sin\Omega_1 T = 2\sin\left(\dfrac{\Omega_1 T}{2}\right)\cos\left(\dfrac{\Omega_1 T}{2}\right)$,

equation (3.63) becomes

$$J = -2m_1\Omega_1\Delta\tan\left(\frac{\Omega_1 T}{2}\right) + \frac{2F_0\Omega_1\tan\left(\dfrac{\Omega_1 T}{2}\right)}{\sqrt{(\Omega_1^2 - \omega^2)^2}} \tag{3.65}$$

and equation (3.64) becomes

$$J = -2m_1\dot{\Omega}_1\Delta\tan\left(\frac{\Omega_1 T}{2}\right) + \frac{F}{\cos\left(\frac{\Omega_1 T}{2}\right)} \cdot \qquad (3.66)$$

If the system is under free vibration ($F = F_0 = 0$), then either equation (3.65) or equation (3.66) provides a result that is identical to the result given in Babitsky and Krupenin [1985] for an impact oscillator, and the frequency characteristic (Figure 3.3) is a typical backbone curve for a nonlinear system. This shape is retained as long as the second term in either equation is small in comparison to the first term.
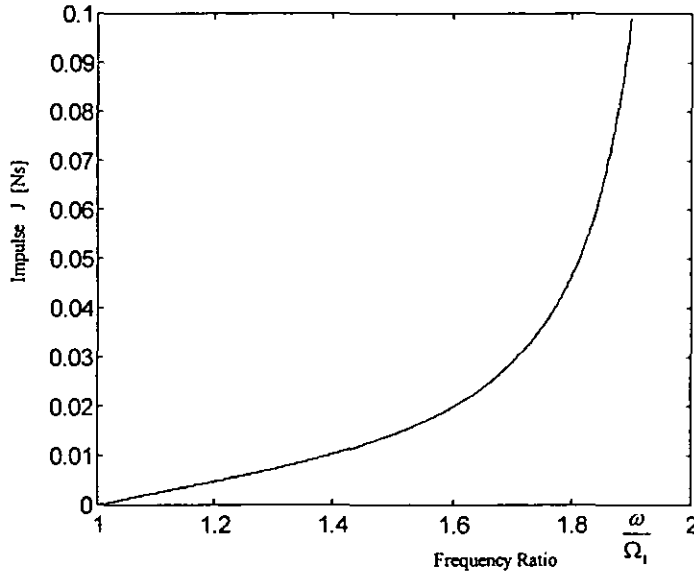
Figure 3.3 The backbone curve

3.6 The dynamic behaviour of the model

In order to illustrate the dynamic behaviour of the two degree of freedom system (Figure 3.2), a suitable set of parameters is obtained from the experiment described in section 5.1 : $m_1 = 0.125$kg, $m_2 = 0.094$kg, $k_1 = 135$N/m, $k_2 = 128$N/m, $c_1 = 0.1$Ns/m, $c_2 = 0.1$Ns/m, $\Delta = 0.001$m.

3.6.1 Sinusoidal excitation
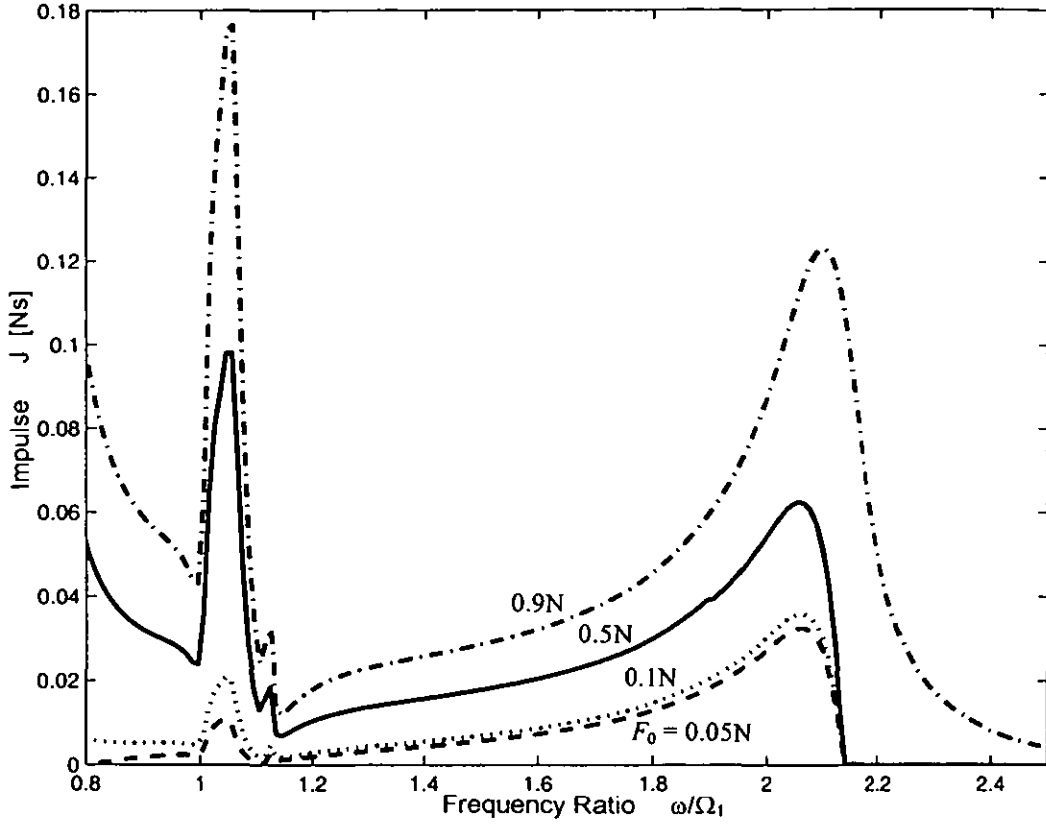
Figure 3.4 Impulse frequency response from sinusoidal excitation: R=1

Using the solution for J from equation (3.33) and varying the frequency of excitation, a frequency response for the impulse J between the two masses can be obtained. The graph shown in Figure 3.4 was generated using a Matlab program, jsnew.m (given in the Appendix). The parameters chosen are those given above with the amplitude of excitation F_0 = 0.05N, 0.1N, 0.5N and 0.9N, and with R = 1. As F_0 increases, the response of J also increases with little change in frequency for the two resonances. There is a peak with a shape like that of the backbone curve (Figure 3.3) at ω/Ω_1 = 2.13. Another peak also occurs at ω/Ω_1 = 1.05.

When F_0 = 0.9N the backbone curve loses its shape suggesting that the second term in equation (3.65) now dominates. If R is reduced to 0.7 and c_1 to 0 and F_0 = 0.5N , the frequency response shows a much reduced second peak (Figure 3.5). The frequency responses of the displacements can also be calculated (using jsdnew.m) and these can be seen in Figures 3.6 and 3.7 . In Figure 3.6 there are two additional

peaks. A large peak appears at $\omega/\Omega=1$, the natural frequency of the active system and another peak occurs on the approach to the natural frequency of the passive system. These two peaks would not occur in a real system because the PGF method allows the masses to pass through one another except at $t = 0$ and at $t = T$. Figure 3.7 shows the displacement response with these two additional peaks removed. The second resonant peak is very small in comparison with the first peak. The passive mass has a greater displacement than the active mass at the minimum between the two resonances (also termed the antiresonance in nonlinear dynamics literature).
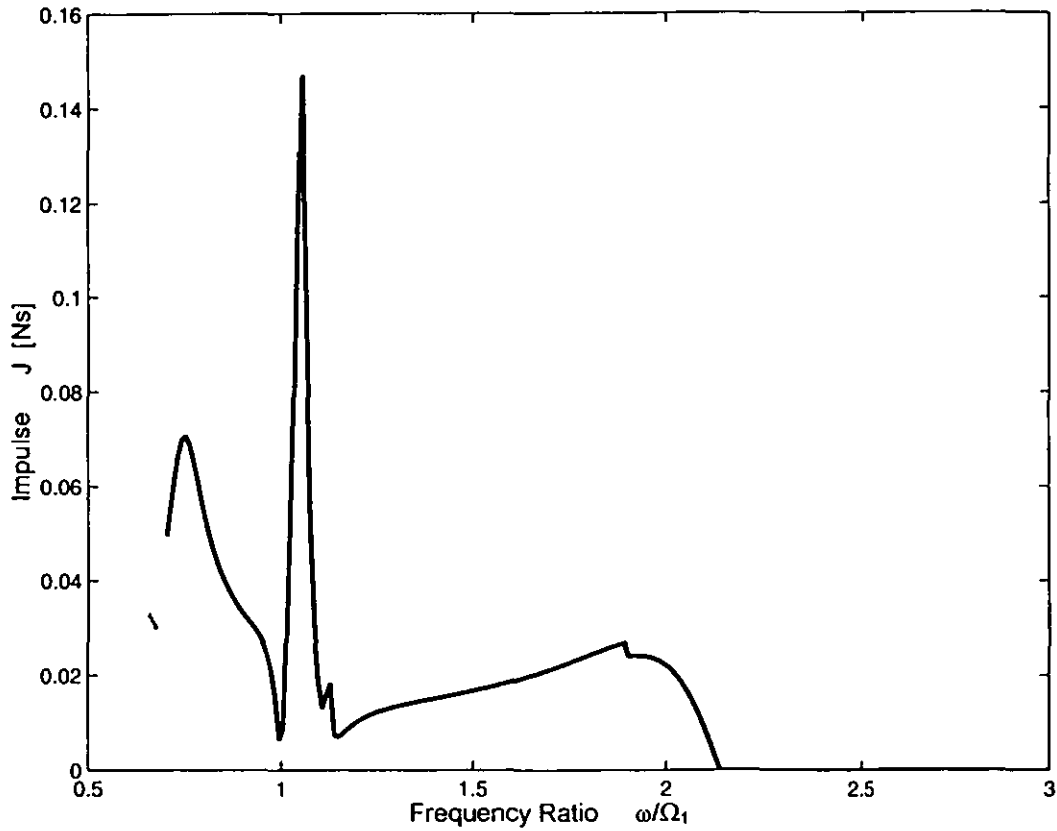
Figure 3.5 Impulse frequency response from sinusoidal excitation: $R = 0.7$, $c_1 = 0$
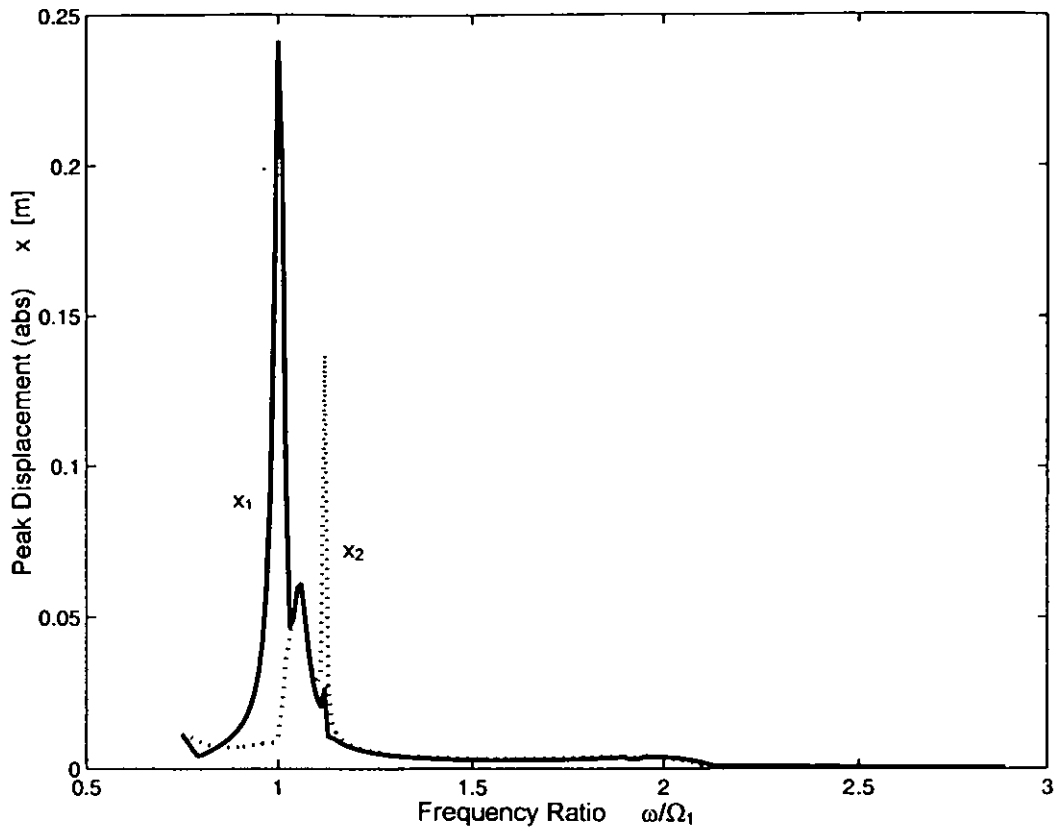
Figure 3.6 Displacement frequency response from sinusoidal excitation: $R = 0.7$, $c_1 = 0.1$
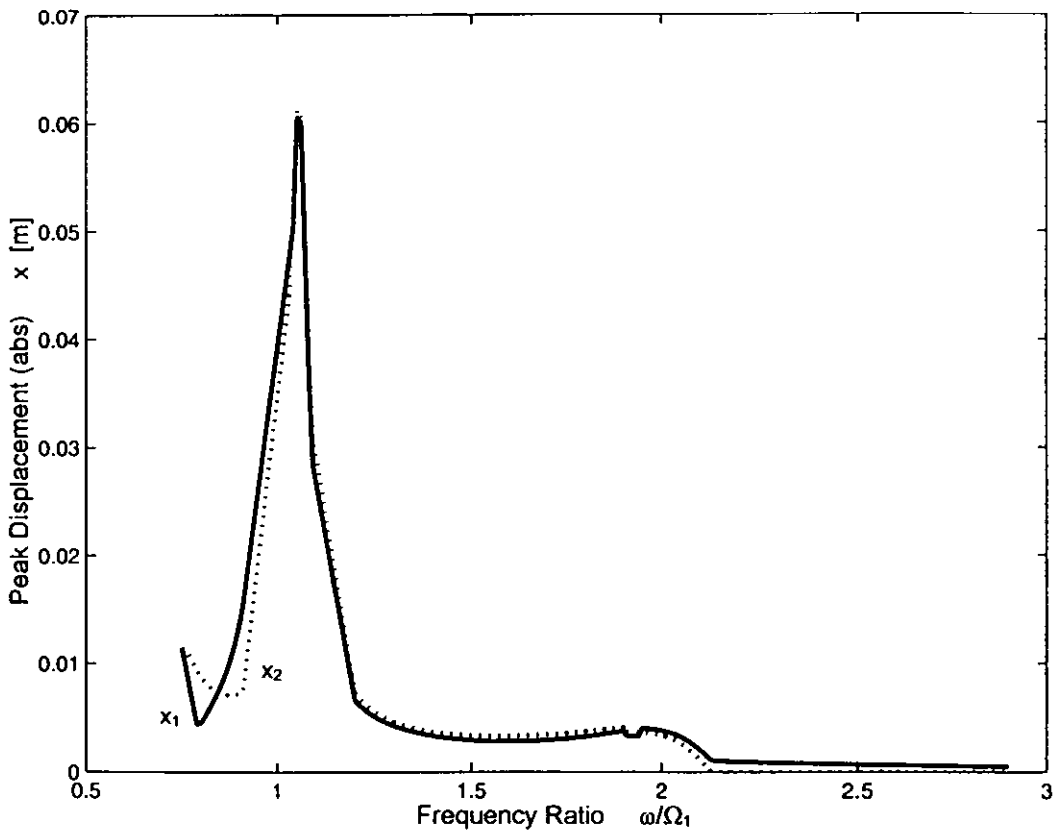
Figure 3.7 Displacement frequency response: additional peaks removed

The displacement behaviour at the two peaks has been calculated (using jsdtw.m). In Figure 3.8 where the frequency ratio is 2.13 (11.1 Hz), and $c_1 = c_2 = 0$ and $F_0 = 0.5N$, the two masses are moving in opposite directions (out of phase) - a *clapping* resonance. The resonance of the active mass has a greater amplitude. Figure 3.9 shows the result for the frequency ratio of 1.05 (5.5 Hz), and $c_1 = c_2 = 0$ and $F_0 = 0.05$. Here the two masses are moving in phase - a *grazing* resonance.
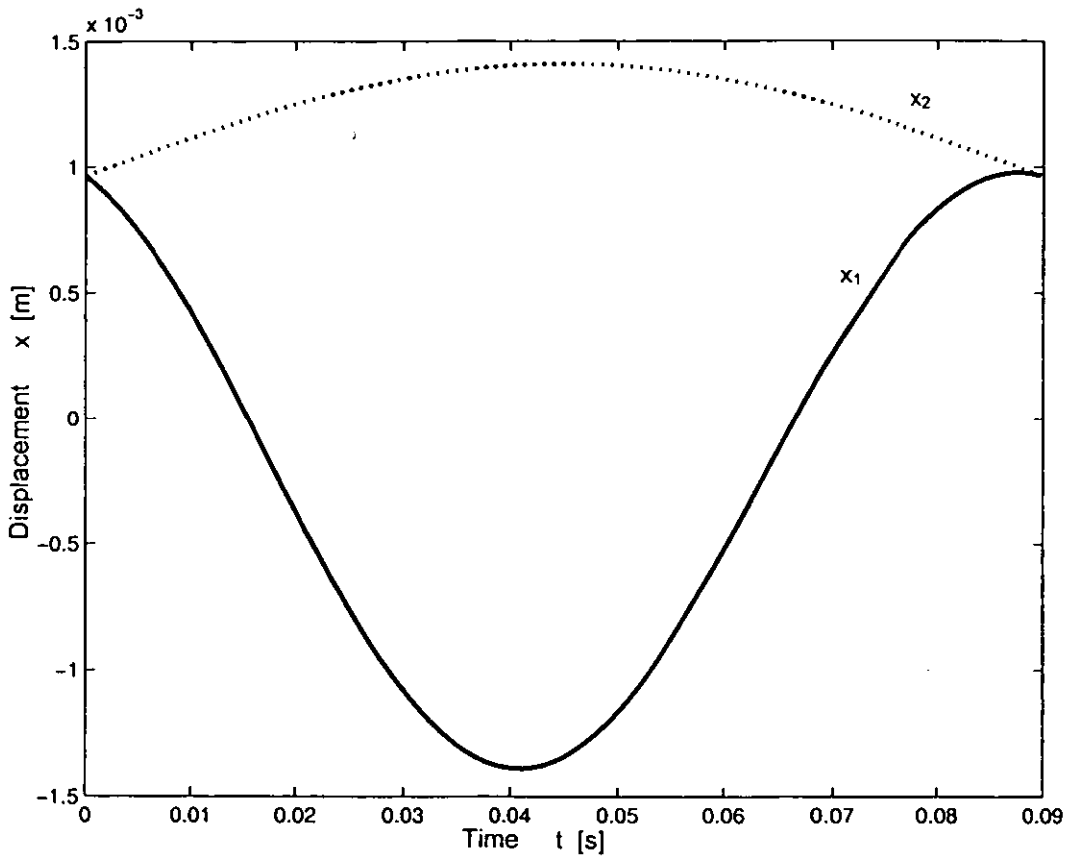
Figure 3.8 Displacements of system under sinusoidal excitation – 11.1Hz
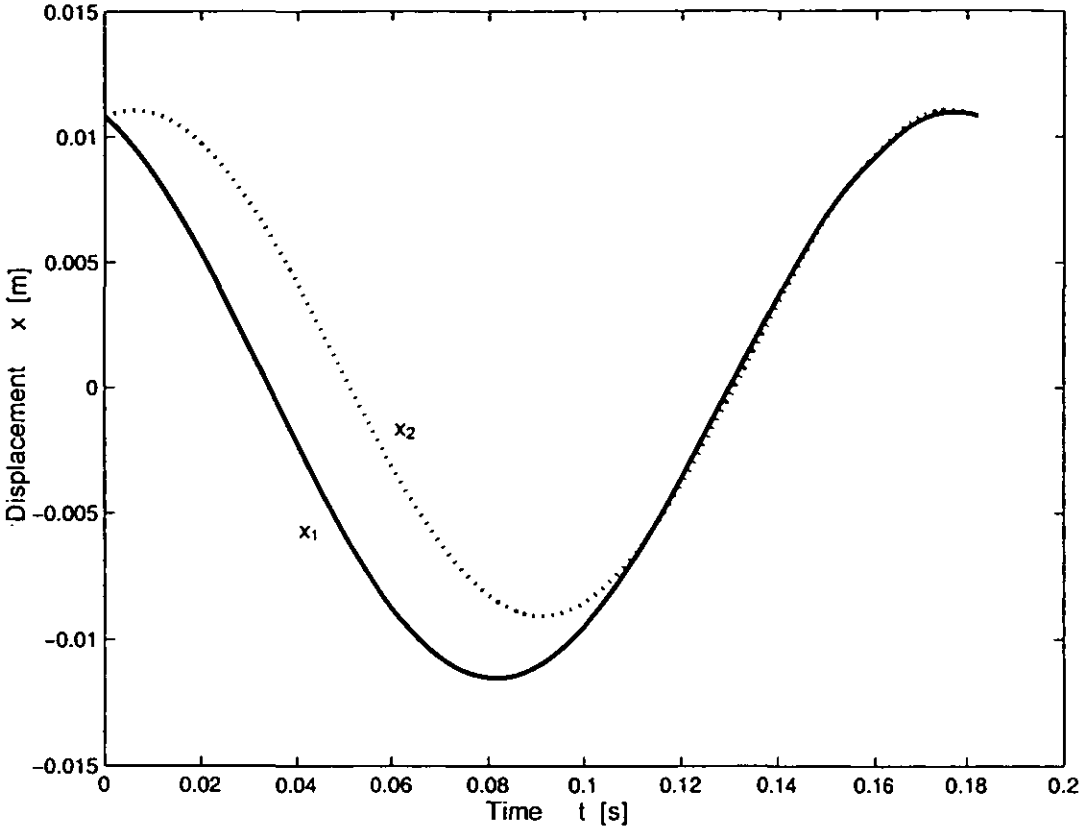
Figure 3.9 Displacements of system under sinusoidal excitation – 5.5Hz

3.6.2 Impulse excitation

This process was repeated for the impulse excitation result (equation 3.42) with similar results. Identical parameters were used except that the excitation impulse F was set at 0.009Ns and initially $R = 1$ and $c_2 = 0$. In Figure 3.10 the frequency response of J is shown. This was calculated from equation (3.42) using the Matlab program jinew.m. There are two peaks at the same frequency ratios with the first peak being very small in comparison with the second peak. It is seen that the second peak is very similar to the backbone curve (Figure 3.3). If R is changed to a more realistic value of 0.7, the impulse response at the frequency ratio of 2.13 is reduced and the first resonance then becomes dominant (Figure 3.11). If in addition $c_2 = 0.1$Ns/m then the amplitude of the first resonance is reduced (Figure 3.12).
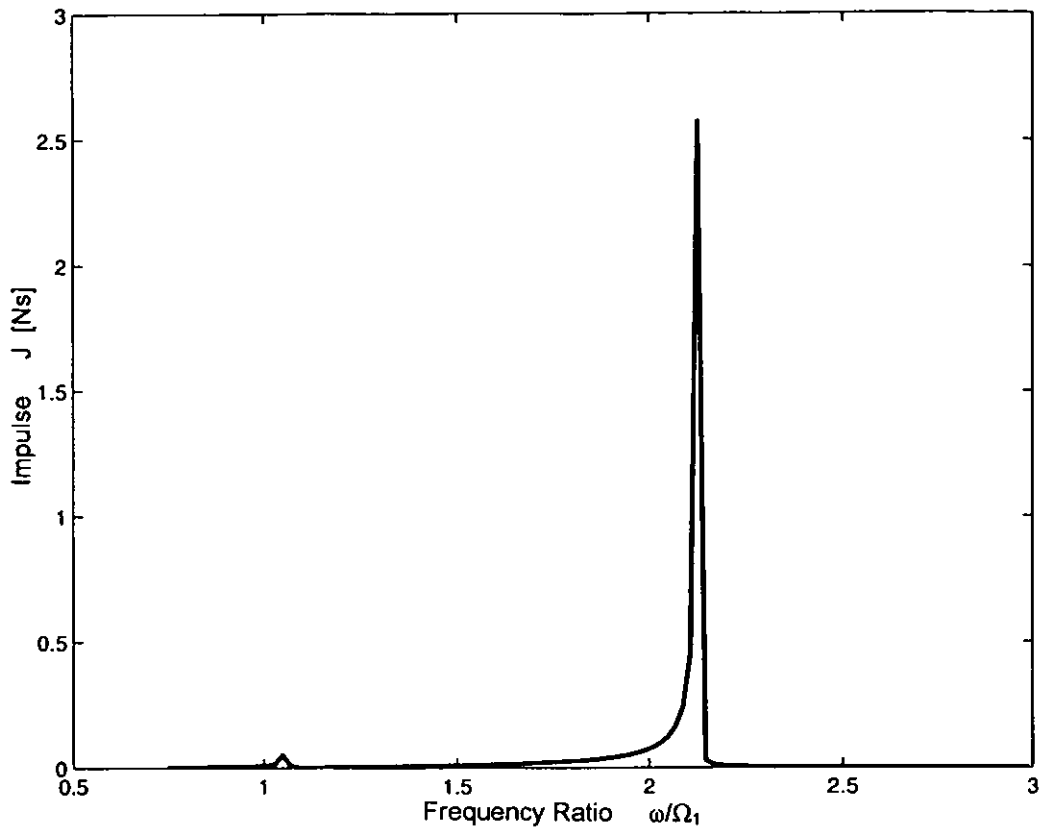
Figure 3.10 Impulse frequency response from impulse excitation: $R = 1$, $c_2 = 0$
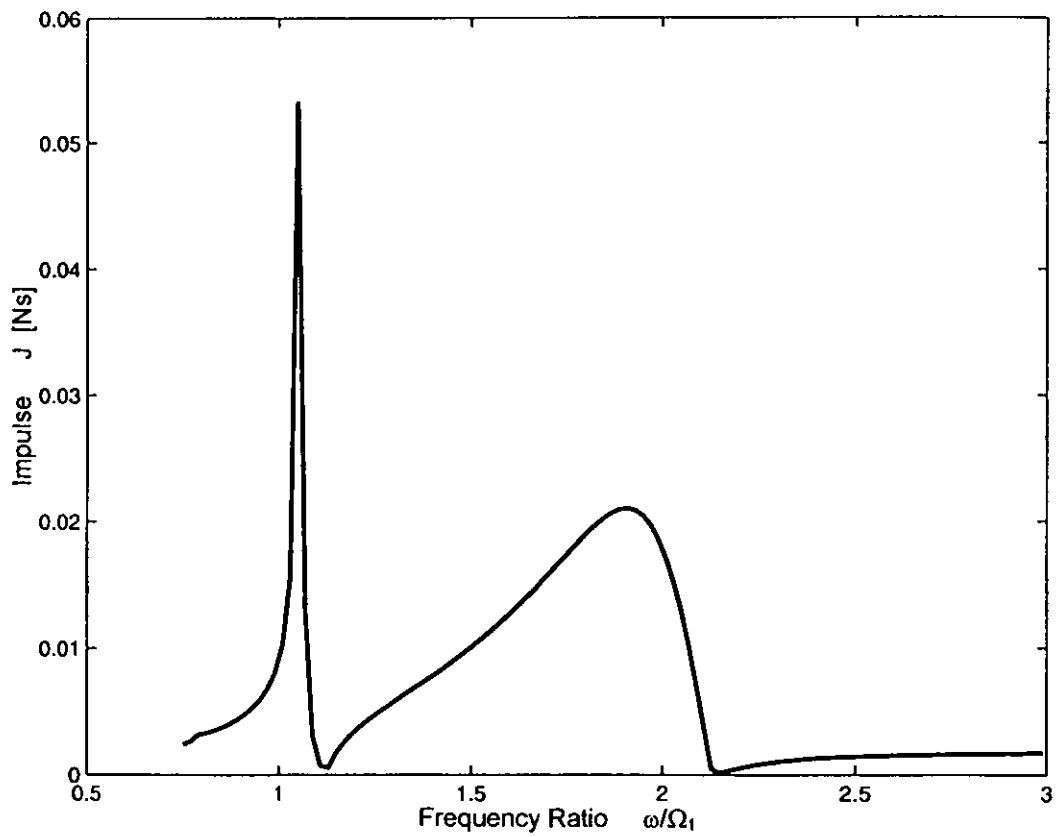
Figure 3.11 Impulse frequency response from impulse excitation: $R = 0.7$, $c_2 = 0$
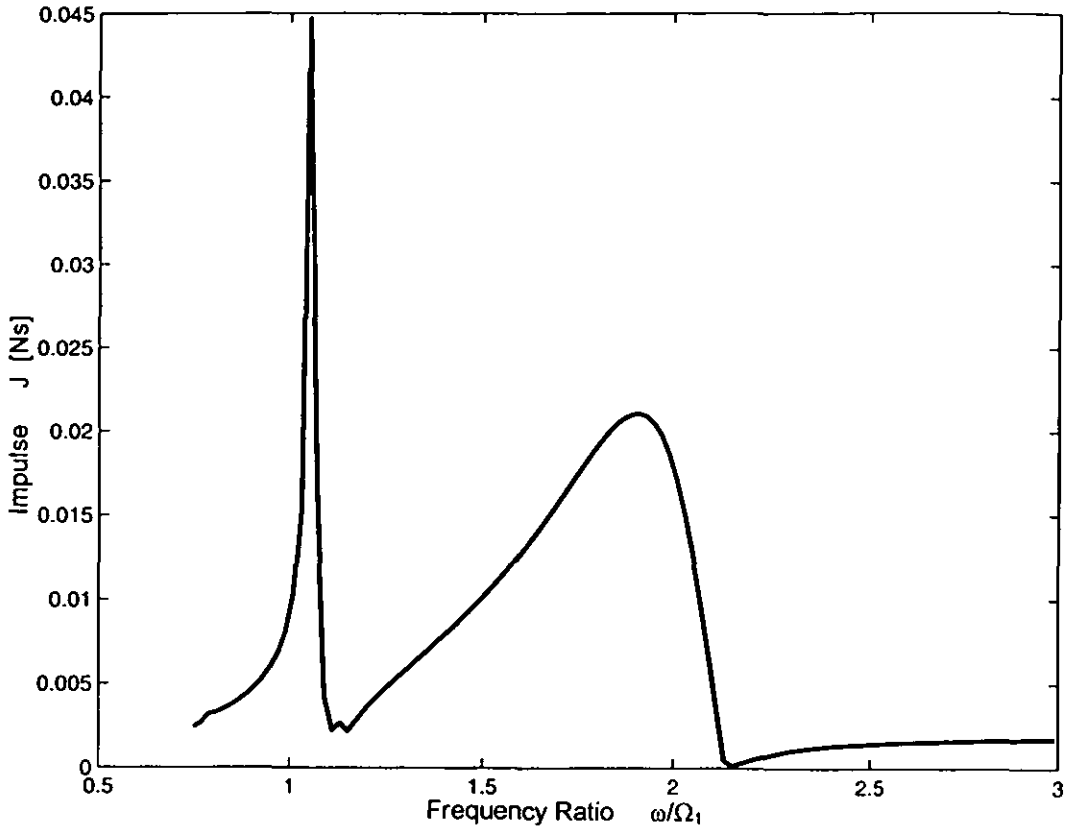
Figure 3.12 Impulse frequency response from impulse excitation: $R = 0.7$, $c_2 = 0.1$

The displacement frequency responses are shown in Figure 3.13 for perfectly elastic behaviour with $R = 1$ and $c_2 = 0$ (calculated by jidnew.m). The passive mass again has a greater displacement at antiresonance than the active mass. Increasing the damping coefficient and reducing the coefficient of restitution have the same effect on the displacement as on the impulse J (Figs 3.14 and 3.15). The additional peak is due to the natural frequency of the active system at the frequency ratio of 1 (5.23 Hz). As in the case of sinusoidal excitation, this peak exists because the masses pass through one another. The notch in the displacement of m_1 at approximately 1.75 is caused by the x_1 having a near zero value as the clapping resonance begins. The displacement of m_1 during the clapping resonance is negative in value. At this notch there is an antiresonance where m_2 has the larger displacement. This region is therefore a possible starting point for optimisation.
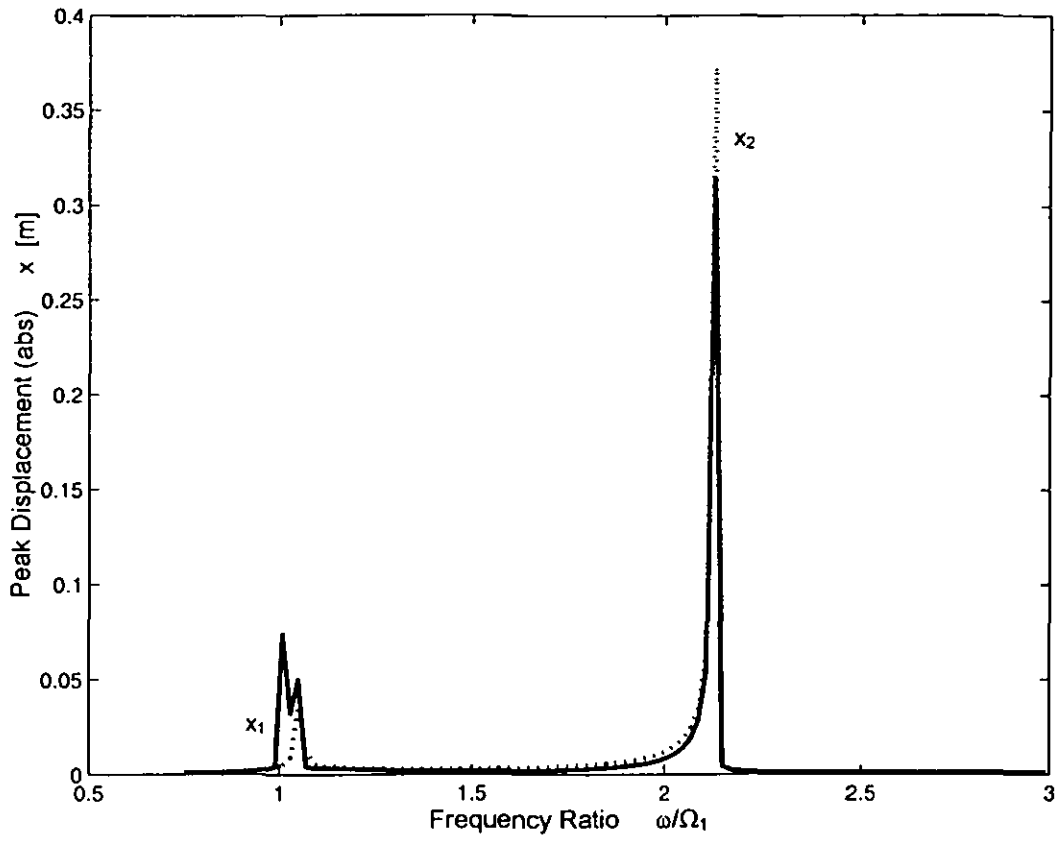
Figure 3.13 Displacement frequency response from impulse excitation: $R = 1$, $c_2 = 0$
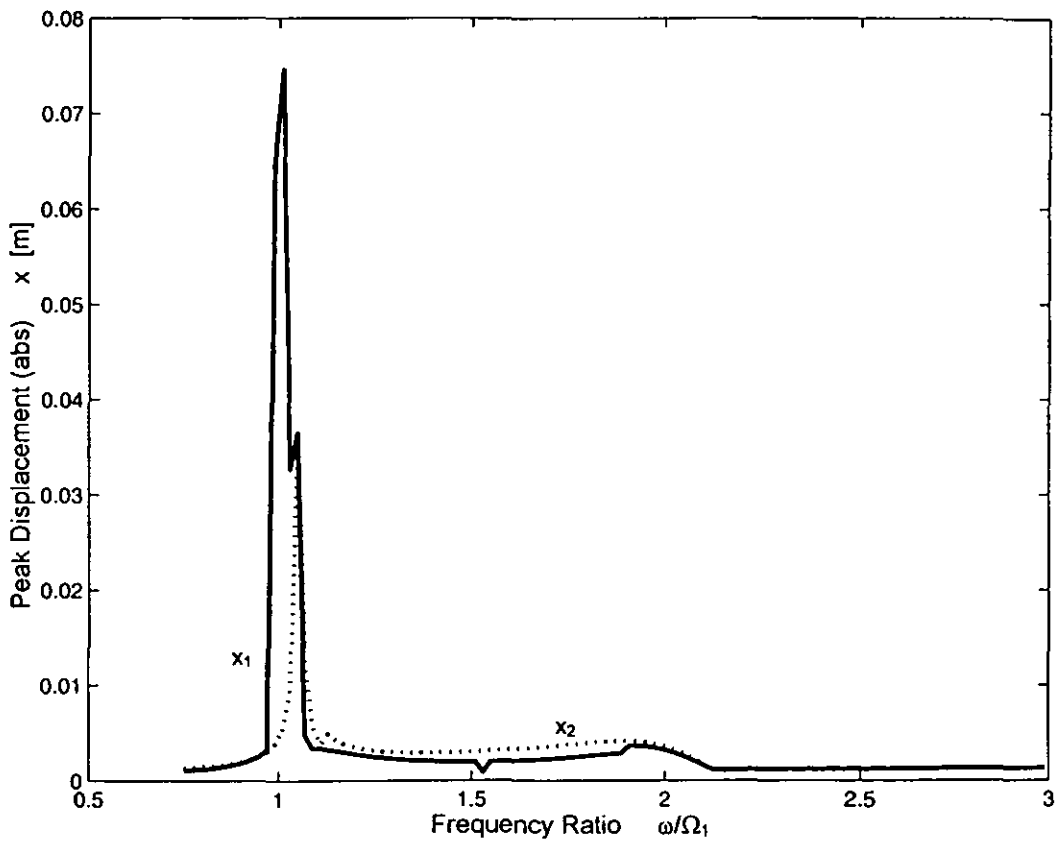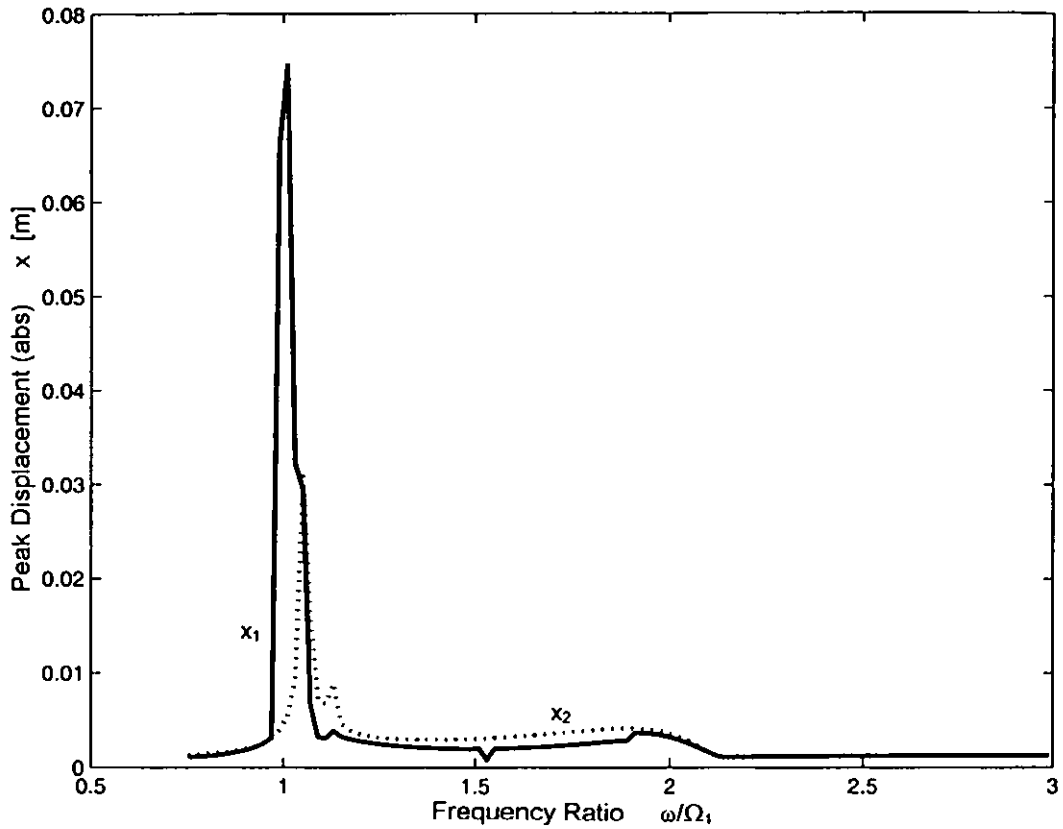

Figure 3.14 Displacement frequency response from impulse excitation: $R = 0.7$, $c_2 = 0$

Figure 3.15 Displacement frequency response from impulse excitation: $R = 0.7$, $c_2 = 0.1$

The displacement behaviour was calculated using jidtw.m with $R = 0.7$ and $c_2 = 0$. At the frequency ratio of 1.05 (5.5 Hz) the behaviour of the system is a grazing resonance (Figure 3.16) while at a ratio of 2.13 (11.1 Hz) the behaviour is a clapping resonance (Figure 3.17 – $R=0.7$ and Figure 3.18 – $R=1$). The effect of the impact excitation is clearly seen in the case where $R=0.7$, probably because the amplitude of the displacements is lower.
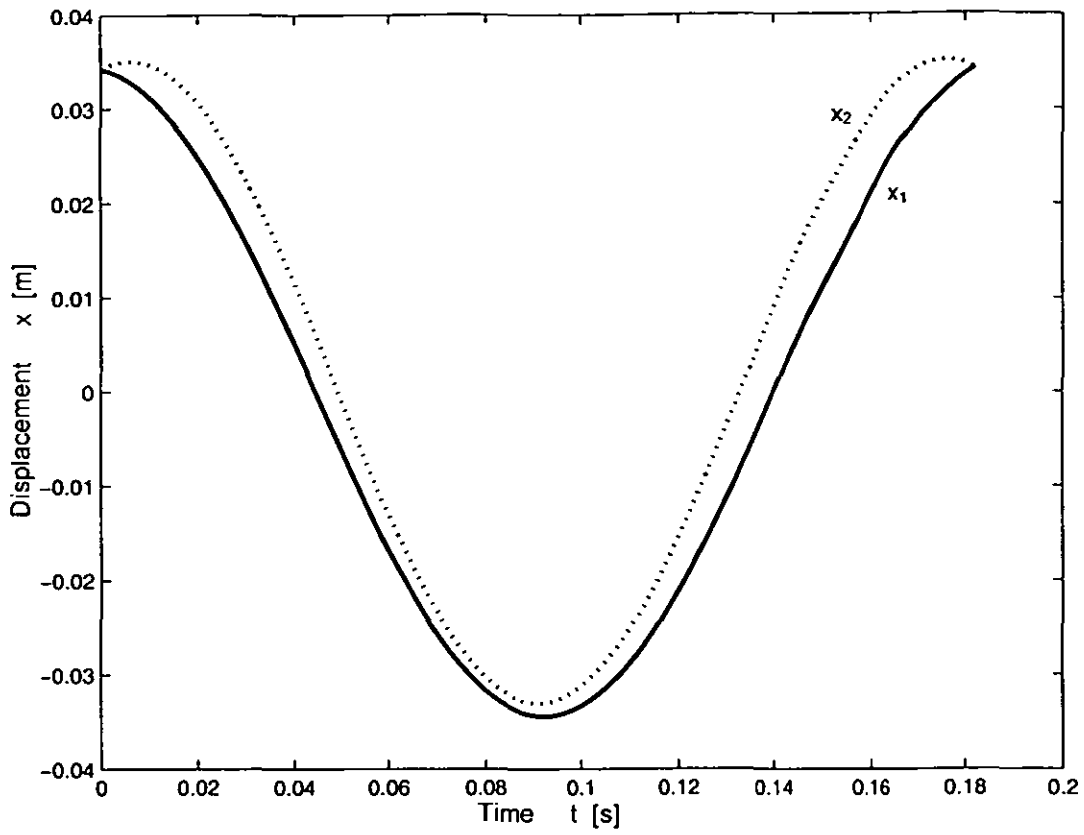
Figure 3.16 Displacements of system under impulse excitation – 5.5Hz
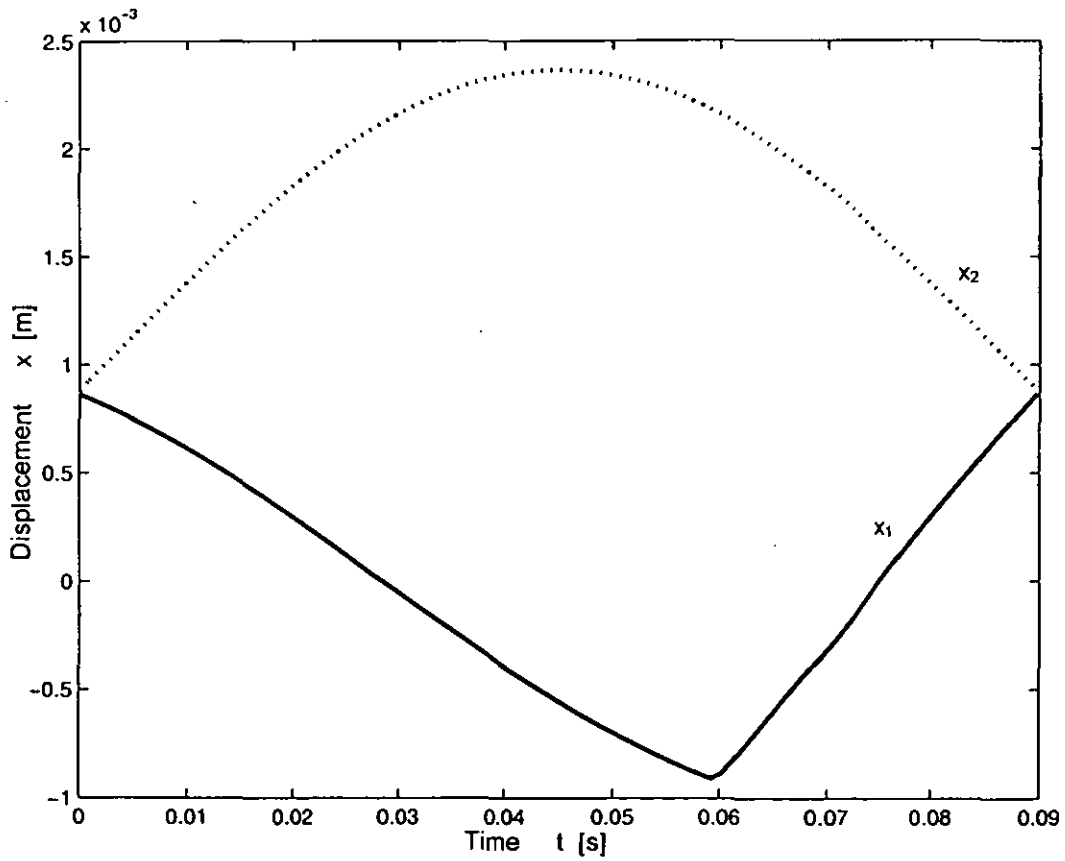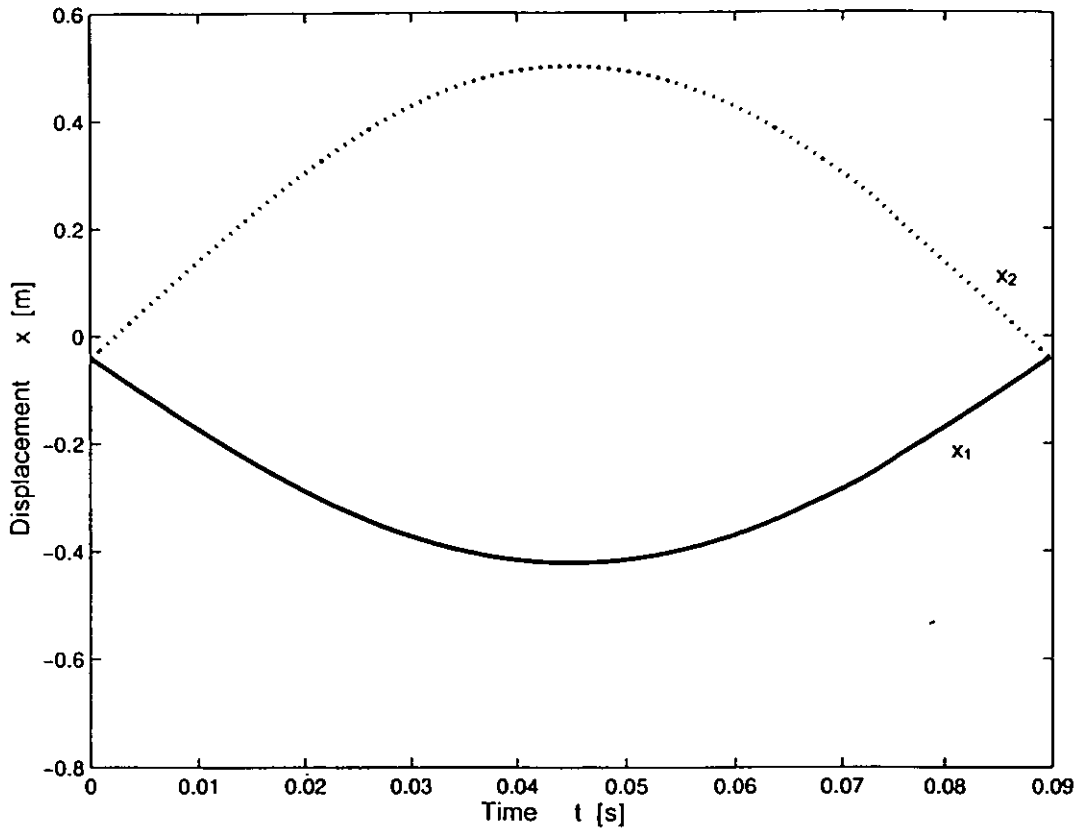

Figure 3.17 Displacements of system under impulse excitation – 11.1Hz, $R = 0.7$

Figure 3.18 Displacements of system under impulse excitation – 11.1Hz, $R = 1$

The PGF method has produced an algebraic solution for both sinusoidal and impulse excitation. The behaviour of the system shows two resonances, one a grazing resonance, the other a clapping resonance while at antiresonance the system behaves like a vibration absorber. This general behaviour occurs for both types of excitation. These results also provide a general background for the simulation study in the next section.

4 NUMERICAL STUDY

The model used for the PGF study was also simulated numerically using Simulink, part of the Matlab suite.

Simulink contains a graphical interface and several block libraries. Using a windows environment, the required blocks are connected to form a system diagram, resembling a control diagram. The blocks include summers, amplifiers, signal generators, integrators, sign blocks, oscilloscopes and other components. The package then simulates the performance of the system. After a simulation has been run, the results can be sent to Matlab for further processing or stored in a file. This chapter describes models developed using this package.

4.1 Impact oscillator

The simplest vibro-impact system to model is the impact oscillator. The model in Simulink has two sections, one that models a single degree of freedom linear system and another to provide the stop.

A single-DOF system has the equation

$$m\ddot{x} + c\dot{x} + kx = f(t)$$

rearranging:

$$\ddot{x} = \frac{f(t) - c\dot{x} - kx}{m}$$

or

$$x = \iint \left(\frac{f(t) - c\dot{x} - kx}{m} \right) dt\, dt$$

This last equation is used as a basis for the Simulink model.

The block diagram in Figure 4.1 shows a sine wave generator, representing $f(t)$, sending a signal through a summation block to an amplifier representing $1/m$: the result is the acceleration of the mass, $\ddot{x}$. This signal passes through two integrators (marked $1/s$) to give x. This result can be displayed on a virtual oscilloscope or sent to the Matlab workspace (the rectangular block marked x). The two upper feedback loops represent $c\dot{x}$ and kx.
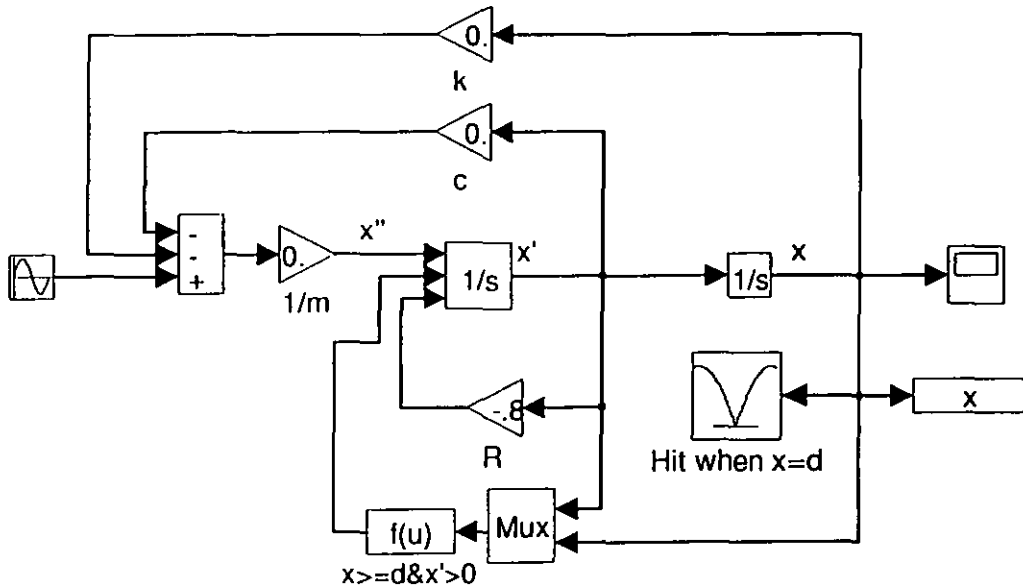
Figure 4.1 Simulink model of an impact oscillator

The lower loops describe the impact with the stop which is modelled using the classical theory of impact. Signals for x and $\dot{x}$ are multiplexed (by the block marked Mux) and then checked to see if the conditions for impact occur (d is the distance between the stop and the mass at rest). If the result is positive, then the integrator (a reset integrator) takes as its next output the input $-R\dot{x}$ from one of the lower feedback loops. If the result is negative the reset integrator continues as a normal integrator. The block marked 'Hit when $x = d$' ensures that simulation takes very small time steps close to the point of contact.

The modelling principles used for this impact oscillator can be extended to more complex models.

## 4.2 Two degree of freedom system with classical impact
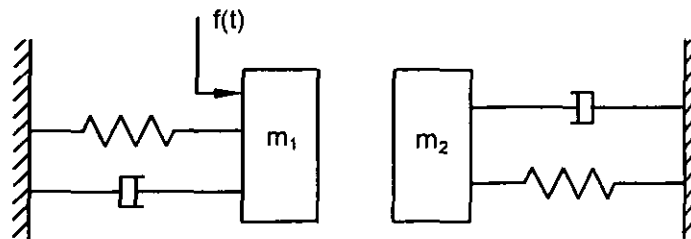
Figure 4.2 Two degree of freedom system

Using Figure 4.1 as a starting point, a Simulink model can be developed for the two degree of freedom (DOF) system described in section 1.5 (Figure 4.2). A system diagram is shown in Figure 4.3.
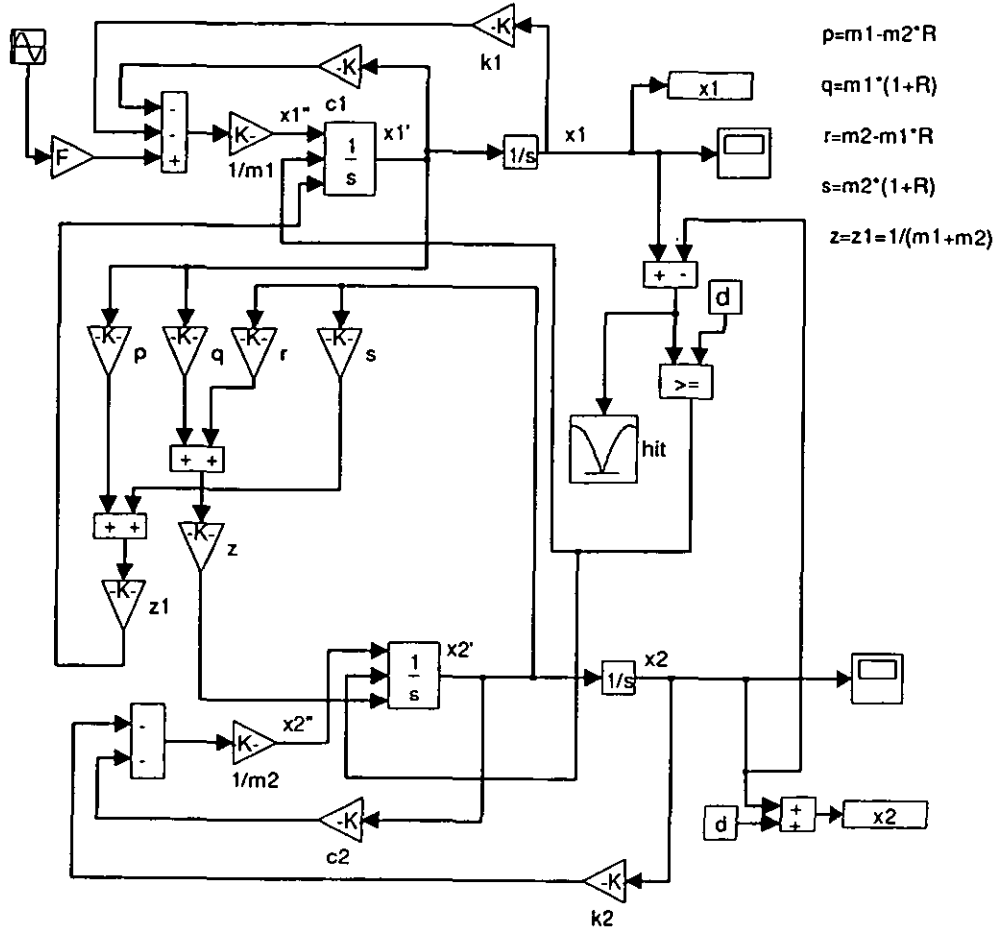
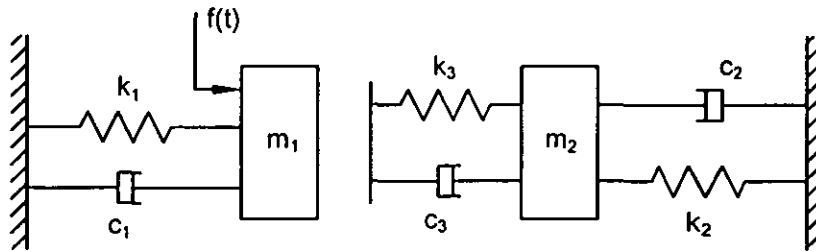**Figure 4.3** Simulink model of two degree of freedom system with classical impact

The upper part is the single degree of freedom (SDOF) system with sinusoidal excitation, the lower part is another SDOF system. Between the two is the impact detection part, and the calculation of the two velocities immediately after impact. The impact detection part does not incorporate detection of the true velocity direction. A similar version was used to produce the result in Figure 4.4, with the solid line representing x_1 and the dotted line for x_2. This model uses the same values as used in the PGF study but produces results that are irregular. The results became more irregular for other excitation frequencies. The integration method (Runge-Kutta with variable step size) was altered to have smaller step sizes, but this did not significantly improve the results.
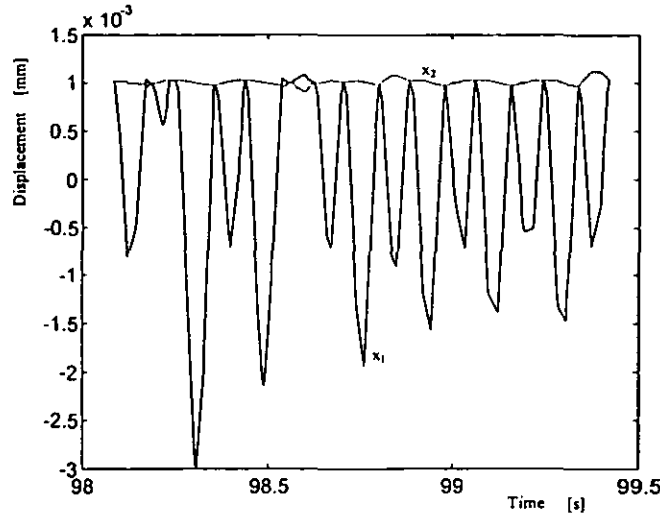
Figure 4.4 Result from Simulink model in Figure 4.3, frequency of excitation 11.1Hz

The Runge-Kutta integrator is the best integrator for discontinuities [Press et al 1992] but can produce errors when there is a sudden change in a parameter. Another factor affecting the results is the use of the classical impact model. As mentioned in section 2.1.1 the moment of collision is poorly defined in the classical impact model and requires infinite acceleration at impact. A simulation of this type should calculate values of acceleration and velocity at impact (which is not required by the PGF method). The impact model was therefore changed to a compliance model, as will be described in the next section.

4.3 Two degree of freedom system with compliance

Figure 4.5 Two degree of freedom system with compliance

In Figure 4.5 a spring and damper pair is incorporated into one of the impacting surfaces, using a method proposed by Babitsky and Veprik [1998]. The equivalent Simulink model is shown in Figure 4.6. Again two separate SDOF systems are

located at the top and bottom of the diagram. The reset integrators used in section 4.2 are no longer required and have been replaced by ordinary integrators. The compliance part is located between the two SDOF systems.
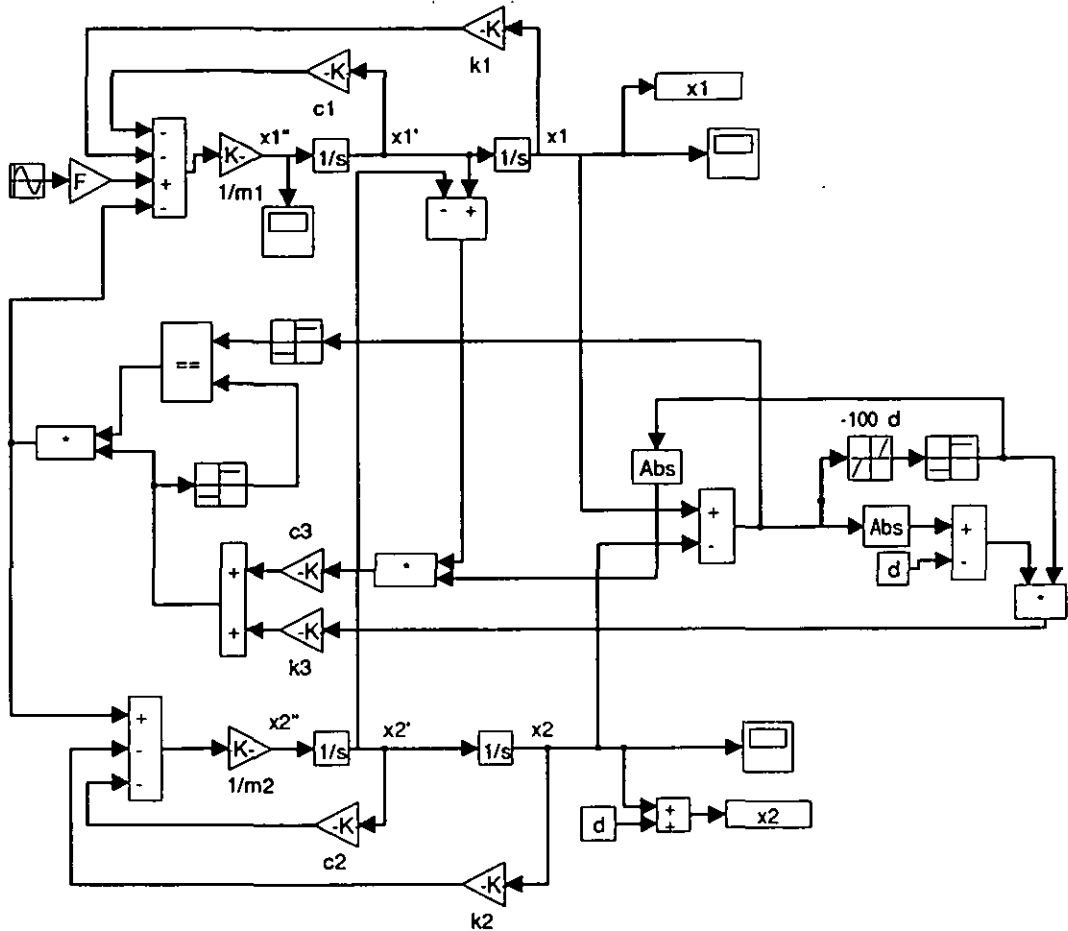

Figure 4.6 Simulink 2-DOF model with compliance

The two displacements x_1 and x_2 are combined to provide a relative displacement which is compared with the distance d to detect contact between the two masses. The Simulink model uses two nonlinear blocks, a backlash block which signals 0 unless the input is greater than d or less than -100. This block could allow double sided impacts but here the choice of -100 ensures that only single sided impact occurs. The result from this block passes through the sign block which converts the signal to 1, 0 or -1 depending on the sign of the input. The two blocks together switch on the compliance, thus allowing the relative displacement to be multiplied by the stiffness k_3 and the relative velocity by the damping coefficient c_3. These are then added to provide the reaction force due to impact.
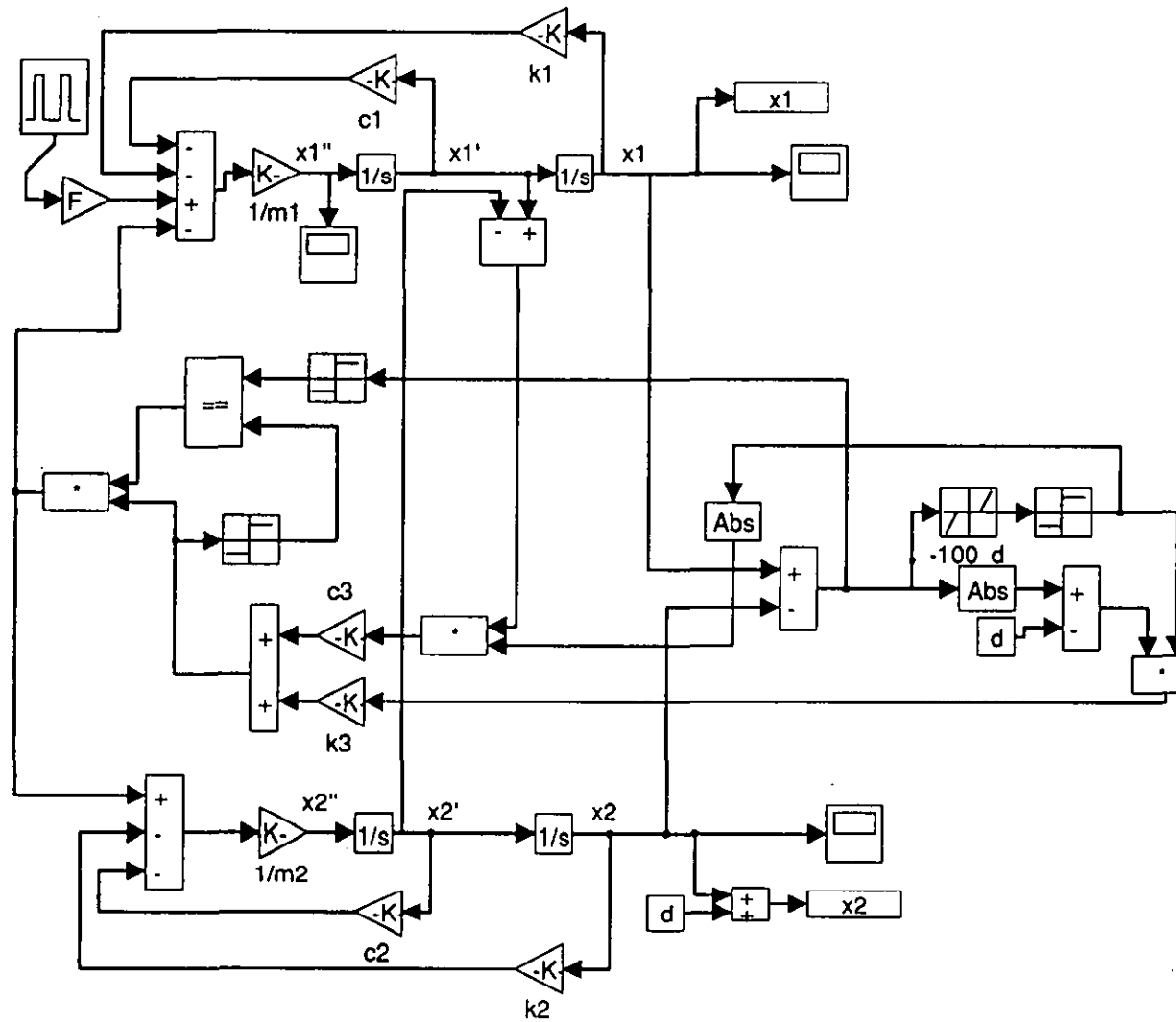
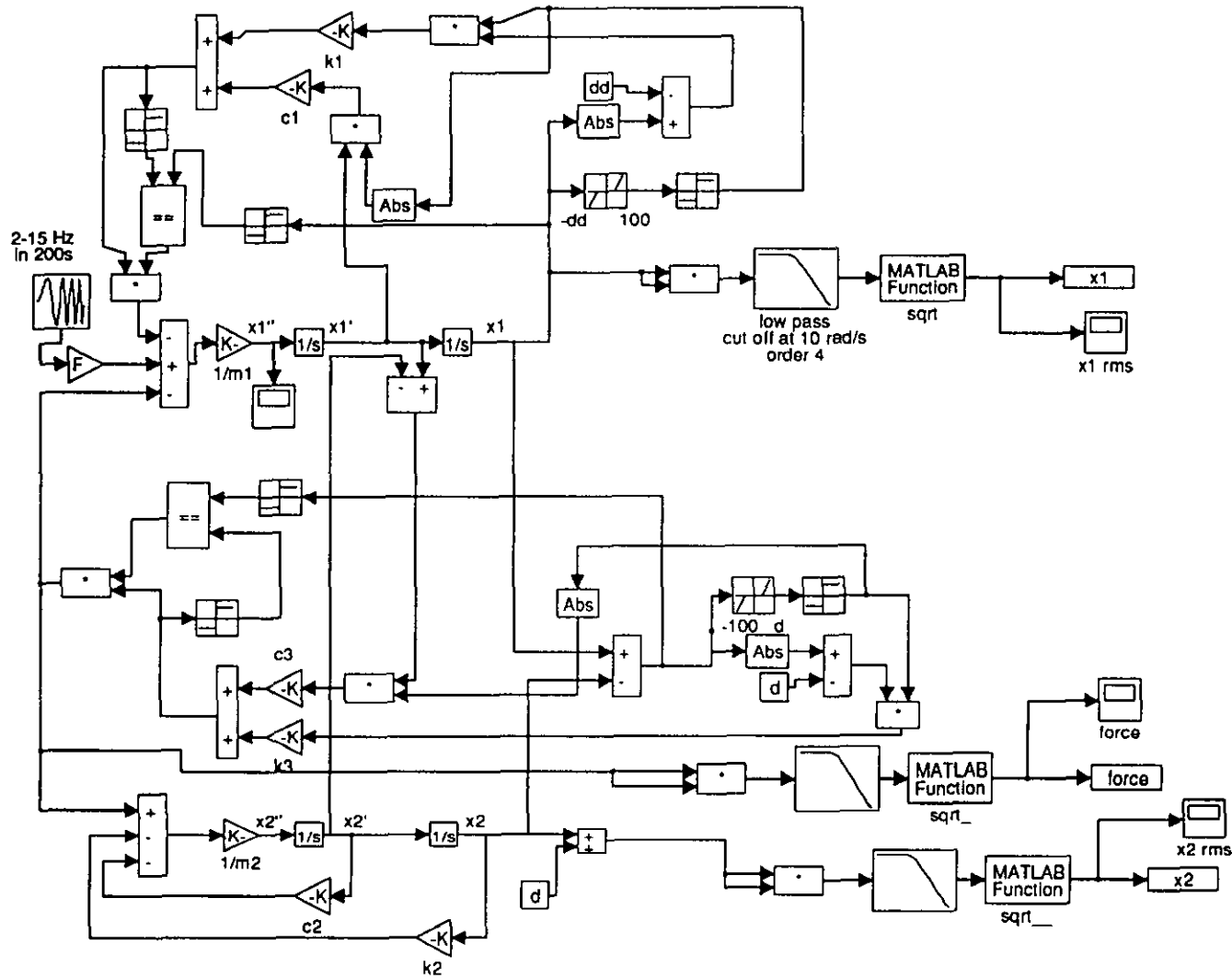**Figure 4.7** Simulink 2-DOF model with compliance and pulse excitation

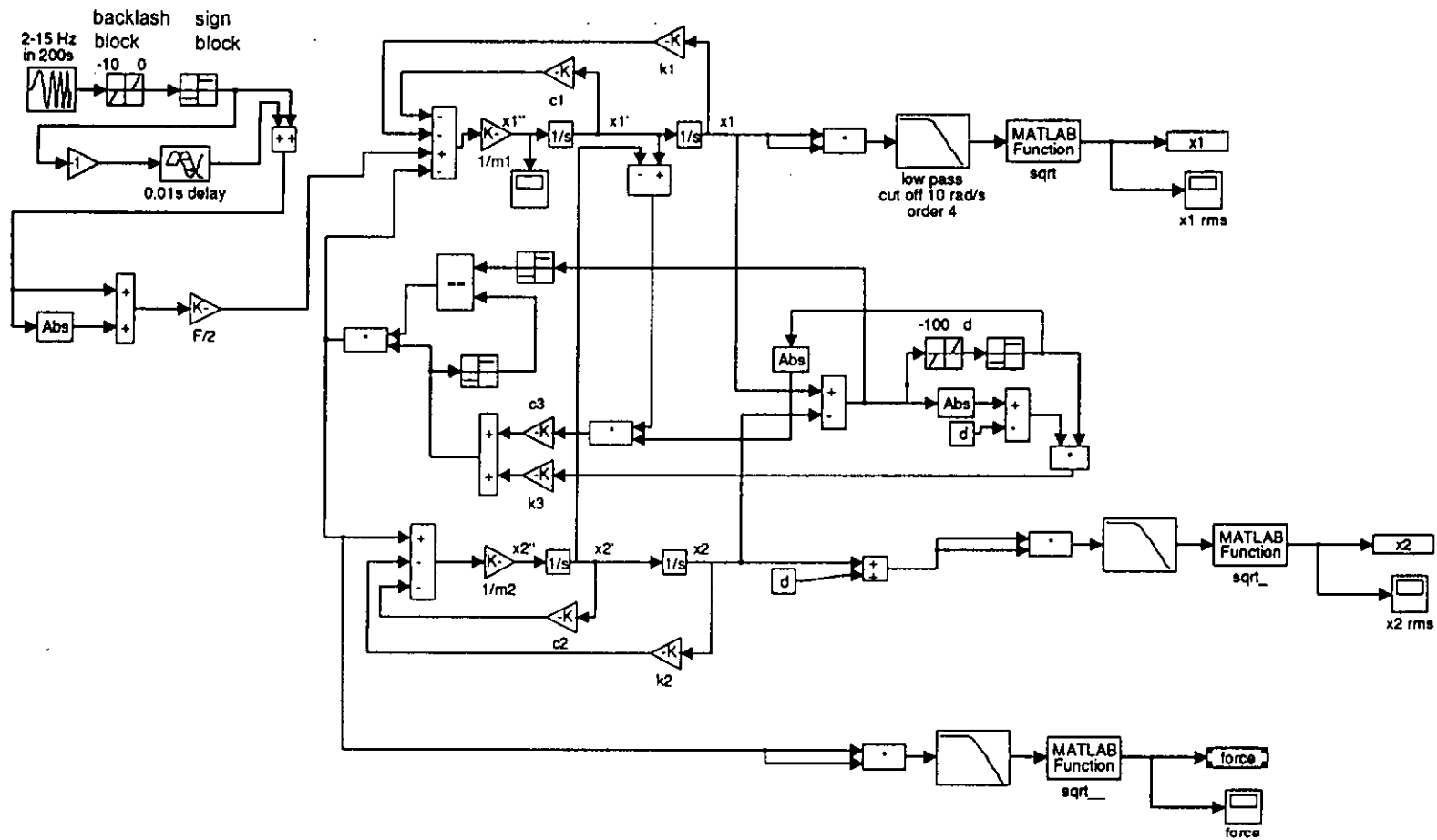**Figure 4.8** Simulink 2-DOF model with sine sweep excitation

Figure 4.9 Simulink 2-DOF model with pulse sweep excitation

Once the masses start to move apart the simulation monitors this reaction force and compares its sign with that of the relative displacement. If the signs are different or if the reaction force is zero, the compliance is switched off. If separation distance alone is used to switch the compliance on and off, then it is possible under some circumstances for the reaction force to become positive [Luo and Hanagud 1998], which is not physically possible.

A second similar model is shown in Figure 4.7 with pulse excitation instead of sinusoidal excitation. These two models produce output at only one frequency and so two further models were created with swept frequency excitation.

Figure 4.8 shows the model with sine sweep excitation (a block provided by Simulink). The output shown is in the form of current root mean square (rms) values to reduce the amount of data provided and to produce a displacement response curve. The conversion to rms is by squaring, filtering (using a low pass Butterworth filter) and calculating the square root.

True rms values are calculated using the following equation:

$$\sqrt{\lim_{T \to \infty} \frac{1}{T} \int_0^T x(t)^2 \, dt}$$

This is not practical for a nonlinear system so the current rms equation is used instead:

$$\sqrt{\frac{1}{T} \int_0^T x(t)^2 \, dt}$$

with the integrator replaced by a low pass filter where the cut off frequency (10rad/s) replaces $1/T$. The result is similar to some rms detectors [McConnell 1995, Randall 1977].

Here three outputs are provided, x_1, x_2 and reaction force and all are converted to rms values by the same method.

Simulink does not provide a pulse sweep excitation block and so the pulse excitation model (Figure 4.9) has a section to create one from a sine sweep signal. The signal is converted to a square wave with range 0 to 1 by a backlash block

followed by a sign block. Figure 4.10 indicates how the square wave is converted to pulses by the use of a delay block. The output from this section is divided by 2 to give unit pulses at a frequency of one pulse for each cycle of the sine sweep signal. The pulses have a length of 0.01s.

These two models required careful choice of the time range for the speed sweep. If the sweep was too fast, the behaviour of interest would be missed. If the sweep was too slow, the PC memory would be swamped with a very large number of data points giving slow running and difficulties with graphs.

One advantage of this modelling method over the PGF method is that the simulation runs like an experiment and it is possible to sweep up and down through the frequencies. The PGF method calculates each displacement value at an individual frequency without reference to previous frequencies.
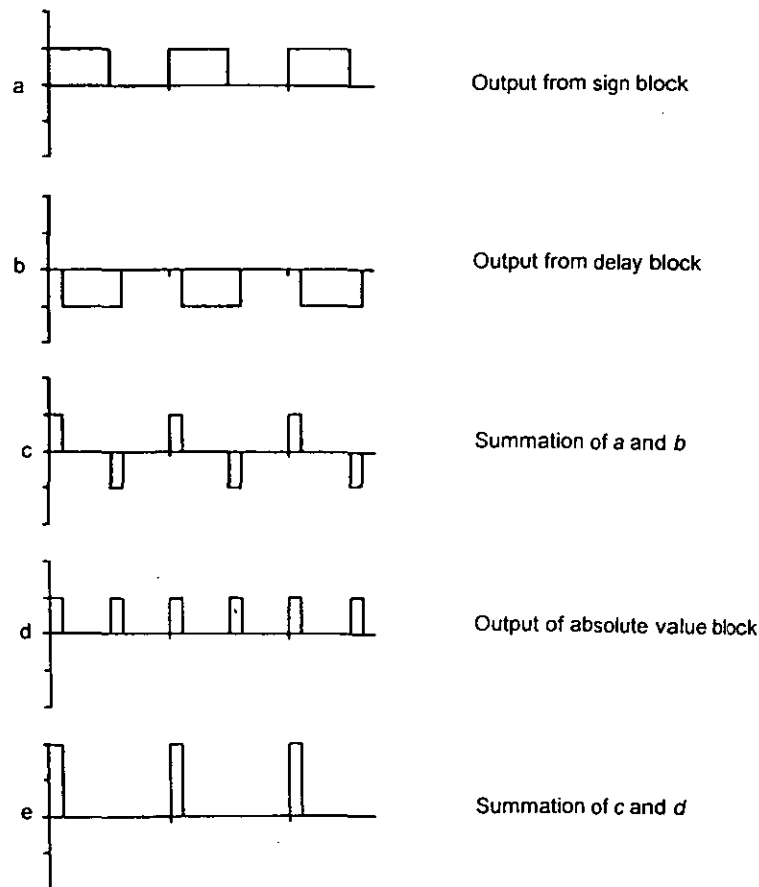

**Figure 4.10** Development of pulse sweep signal

4.4 Results from the two degree of freedom system with compliance

For this model the same masses and stiffnesses were used as in the PGF method (m_1=0.125kg, m_2=0.094kg, k_1=135N/m, k_2=128Nm). The gap was set to 0.001m, the stiffness of the compliance (k_3) to 100000N/m and all the damping values to 0.1 Ns/m. Vibrating system models in Simulink require some damping to avoid very large displacements at resonance. Some adjustment to the excitation magnitudes was necessary to achieve vibro-impact behaviour so comparison of amplitude values with the PGF results is not possible.

Using sine sweep excitation (Figures 4.11 to 4.13), the 2-DOF system shows the same type of behaviour that was also shown by the PGF model. The first peak at 4.66Hz has a greater amplitude and is more symmetrical in form than the second peak at 10.61Hz. The second peak has the backbone curve shape of Figure 3.3. Figure 4.12 shows the displacement response of the passive mass (note that the passive mass starting position is at 1mm). The passive mass has no motion until the active mass begins to strike it. The reaction force (Figure 4.13) shows that the force between the two masses is greatest for the second resonance. At the first resonance the force reduces which is expected in linear vibrating systems at resonance.
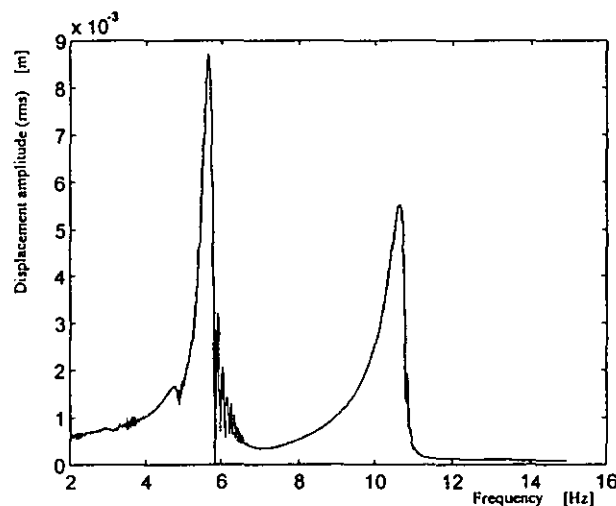
Figure 4.11 Displacement frequency response of active mass to sinusoidal excitation
– up sweep
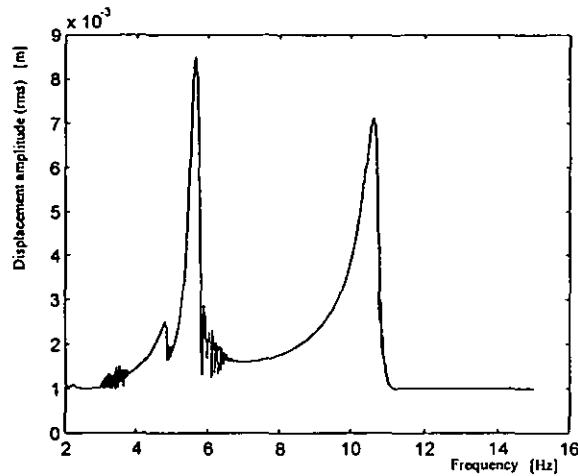
Figure 4.12 Displacement frequency response of passive mass to sinusoidal excitation
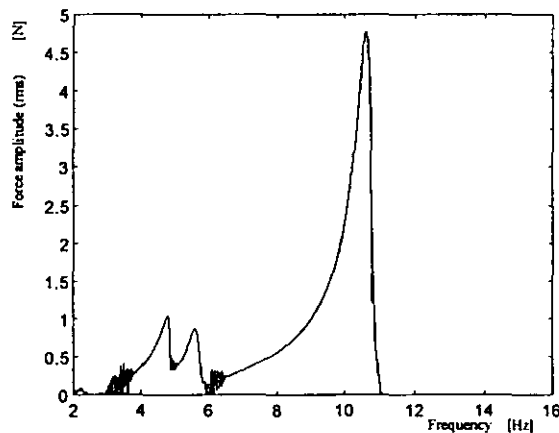
– up sweep

Figure 4.13 Displacement frequency response of reaction force between the two masses

– up sweep

When the frequencies are swept down (Figures 4.14 and 4.15) the second peak does not occur. This is particularly obvious when looking at the response of the passive mass. The second resonance is therefore nonlinear while the first is linear.

The patches of noise may be due to transients if the sweep speed is not sufficiently slow or may be due to chaotic behaviour at the points where impacts start of finish.
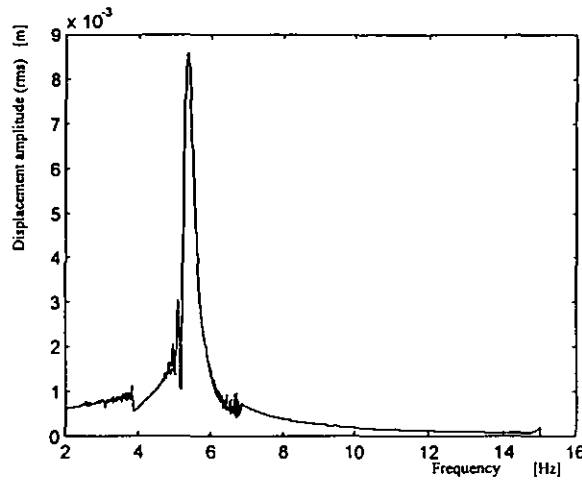
Figure 4.14 Displacement frequency response of active mass under sinusoidal excitation
– down sweep

Figure 4.15 Displacement frequency response of passive mass under sinusoidal excitation
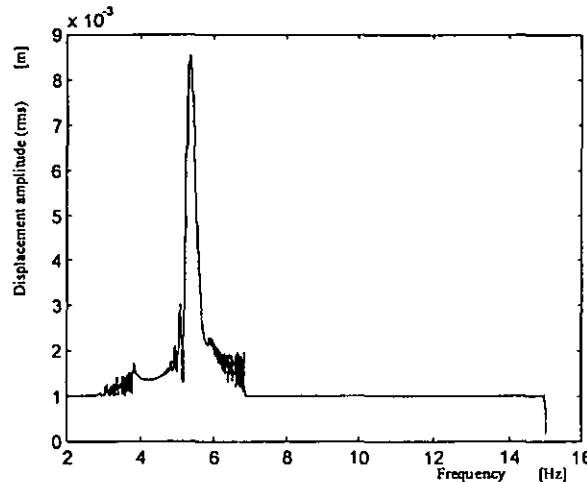– down sweep

Similar behaviour is obtained from the model with pulse excitation. For a sweep up through the frequencies (Figures 4.16 and 4.17) the two peaks are at 5.66Hz and 10.72Hz. The greater levels of noise in the results are due to errors in the integration process caused by the use of pulses. The small peak at low frequencies is a subharmonic response, an additional solution which is caused by the nonlinear nature of the system and is especially apparent with pulse excitation. Figures 4.18 and 4.19 show the responses when the frequencies are swept down. Again no second resonance occurs. The small peak at high frequency is probably due to errors at the start up of the simulation.
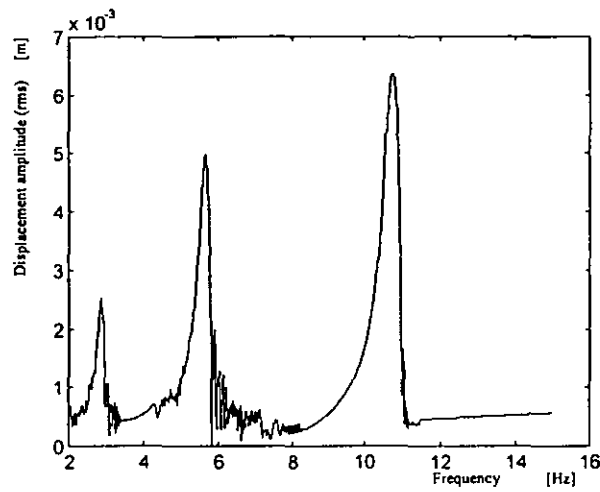
Fig 4.16 Displacement frequency response of active mass under pulse excitation – up sweep
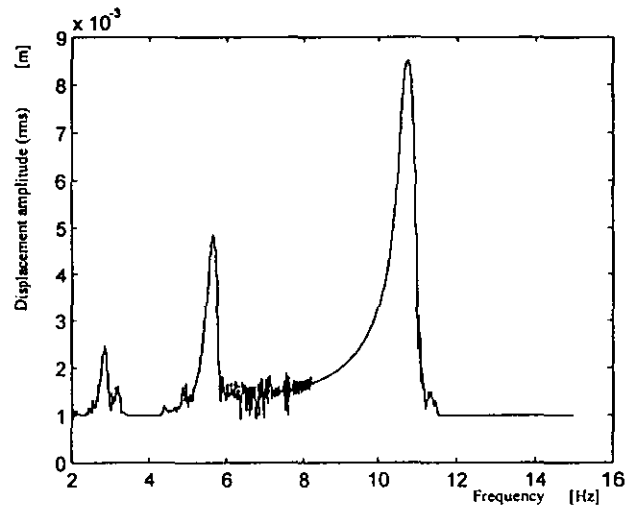
Fig 4.17 Displacement frequency response of passive mass under pulse excitation – up sweep
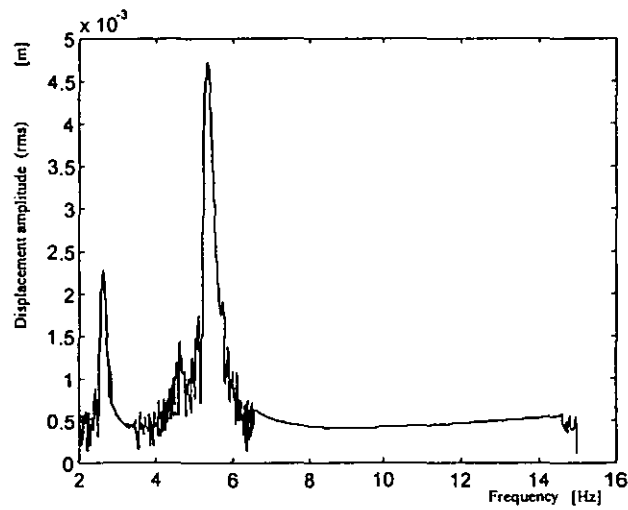
Fig 4.18 Displacement frequency response of active mass under pulse excitation – down sweep
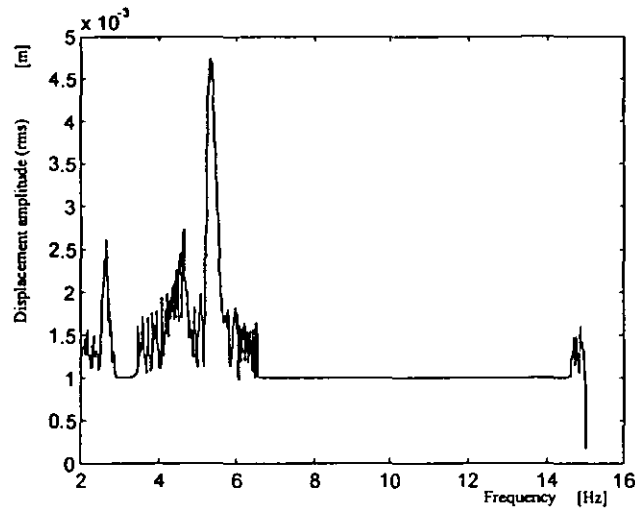
Figure 4.19 Displacement frequency response of passive mass under pulse excitation – down sweep

In the time domain, the behaviour of the system under both types of excitation is similar. At the first resonance (Figures 4.20 and 4.21) the behaviour shows a grazing resonance. The second resonance is a clapping resonance (Figures 4.22 and 4.23). Generally the results are similar to the results obtained by the PGF method.
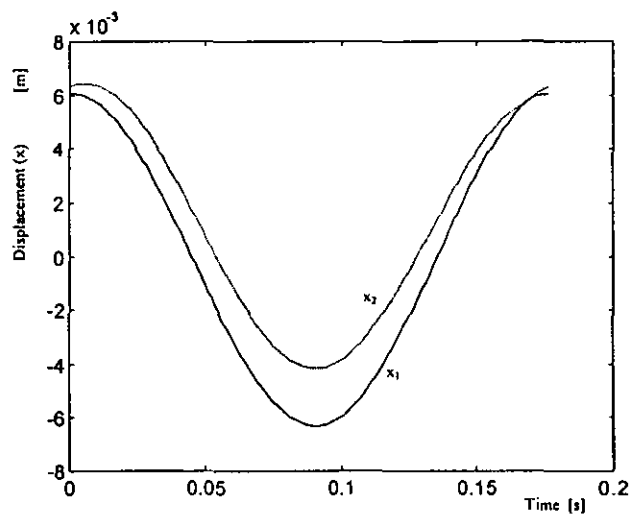
Figure 4.20 Grazing resonance at f = 4.66Hz sinusoidal excitation
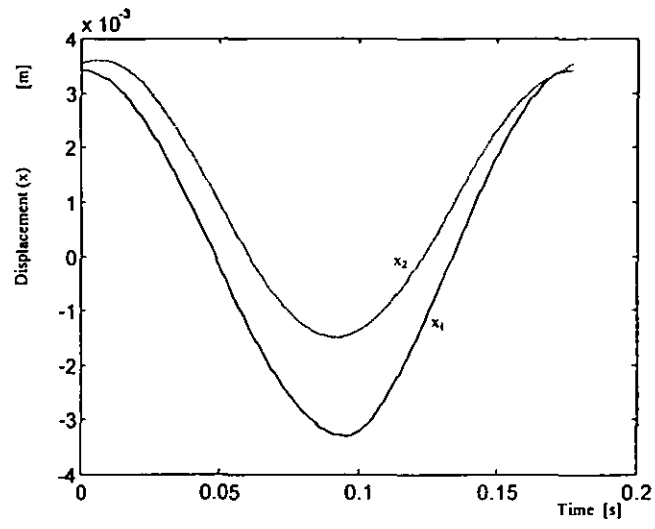
Figure 4.21 Grazing resonance at f = 5.66Hz pulse excitation
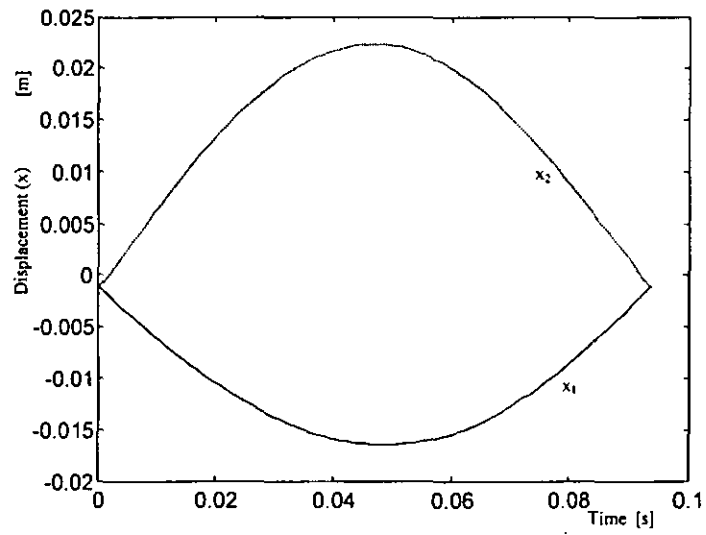
Figure 4.22 Clapping resonance at f = 10.61Hz sinusoidal excitation
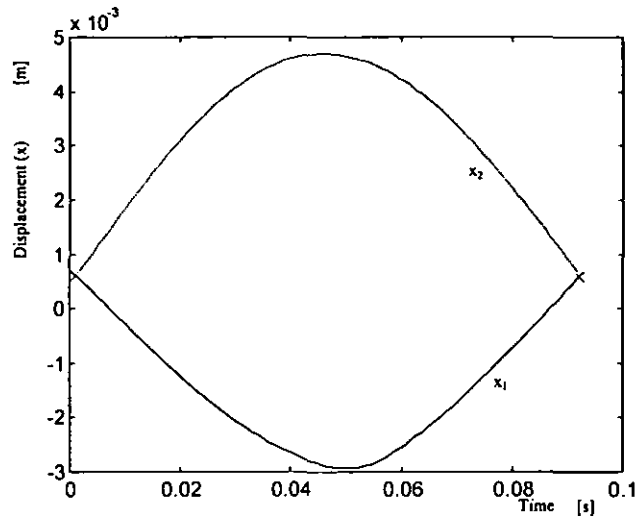
Figure 4.23 Clapping resonance at f = 10.72Hz pulse excitation

However when comparing the clapping resonance result for impulse excitation with the PGF result when $R = 0.7$ (Figure 3.11), the shape in the time domain is not the same, probably because the pulses in the simulation are not narrow enough to model impact adequately. Narrowing the pulses would increase the noise level as more errors in the integration would occur.

4.5 Further models
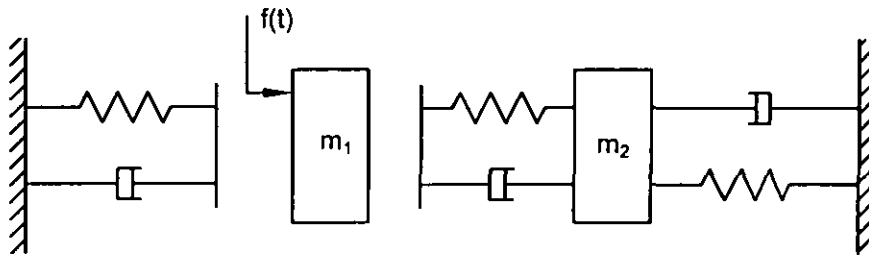
Figure 4.24 2-DOF system with loose mass

It is straightforward to add extra features to the models developed in Simulink by adding further blocks. An example is shown in Figure 4.24 and the Simulink model is in Figure 4.25. This model is closer to a real hammer drill than those studied so far, since the active mass is now not always in contact with the spring and damper representing the buffer. The identical method for applying compliances to the impacting surfaces is now applied to switch the buffer spring and damper on and

off. The initial gap between the active mass and its spring and damper was set to 1mm. The other parameters remained the same as the previous models. Figures 4.26 and 4.27 show the displacement response as the frequencies are swept up while Figures 4.28 and 4.29 show the response for the sweep down.
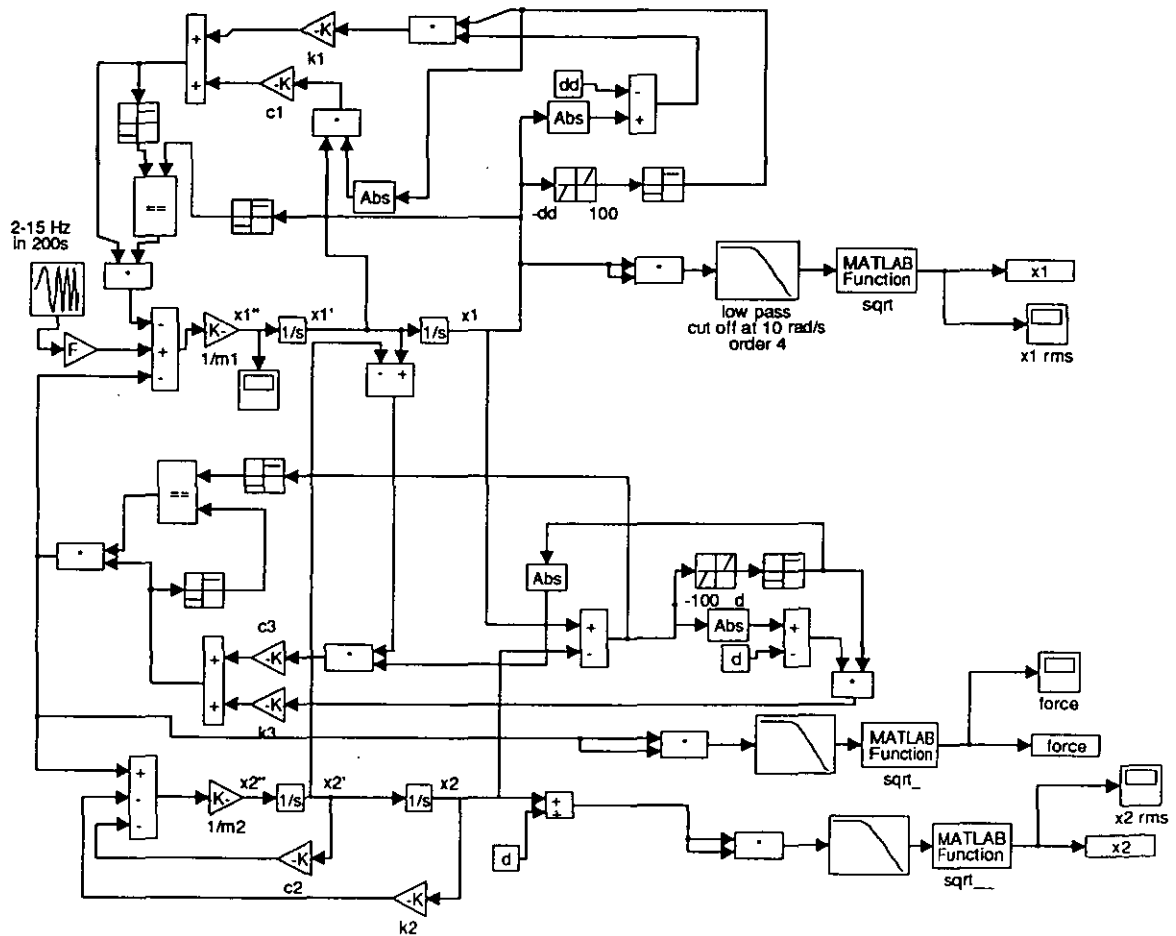
Figure 4.25 Simulink 2-DOF model with loose mass
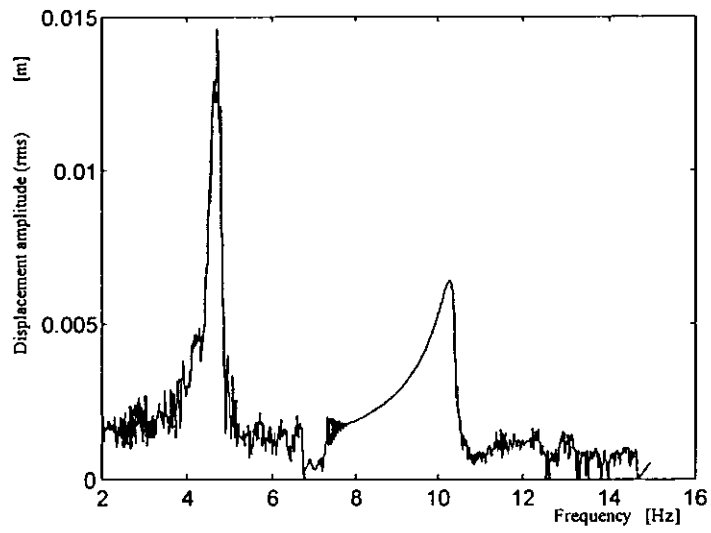
Fig 4.26 Displacement frequency response of active mass (loose mass model) – up sweep
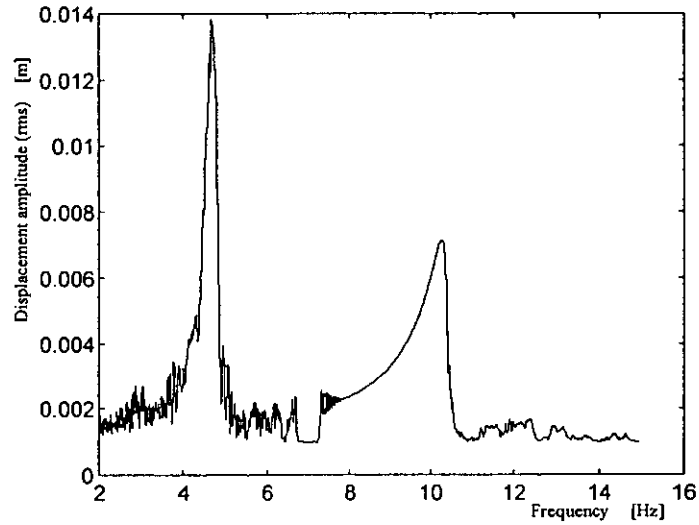
Fig 4.27 Displacement frequency response of passive mass (loose mass model) – up sweep
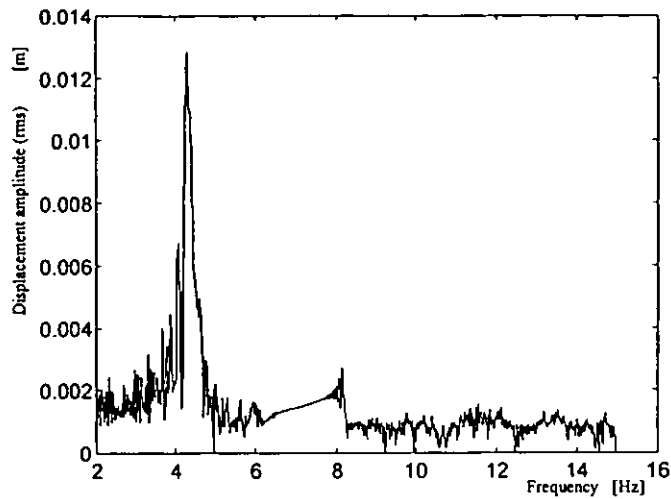
Figure 4.28 Displacement frequency response of active mass (loose mass model)
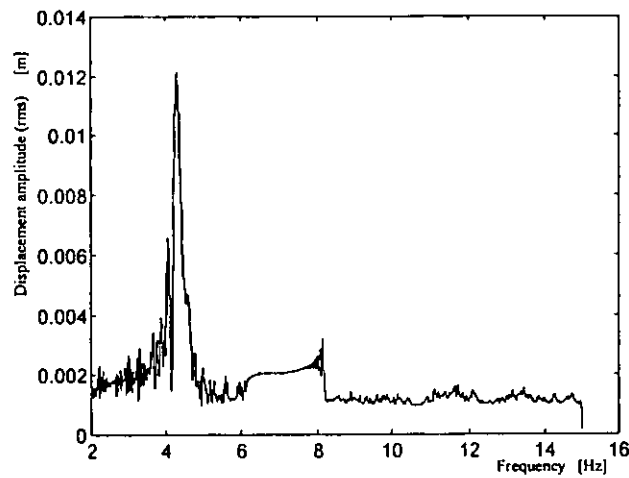
– down sweep

Figure 4.29 Displacement frequency response of passive mass (loose mass model)

– down sweep

Again there are two peaks, one at 4.73Hz and one at 10.27Hz. The second resonance is nonlinear in form and occurs with reduced amplitude in the sweep down. If the active system is linearised, the linearised stiffness would be less than the system with the mass attached to the spring due to the presence of the gap. This causes the reduction in resonance frequency for the first resonance. Unlike the previous models there is a peak in the reaction force during the first resonance (Figure 4.30).
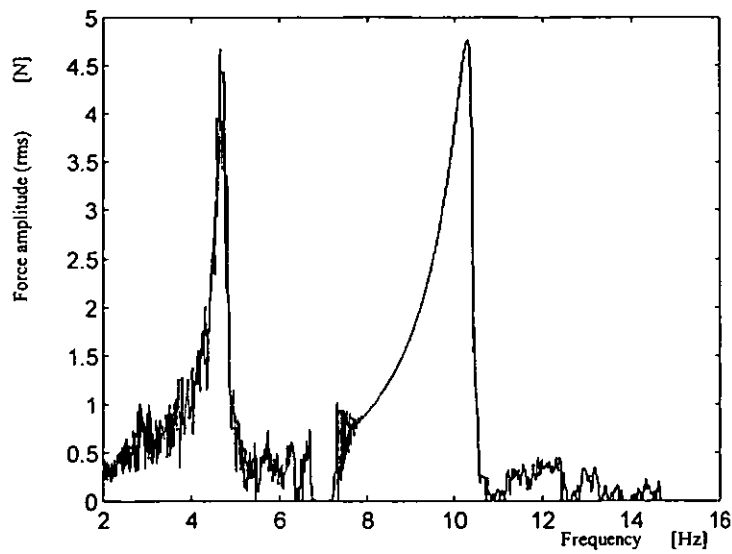
Figure 4.30 Frequency response of reaction force (loose mass model) – up sweep

These Simulink models compare well with the behaviour of the PGF model although amplitudes cannot be compared due to the modified excitation amplitude. Adding extra features has been shown to be straightforward but with some increase in noise levels. Results from both the PGF method and Simulink models will be compared with the results from a two mass test rig.

5 EXPERIMENTAL STUDY OF A TWO MASS VIBRO-IMPACT SYSTEM

An experimental study was carried out to obtain a better understanding of the impact unit behaviour and to provide data for comparison with the analytical and numerical models. The initial experimental work was carried out on a two mass test rig described here and measurements were also carried out on a test rig based on an actual hammer drill, explained in Chapter 6.

5.1 Two mass experiment

5.1.1 Test rig development

The experimental rig consisted of a pair of masses, each attached to a strip of spring steel as shown in Figure 5.1. The masses were made from hexagonal steel bar with domed contact surfaces to obtain point contact.

The steel strips acted as cantilevered beams and were attached to a steel block such that the motion of the masses was horizontal. Washers were placed between the strips and the block to enable the gap to be adjusted. The whole assembly was clamped to a table isolated from external vibrations.
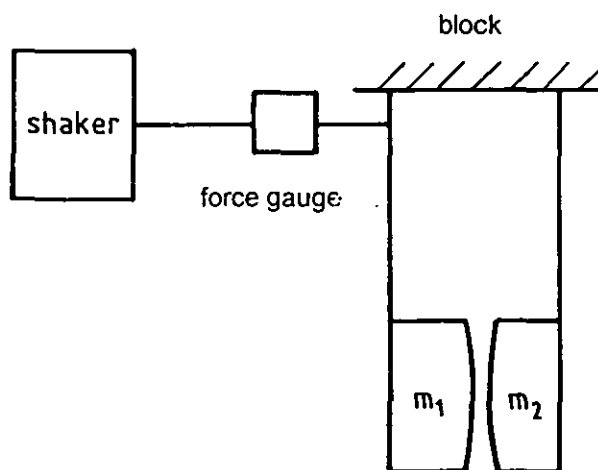
Figure 5.1 Diagram of the two mass experimental rig

Excitation was initially provided by a small electrodynamic shaker (Ling 101 with amplifier TPO20) fitted with a rod which was pressed against one of the beams close to the block. Attaching the end of the rod to the beam was not possible since the rod would bend due to the fact that the beam moved in an arc and not in a straight line. Applying the excitation to a mass was not possible because of the large displacements at resonance. Sinusoidal excitation was used since impact excitation was found to be difficult to maintain and damaged the shaker.

Since the displacements and accelerations were large, difficulties with using accelerometers were encountered because they overloaded the charge amplifiers. It is possible that this could be overcome by the use of accelerometers with lower sensitivities. A laser vibrometer which measured velocity (Polytec OFV 302 with controller OFV 3000 described in section 6.2) was then employed. A force gauge (Brüel&Kjær type 8200 with charge amplifier type 2635) was also used and this was connected to the beam end of the shaker rod. Attached to the force gauge was a small piece of aluminium used as a contact surface for the rod against the beam. The diameter of the rod end contact area was approximately 3mm which produced a small variation in contact point location. It would have been better to use a point contact stinger and put the force gauge closer to the shaker as the mass of a force gauge can affect the results, especially when attached to a light structure like this experimental rig. Maia and Silva [1997] suggest putting the force gauge next to the shaker as a possible arrangement but Ewins [1984] considered this to be a poor arrangement.

The data from the force gauge and the vibrometer were acquired and analysed in a Signal Processing Systems SPS390 FFT analyser. After carrying out trials with different methods of data collection, including random excitation (from the analyser) and automatic sine sweep (from both the analyser and a Hewlett Packard HP3330A automatic synthesizer), manual sine sweep was chosen as the most informative method of showing system behaviour. The two mass rig proved to have very long transients, sometimes as long as several seconds, so that more automated methods could only capture the transients since these methods acquired data or swept the excitation over periods of time that were too short. The spectrum

from the force gauge data was used to obtain the excitation frequency. The sine frequency was set manually to a given value and measurements were taken after allowing any transients to decay. The next frequency was then set and the process repeated. Both up and down sweeps were carried out. As only one laser vibrometer was available and the analyser had only two input channels, the behaviour of each mass was studied separately. Within the analyser, the data were integrated to provide displacement behaviour rather than velocity and displayed as a displacement spectrum (consisting of the magnitude of the signal following a fast Fourier transform). These spectra were further analysed in Matlab to produce the graphs shown in this thesis. The programs developed for this are given in Appendix A.1.

The general behaviour of the experimental rig is now described. During the up-sweep phase, initially there were no impacts, impacts then commenced and the motion of both masses increased until the first (grazing) resonance was reached at approximately 5.6 Hz. The two masses were moving in phase with such violence at this point that no measurements were taken. After passing this resonance, the displacement amplitude of the motion and the noise of the impacts declined and then increased to reach the second (clapping) resonance where the two masses moved out of phase. As the clapping resonance was reached the impacts became louder until the impacts suddenly ceased.

When the excitation frequency was swept downwards, there was a long period without impacts until, at a frequency lower than the clapping resonance, impacts commenced. The displacement amplitude then increased until the grazing resonance was reached at about the same frequency as before. As the frequency was decreased further, the displacement amplitude decreased and impacts ceased. The clapping resonance was completely absent. This indicates that the first resonance was linear while the second resonance was nonlinear.

Difficulties were encountered with repeatability of the test rig behaviour. This was probably due to several factors such as the positioning of the shaker, the force which the shaker exerted against the beam and the amplitude of the forcing

function. The grazing resonance being linear was not affected by the amplitude variation, it consistently occurred at approximately 5.6 Hz. However, the clapping resonance was affected, especially the maximum frequency at which impacts occurred.

The nature of the impact patterns was studied using electrical contact so that when an impact occurred, the circuit was completed and a spike would appear in the analyser display. The circuit is described in section 5.2.3. At $f = 5.61$Hz irregular impacts occur (Figure 5.2) while in Figure 5.3, at $f = 7.49$Hz, one impact per cycle occurs (checked by averaging the time difference between the peaks using a Matlab program timeav.m, given in Appendix A.1). There was some mains noise present which was removed by a Kemo VBF8 analogue filter (48dB cut off) set up as a 30Hz low pass filter. The ringing after each impact may be due to mechanical chatter or the electrical circuit, but as the main impacts stand out clearly the side peaks may be disregarded.
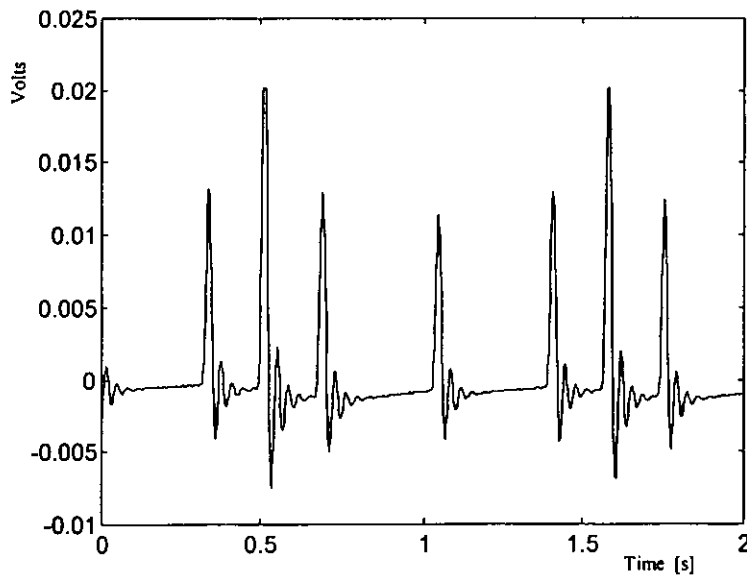
Figure 5.2 Signal from electrical impact detection circuit at 5.61Hz
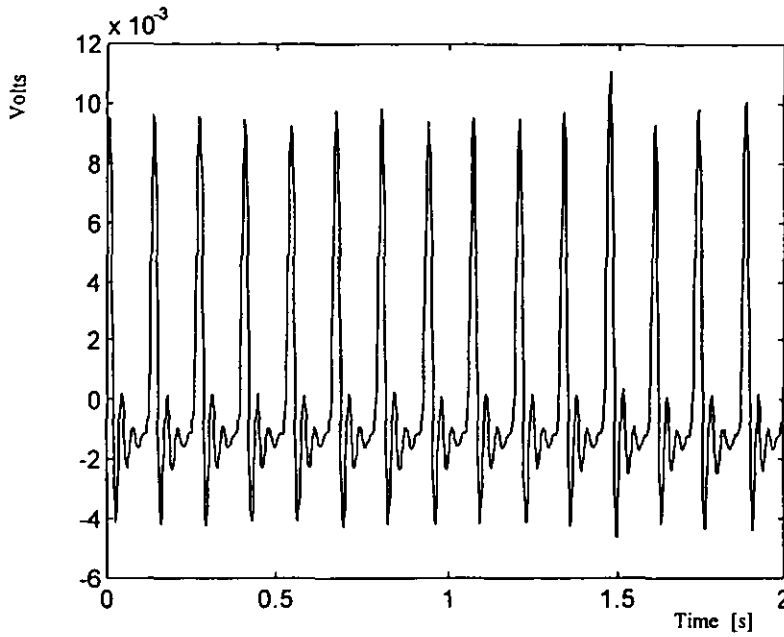
Figure 5.3 Signal from electrical impact detection circuit at 7.49Hz

The sweep experiments were then repeated with a large shaker (Ling V406 with amplifier PA100) as the small shaker was not able to provide enough power for a good comparison with the analytical studies in the region of the clapping resonance. Similar difficulties were encountered with the positioning of the shaker and with consistency of the amplitude setting. As the large shaker had a higher power level than the small shaker, care had to be taken with the amplitude setting on the power amplifier as at high settings the amplitude of the shaker's motion became excessive and contact with the beam would be lost for part of the excitation cycle. A maximum frequency of 11.5 Hz was achieved for the second resonance but when the spectra were collected in a repeat test the maximum frequency was only 9.5 Hz, suggesting that the clapping resonance was very sensitive to small changes in excitation amplitude.

One additional problem was that the shaker contained a powerful permanent magnet and this was seen to cause some attraction between the two masses. As a consequence when the impact forces were low, the two masses stuck together on some occasions with an adverse effect on the results.

5.1.2 Results

The results are shown in two forms, as a waterfall plot displaying all the spectra, and as a displacement frequency response created by taking the peak value from each displacement spectrum and plotting this against the excitation frequency used for that spectrum. The graphs were created using the Matlab programs sineswf.m, sinesw.m and sinesw3.m, given in Appendix A.1.

Figures 5.4 and 5.5 are the upsweep results for the excited system, Figures 5.6 and 5.7 are the upsweep results for the passive system, Figures 5.8 and 5.9 are the downsweep results for the excited system and Figures 5.10 and 5.11 are the downsweep results for the passive system. It is seen that the first peak is larger than the second peak and that at the antiresonance between the two resonances the passive mass has the greater amplitude. In the waterfall plots the peaks at very low frequencies are due to the analyser's simple method of integration. The analyser divides each value by $2\pi f$ where f is the frequency at that point. Thus when f is close to zero the displacement amplitude is large. When these sets of data were collected, the large shaker was used to provide the excitation.
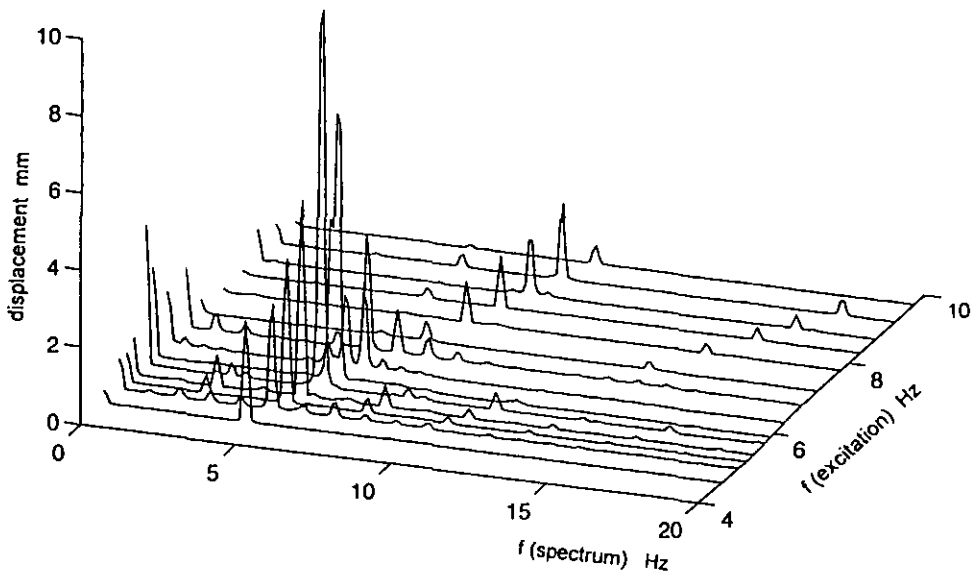
Figure 5.4 Waterfall plot for active system – up sweep
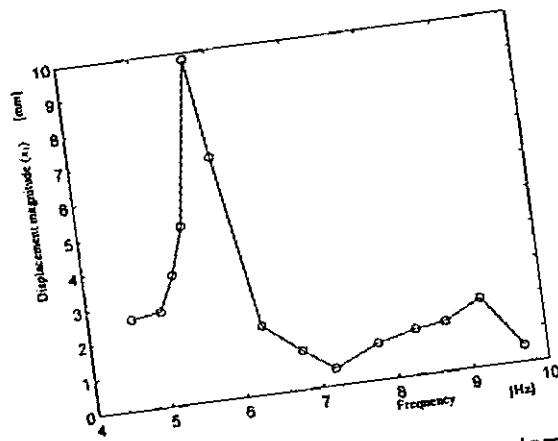
Figure 5.5 Displacement response of active system - up sweep
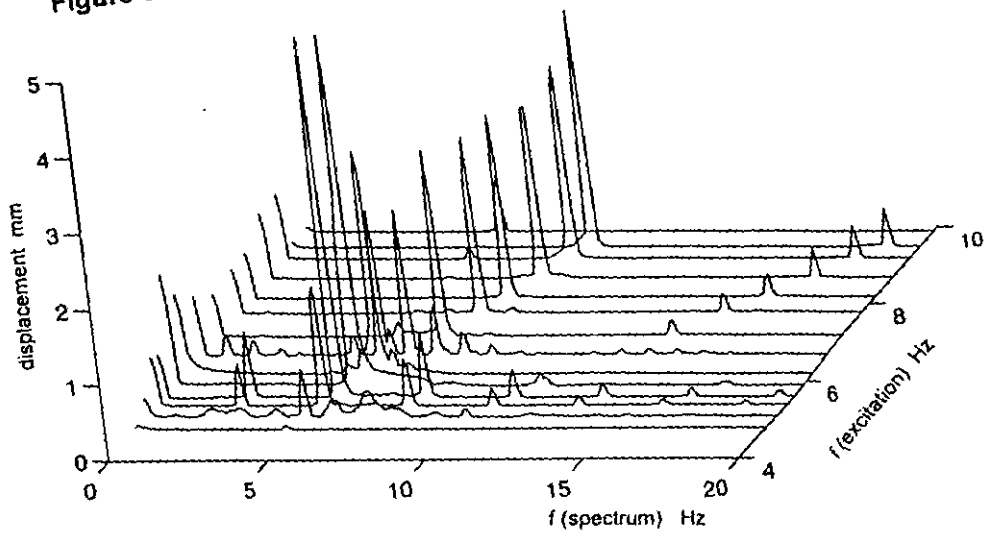
Figure 5.6 Waterfall plot for passive system – up sweep
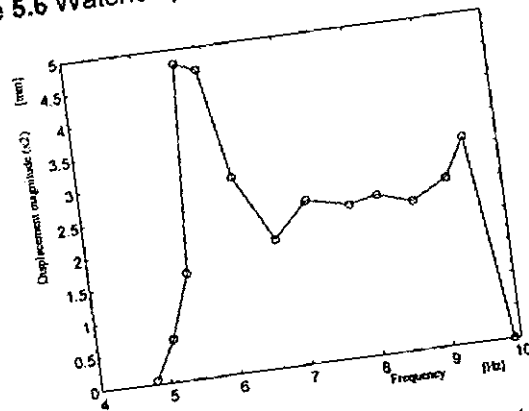
Figure 5.7 Displacement response of passive system - up sweep
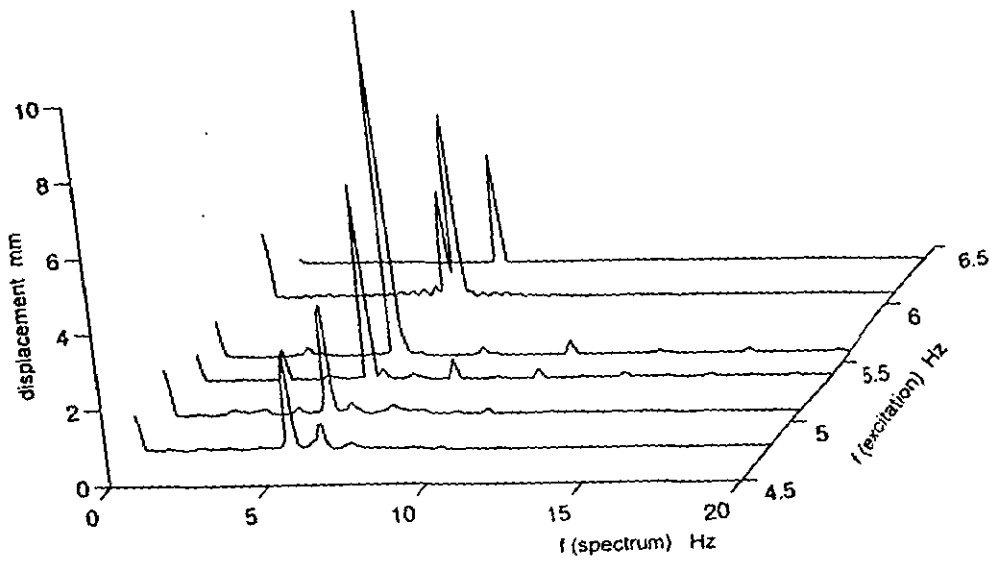
Figure 5.8 Waterfall plot for active system – down sweep
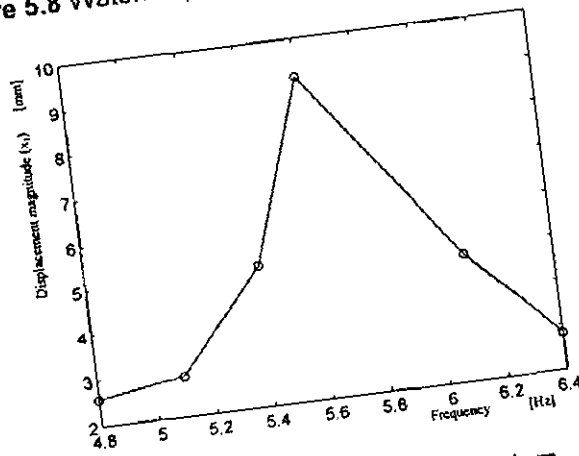
Figure 5.9 Displacement response of active system - down sweep
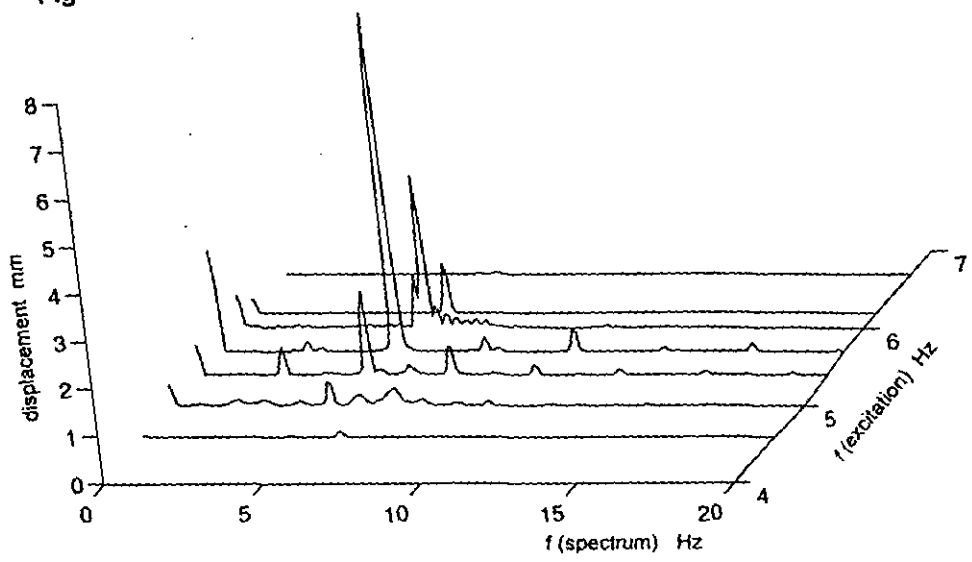
Figure 5.10 Waterfall plot for passive system – down sweep
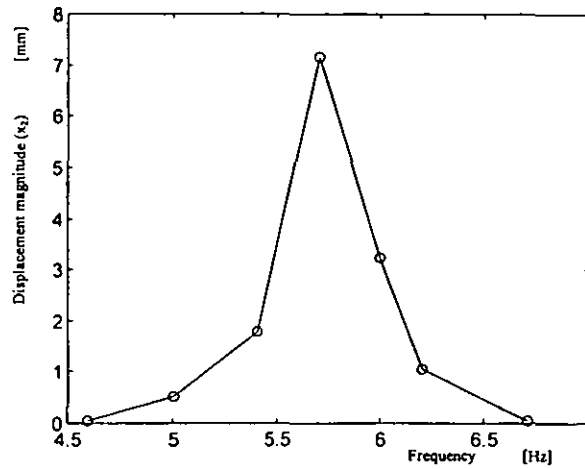
Figure 5.11 Displacement response of passive system (down sweep)

5.1.3 Determination of system parameters

Data from the experiments including information on the masses, stiffnesses and forcing function were necessary to allow comparison with the analytical and numerical models. The amplitude of the forcing function is difficult to determine since during a sweep, even if the amplitude setting did not change, the force applied to the structure varied as seen in Figure 5.12. This variation is due to feedback from the structure, which is especially noticeable at resonance when the force level required drops. The variation may also be due to the low frequencies used so that the shaker may not be behaving linearly [McConnell 1995, Ewins 1984, Maia and Silva 1997]. Therefore for this study the amplitude of the forcing function was not considered.
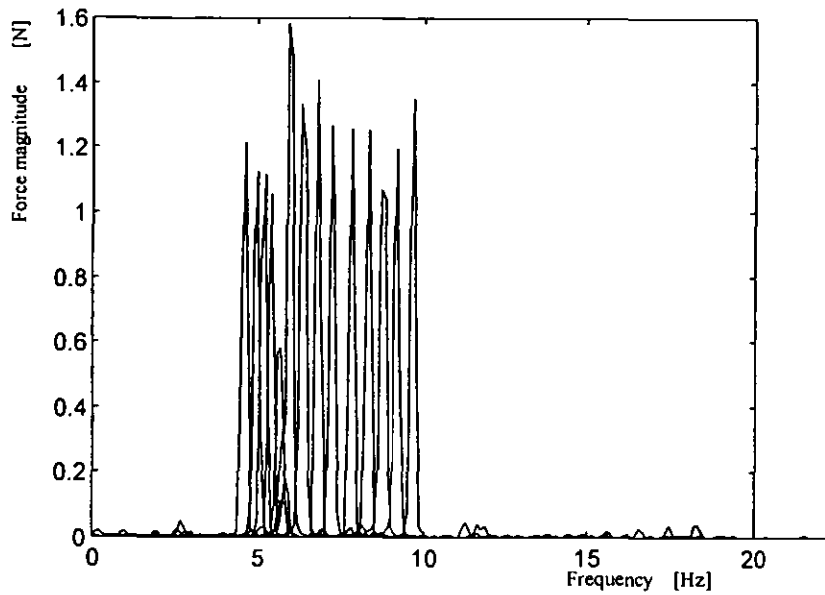
Figure 5.12 Typical force spectrum (up sweep)

The natural frequencies for the two systems were measured. One of the masses was removed so that no impacts occurred. The system was excited with random excitation from the analyser and a transfer function was calculated by the analyser from data collected by the force gauge and the laser vibrometer. The magnitudes of the transfer functions are shown in Figure 5.13 for the excited system and in Figure 5.15 for the passive system. The damping can be calculated from the Argand diagram [Ewins 1984] but requires at least six clear points on the circle for a good fit. The Argand diagram for the excited system (Figure 5.14) is not a well defined circle and does not have enough points to calculate the damping reliably. The small number of points on the circle and the sharpness of the resonant peak suggest that the damping level is low. This is also evident from the sweep experiments where transients sometimes took several seconds to die away. After taking several measurements and averaging, the natural frequency of the active system had a value of 5.23Hz while that for the passive system was 5.87Hz. For the active system mass of 0.125kg, this gave a beam stiffness of 135N/m. For the passive system mass of 0.094kg, this gave a beam stiffness of 128N/m. The damping in such systems is generally small and was estimated to be 0.1Ns/m for both systems. The gap between the two masses at rest was estimated to be 1mm.
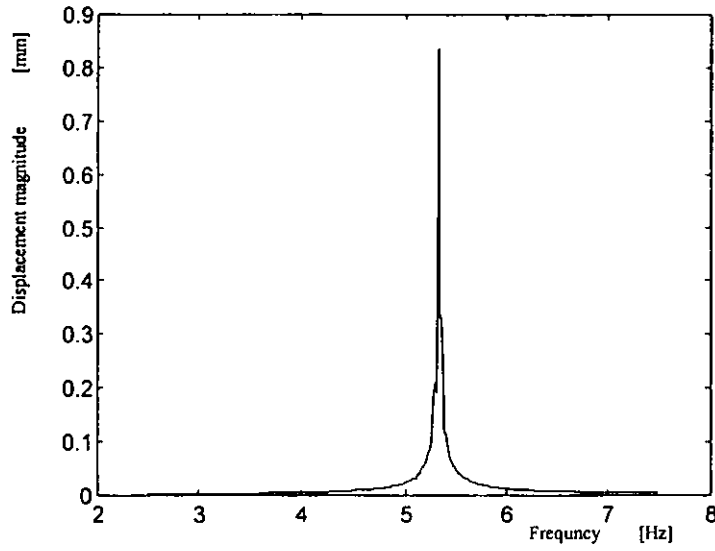
Figure 5.13 Displacement spectrum for the active system
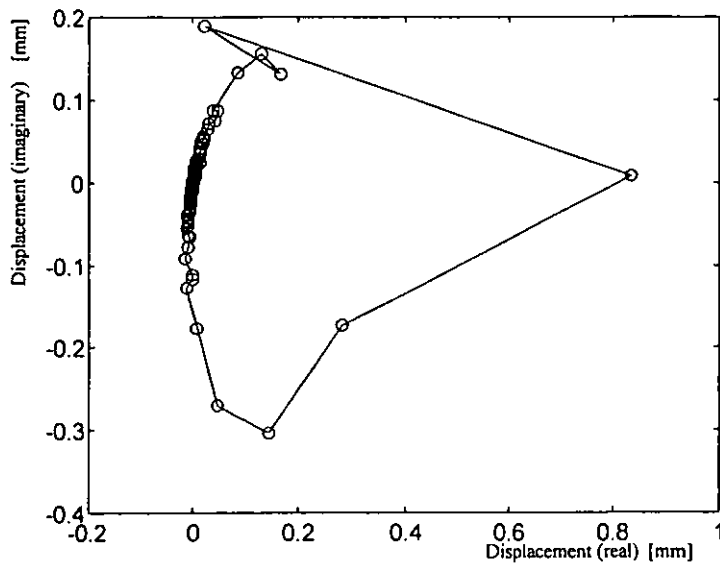
Figure 5.14 Argand diagram for the active system
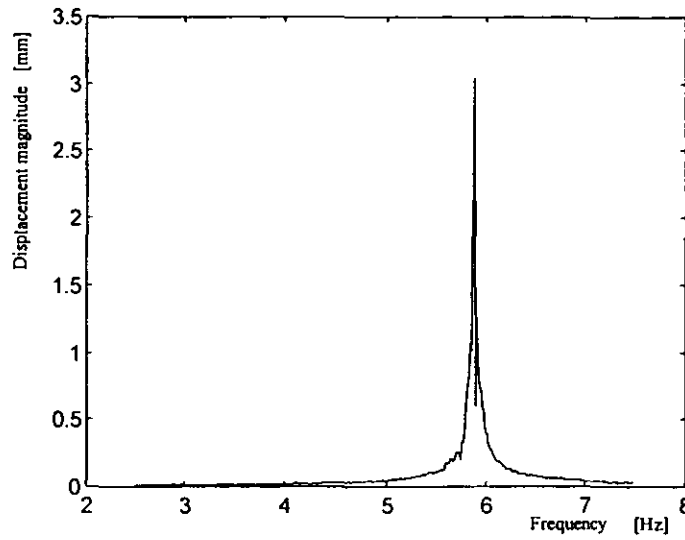
Figure 5.15 Displacement spectrum for the passive system

The beam mounting was not symmetric, as shown in Figure 5.16*b*. This would produce a greater stiffness in one direction than the other, making the spring nonlinear. However, experiments with and without a washer between the beam and the fixed block showed no measureable difference observed in the natural frequency, suggesting that the effect was negligible.
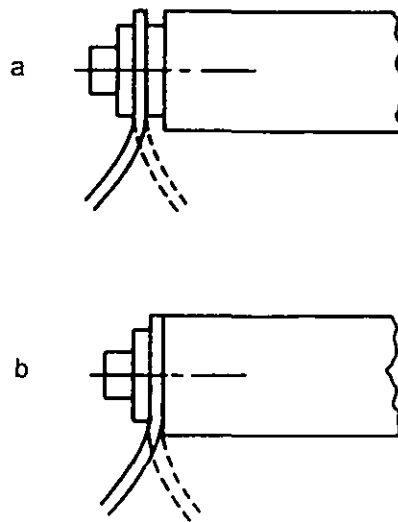
Figure 5.16 The beam mounting methods with and without a washer

5.1.4 Coefficient of restitution

An approximate method was used to measure the coefficient of restitution between the two masses [Goldsmith 1960]. One mass was placed on a sheet of paper on top of a large flat 10kg weight. The paper deadened the impacts between the mass and the weight. A tube was placed over the weight so that the first mass was approximately in the middle and the second mass was dropped from the top of the tube (Figure 5.17). The second mass had a thin wire attached to it so that when impact between the two masses occurred an electrical circuit (identical to the one used to study impact patterns, in section 5.2.1) was completed. The analyser was used to collect the time trace.
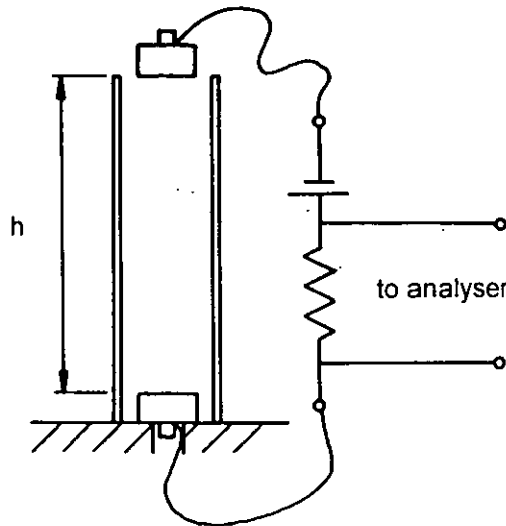
Figure 5.17 Diagram of the coefficient of restitution measurement rig

Drops were made with h = 0.57m and Figure 5.18 shows a typical trace. From these traces it was difficult to measure the time between impacts Δt and there was some variation between runs. The measured average was 0.144s. This average gives a value for the coefficient of restitution of 0.2 using equation 5.2 given below. This is probably too low due to errors in the estimation of Δt and the variation of initial height. Other sources of error are: non-central impact, friction in the pipe, restrictions on the falling mass due to the attached wire, air damping and ideal solid body assumptions.
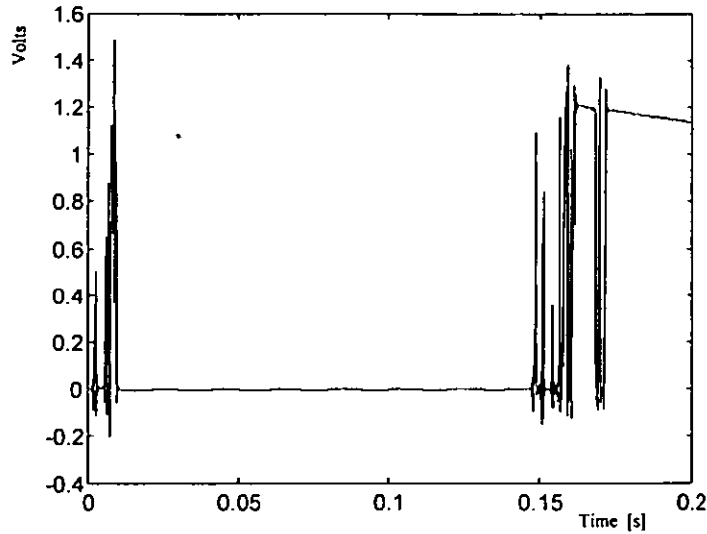
Figure 5.18 Time trace showing first and second impacts, estimated time between impacts: 0.14s

The equation to calculate the coefficient of restitution was developed using the following method.

By conservation of energy if m is the dropped mass, h is the height and v is the velocity of the mass just before impact:

$$\tfrac{1}{2}mv^2 = mgh$$

or:

$$v = \sqrt{2gh}$$

The velocity after impact is:

$$v_a = Rv = R\sqrt{2gh}$$

where R is the coefficient of restitution.

If the maximum height reached after the first impact is x, then by conservation of energy:

$$\tfrac{1}{2}mv_a^2 = \tfrac{1}{2}mR^2 2gh = mgx$$

or

$$R^2 = \frac{x}{h}$$

This equation is often used to measure coefficient of restitution. However, in this experiment the time Δt between the first and second impacts was measured. This is

twice the time that the dropped mass takes from the first impact to reach the height x and we thus have:

$$x = v_a \frac{\Delta t}{2} - \tfrac{1}{2} g \left(\frac{\Delta t}{2} \right)^2 = R\sqrt{2gh}\, \frac{\Delta t}{2} - g \frac{\Delta t^2}{8}$$

Dividing by h gives

$$\frac{x}{h} = R\sqrt{2gh}\, \frac{\Delta t}{2h} - g \frac{\Delta t^2}{8h}$$

$$R^2 = R\Delta t \sqrt{\frac{g}{2h}} - \frac{g\Delta t^2}{8h}$$

$$R^2 - R\Delta t \sqrt{\frac{g}{2h}} + \tfrac{1}{4}\left(\Delta t \sqrt{\frac{g}{2h}} \right)^2 = 0$$

$$\left(R - \frac{\Delta t}{2} \sqrt{\frac{g}{2h}} \right)^2 = 0$$

$$R = \frac{\Delta t}{2} \sqrt{\frac{g}{2h}} \qquad\qquad (5.2)$$

5.2 Comparison with the PGF and Simulink models

Repeatability of measurements from the two mass rig was poor due to variation in the amplitude of the excitation force. However, the experimental results were in qualitative agreement with the analytical and numerical results. It should be noted that the PGF and Simulink models required different levels of excitation amplitude in order to avoid singularities or simply to achieve vibro-impact behaviour.

Generally the Simulink model behaves much more like the experimental system and it shows the same variation with sweeps up and down which is not possible with the idealised PGF model.

The experiment, the PGF model and the Simulink model all show the same general behaviour with two resonances. The grazing resonances all occur at approximately the same frequencies. The clapping resonances are more variable in frequency due to the nonlinear nature of these resonances. It should be noted that the PGF model frequency does not vary with excitation amplitude. The frequency in the Simulink

model varies only slightly. This is due to the dominance of the damping curves in determining resonance frequency rather than the excitation amplitude (section 1.2). The fact that the experimental value was dependant upon excitation amplitude suggests that the experiment has some nonlinear parameters, probably the stiffness and perhaps the damping. This indicates that the backbone curve/calculated response curve for the second resonance has a different formation from the idealised model that was used in the PGF and Simulink studies.

The experimental results have a much lower displacement amplitude at the second resonance than suggested in the models. This may be due to the spring nonlinearities or additional features not accounted for in the models. The loudness of the impacts increased as the second resonance was approached, which would agree with an increase in impulse value between the two masses as shown by the graphs for J (Figures 3.4 and 3.10).

6 DEVELOPMENT OF AN EXPERIMENTAL HAMMER DRILL RIG

In order to obtain experimental data that can be used directly in hammer drill development, it is necessary to take measurements on a test rig that is similar to an actual hammer drill. The design of an experimental hammer drill rig is described, together with measurements taken from the impact unit.

6.1 Rig design

The hammer drill used as the basis of this test rig was a Hilti TE74, the impact unit mechanism of which was discussed in section 1.3. The impact unit is located within a tight fitting tube which can rotate for drilling or be held stationary for chiselling. This tube is surrounded by seals, springs, bearings and a clutch mechanism and all the parts are located within the outer casing of the drill. To take measurements from this drill it was decided to use it in chiselling mode only (so that the inner tube does not rotate). When measuring the vibration levels at the handle of a hammer drill, it is usual to drill into concrete according to BS EN 28662-3:1995. Larger devices are operated against a damper specified in the same British Standard. Drilling into concrete causes the destruction of the concrete and the whole device will move downwards which could confuse some types of measurement. Operating the hammer drill against a damper would produce results with greater repeatability without the whole body motion. Within the inner tube, there is a lack of space for contacting methods of measurement such as accelerometers to be attached to the moving parts. Strain gauges could be used but their wires might be trapped in the mechanism or suffer fatigue failure due to the rapid motion of the parts. The remaining options are telemetry or a non-contacting optical method.

Figure 6.1 Overall view of experimental hammer drill rig (the red glow in the lower acrylic window is due to the laser beam reflecting off the intermediate piston)
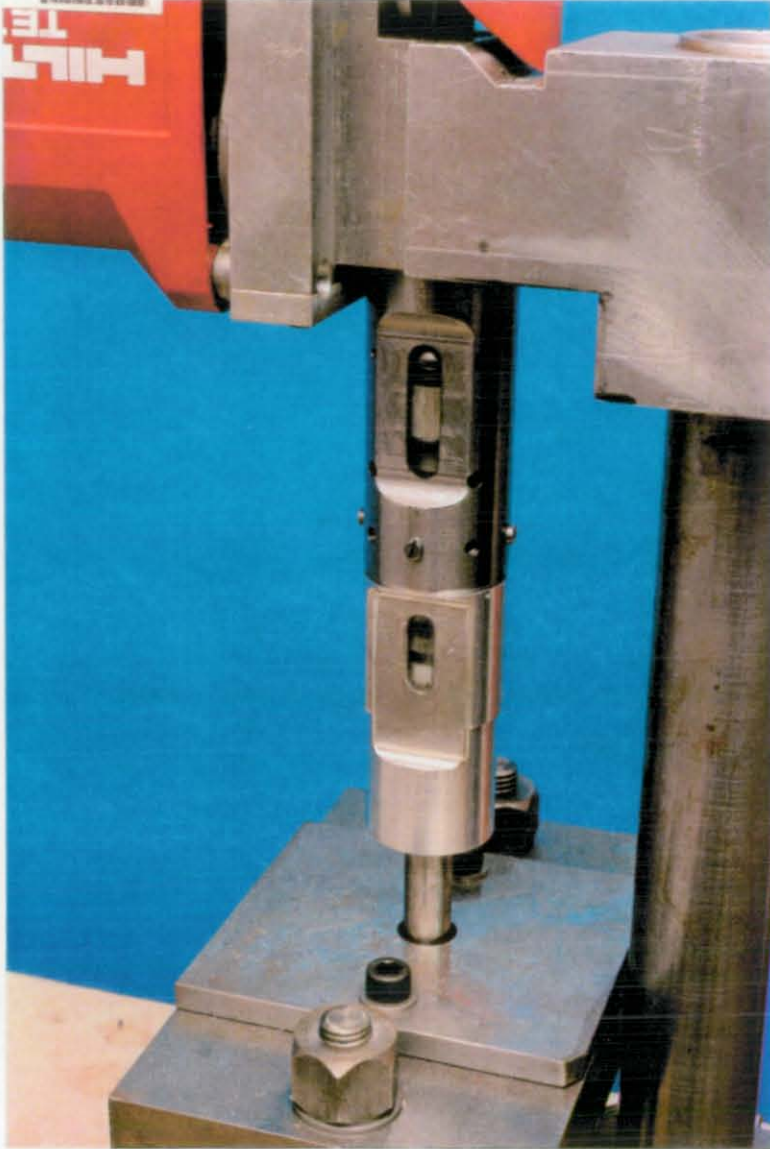
Figure 6.2 Close up of tube – the striker can be seen through the upper window and the intermediate piston through the lower window

Veluswamy and Crossley [1975] used an impacting device with an internal accelerometer. In the case of a hammer drill this would require the use of internal parts specially modified to take such an accelerometer and the use of telemetry. Optical methods require optical access. It was decided not to machine holes into the original inner tube because the thin tube wall made it difficult to attach acrylic windows. The presence of the various components surrounding the impact unit also made optical access difficult. The section of the drill containing the impact unit was therefore replaced by a tube with acrylic windows to allow optical access without loss of pressure (Figures 6.1 and 6.2). This tube was attached to the rest of the drill so that the original excitation mechanism was retained. The tube was bored to the same internal diameter as the original machine so that the original impact unit parts could be used. The tube was made in two parts for ease of assembly. Initially both parts of the tube were made from aluminium. However, friction between the striker O-rings and the aluminium bore prevented the striker from moving. The upper part of the tube containing the piston and striker was then replaced with mild steel which could be honed to provide the right degree of friction and gas sealing.

The damper was also designed in accordance with BS EN 28662-3:1995. It consists of a hardened steel tube containing approximately 11000 4mm diameter ball bearings. The damper was attached to a large concrete block (also was used for whole drill experiments as specified in the same standard) To prevent the ball bearings embedding into the concrete, a hardened steel disk was used as the base of the damper. A second hardened steel disk was used as the contact surface between the drill bit and the balls. The drill bit was a case hardened steel rod with spherical ends. The drill bit passed through a brass bush. A steel column was used to support the drill and to prevent rotation during measurements. The modified drill weighed 8.4kg while the original drill weighed 7.9kg.

A check of the experimental rig behaviour compared to the original machine was made by taking measurements using an accelerometer (B&K type 4367) fitted to the main handle of the drill and comparing these with measurements taken (at the same point) when drilling with the original drill into concrete. The two sets of

results are in Figures 6.3 & 6.4. It can be seen that the experimental rig has lower acceleration amplitude and an additional 5th resonance. Ideally, an additional experiment would include testing the original drill on the damper. However as this would require modifications to the drill (to remove the hardened steel lugs used to provide orientation for the drill bits in the drill holder, and as means of transferring the rotation to the drill bit), this experiment was not carried out.
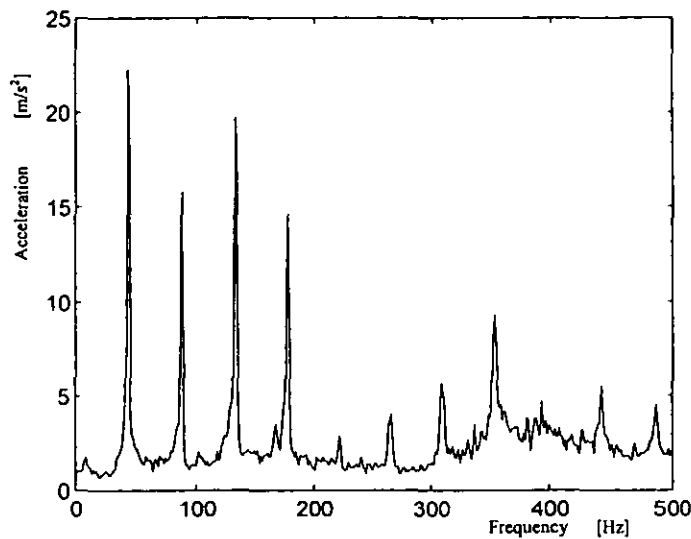
Figure 6.3 Acceleration frequency spectrum of hammer drill drilling into concrete
– accelerometer on main handle
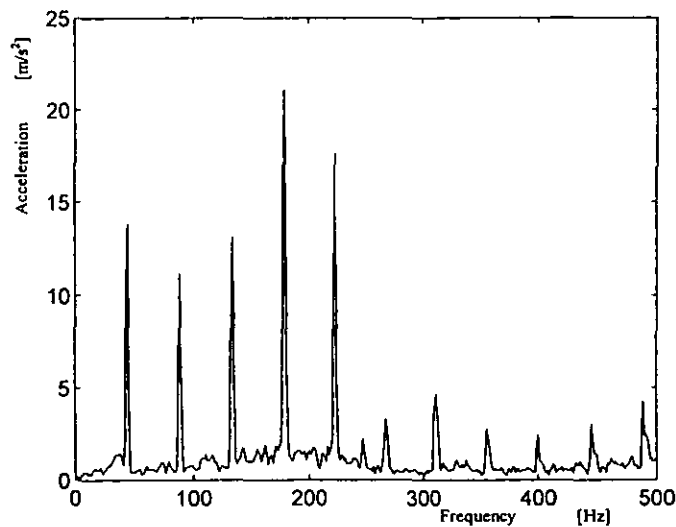
Figure 6.4 Acceleration frequency spectrum of experimental rig chiselling against damper
– accelerometer on main handle

6.2 Transducers

The choice of laser vibrometry was partly due to the fact that this is a technique that the Department of Mechanical Engineering has expertise in and many years of experience.

The laser vibrometer is based on a technique used to measure fluid flow velocity known as laser doppler velocimetry. A laser beam is pointed at the structure. The beam is reflected from the structure but with a change of frequency proportional to the velocity of the surface parallel to the beam (the Doppler effect). The instrument measures the change in frequency by comparing the reflected beam with the original beam. The device used in these experiments was the Polytec laser vibrometer OFV302 with processor OFV3000. This vibrometer is based on a helium neon laser. The beam is polarised and split into a signal beam and a reference beam using a beam splitter. The signal beam passes through a lens, strikes the object and returns. The reference beam is frequency shifted by a Bragg cell (an optical/acoustic device requiring radio frequency input). This frequency shift is required to detect the direction of motion. The signal and reference beams mix together and are detected by two photodetectors. The processor provides the power and the radio frequency signal for the Bragg cell, and demodulates the signal from the photodetectors (in a similar manner to an FM radio receiver) to produce an output in terms of velocity. The Polytec OFV302 has a frequency range of 150kHz. The optimum distance between the object and the vibrometer is 100mm. Other distances for quality results are 305mm, 510mm and so on in steps of 205mm (twice the cavity length of the laser).

When the laser beam strikes the surface of the object the light is scattered and the scattered waves interfere with each other to produce a pattern of light and dark spots known as laser speckle. To improve the scattering back to the instrument, the object is often coated in retroreflective tape or retroreflective paint. In this experiment retroreflective tape was used. If the motion of the object is only normal to the surface then the detector will be looking at the same speckles throughout the measurement. However, if the speckle pattern changes because of motion in other

planes, the detector interprets this as motion aligned with the beam which is known as pseudovibration. In the case of this experiment, pseudovibration must be considered as it was not possible to have the laser beam aligned with the direction of motion and the beam was therefore angled to measure a component of the motion (Figure 6.5) [Halliwell 1993].
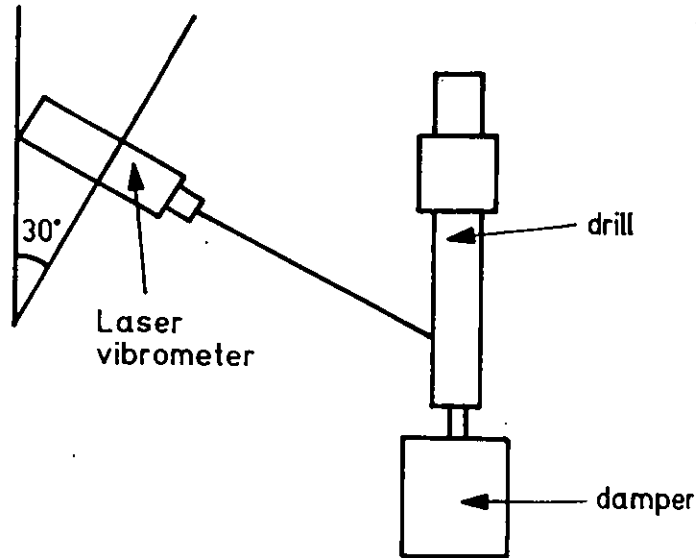
Figure 6.5 Laser vibrometer setup for measurement
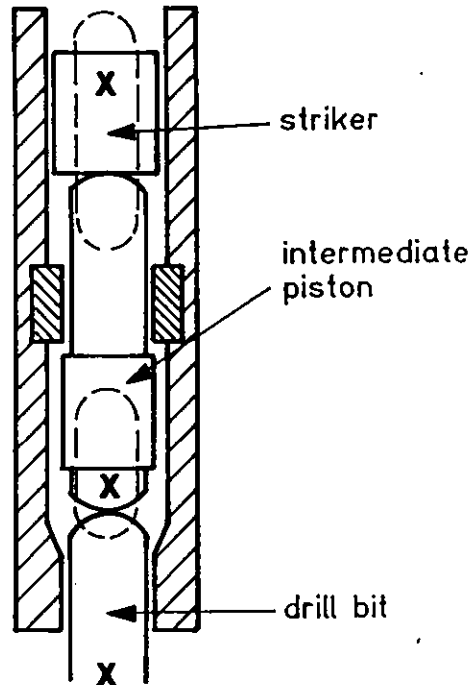
Figure 6.6 Impact unit showing the measurement points

The hammer drill rig had periodic excitation. In order to know at what point in the excitation cycle events occurred, the crank disk and surrounding metal work were painted matt black and a small strip of retroreflective tape was placed on the edge of the disk. The detector used was based on a reflective optoswitch working in the infrared region which produced a pulse every time the strip of tape passed the detector. This pulse indicated the point in the cycle when the piston was at top dead centre.
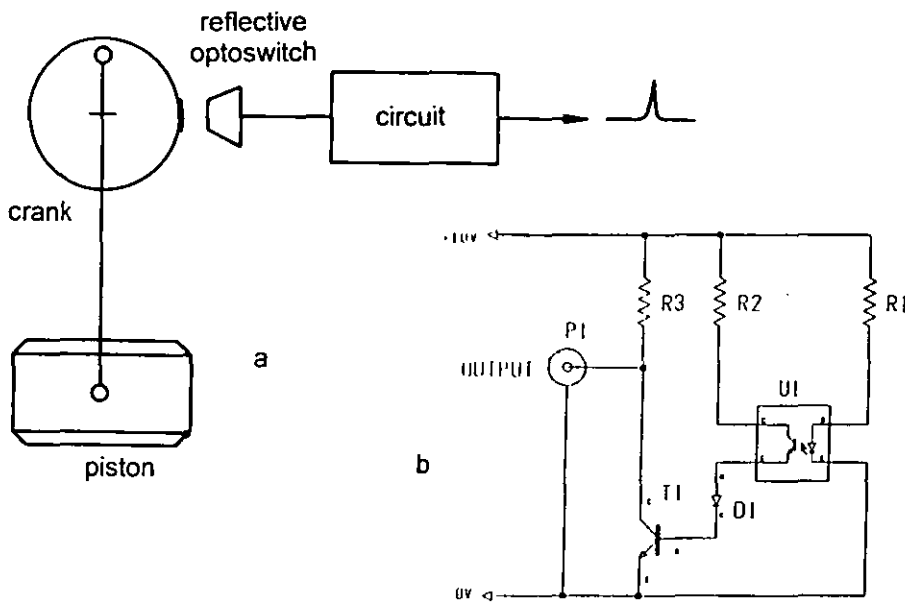
Figure 6.7 Method of indicating piston top dead centre: *a* Crank disk with reflective optoswitch, *b* Electronic circuit for optoswitch

6.3 Results

The rig was set up as shown in Figures 6.1, 6.2, 6.5 and 6.6 and the behaviour of three parts of the impact unit were studied in turn. With the 30° beam angle, the velocity output was multiplied by two to obtain the actual velocity.

The signal quality was always first checked by taking measurements from the rig without motion to check that the acrylic windows were not causing excessive noise. This gives a noise floor for each set of measurements. Figure 6.8 shows the noise floor for the striker. Figure 6.9 shows the measurement repeated when the rig was operated (over a smaller frequency range). At 2kHz the striker spectrum has reduced to a level of –45dB. The noise floor does not reach –45dB until 30kHz. At

low frequencies (below 500Hz) the motion signal is above –40dB while the initial peak of the noise floor peaks at –37dB and drops rapidly to below –50dB. The noise present in the motion signal is therefore not an important feature.
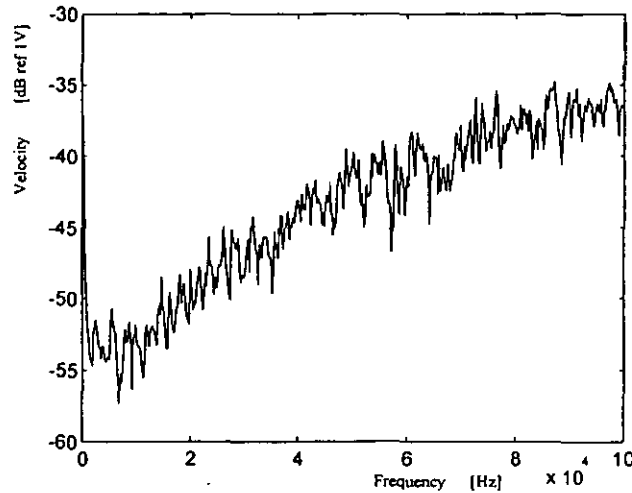
Figure 6.8 Velocity frequency spectrum of striker without motion (1V≡2m/s)
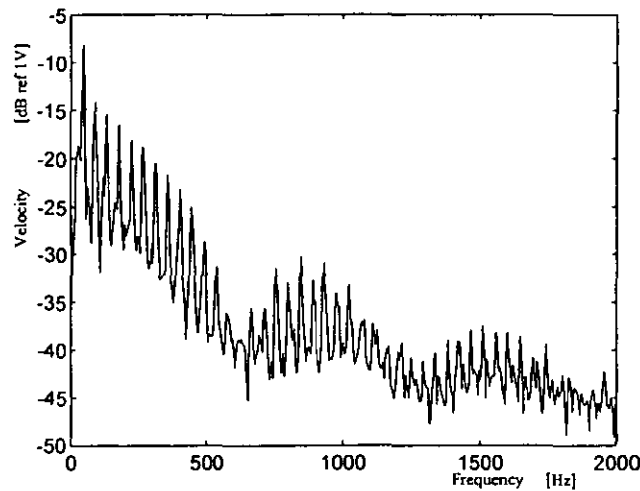
Figure 6.9 Velocity frequency spectrum of striker with motion (1V≡2m/s)

The velocity of the striker is also shown in the time domain in Figure 6.10. The positive values indicate velocity directed upwards towards the handle. The behaviour is periodic but it is difficult to obtain further information. The experiment was therefore repeated with different pressures on the trigger. Figure 6.11 shows the velocity of the striker when the trigger was lightly pressed. The motor operated at a slow speed and no impacts were audible. The data were exponentially smoothed using Excel but was not scaled by 2 to take into account

the beam angle. At this speed the motion of the striker is entirely due to the action of the piston, and the induced air pressure between the piston and the striker.
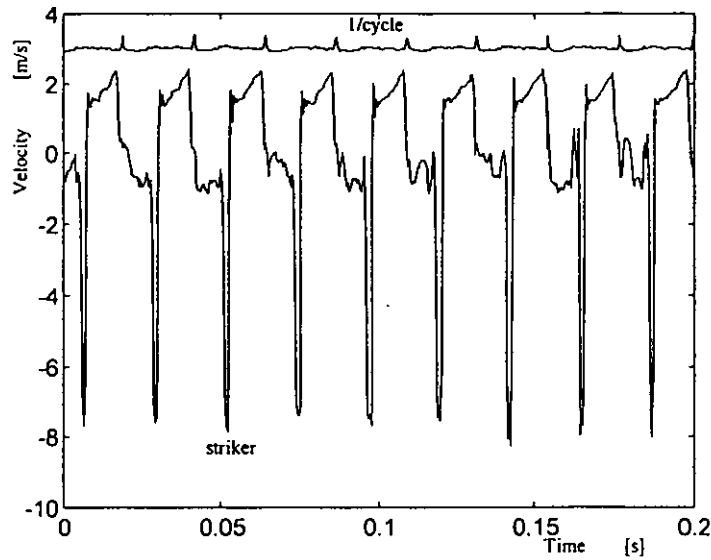
Figure 6.10 Velocity of the striker with 1/cycle signal
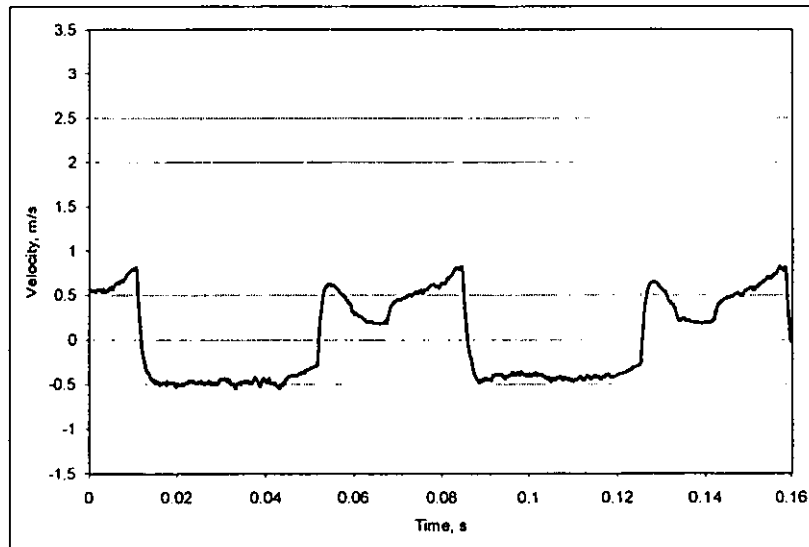
Figure 6.11 Striker motion at low speed

In Figure 6.11, at approximately 0.05s, the striker is sucked vertically upwards so that it accelerates to aproximately 0.5m/s when its speed drops. The pressure in the air gap builds up, the striker is accelerated downwards and it reaches a velocity of -0.5m/s at approximately 0.09s.
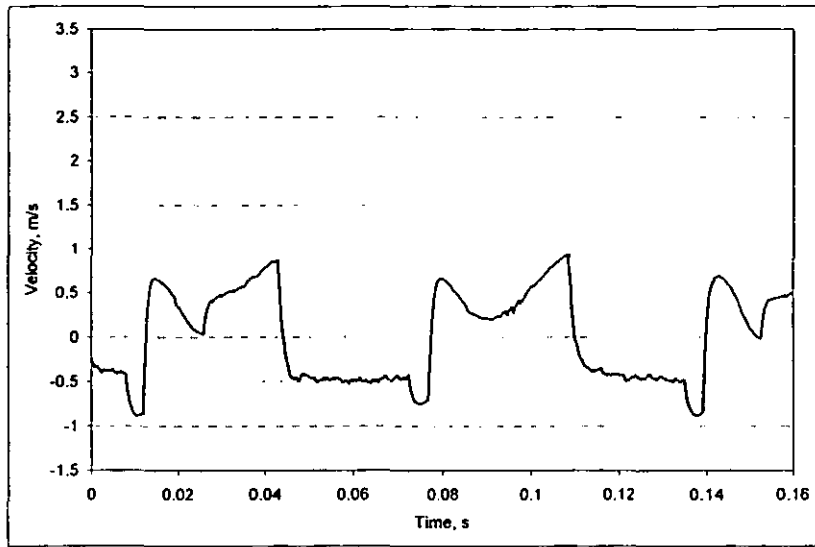
Figure 6.12 Striker motion at medium speed

When the trigger pressure is increased, the motor speed is increased and impacts occur between the striker and the intermediate piston. The velocity trace is shown in Figure 6.12. The positive sections of the velocity trace are similar to Figure 6.11 indicating that this portion of the trace is controlled by the piston behaviour. Since the motor speed has increased, the positive velocities have also increased in magnitude. After the striker has travelled at –0.5m/s for approximately 0.02s, there is a sudden increase in velocity, probably induced by the pressure spike, followed by a sudden change in direction which suggests that impact has occurred.
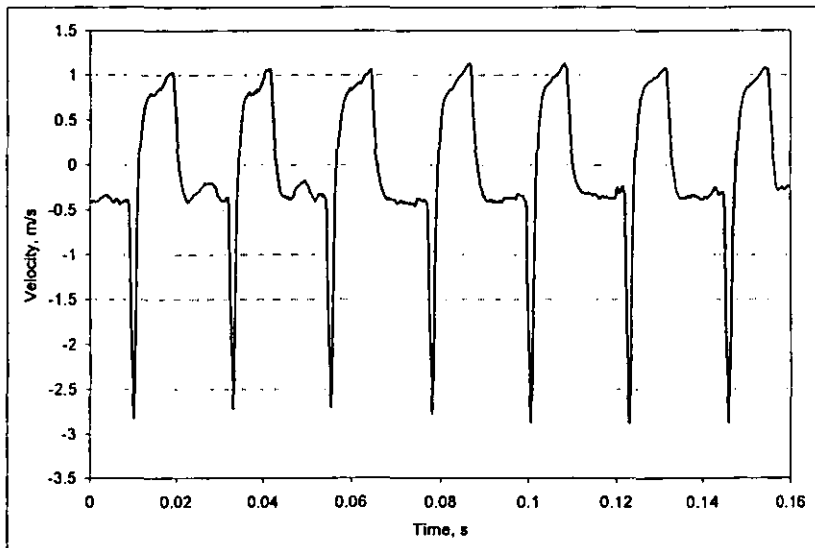
Figure 6.13 Striker motion at high speed

Figure 6.13 shows the striker motion when the trigger is fully depressed and the motor is operating at maximum speed. The shape of the trace is similar to Figure 6.10. The positive velocity values are greater than in Figure 6.12 and the negative velocity reached just before impact is greatly increased.

Returning to Figure 6.10, piston top dead centre occurs at the maximum positive velocity. The air pressure is then at its lowest value and the upward force of the piston is therefore at a maximum. The striker decelerates and, as the pressure builds, starts to descend. As the piston approaches bottom dead centre, the pressure peaks and rapidly accelerates the striker towards the intermediate piston. Impact occurs and the striker changes direction and, with the help of the piston's suction effect, returns to its start position. The pressure peak dissipates after the striker starts to move downwards because the striker uncovers vent holes in the tube.
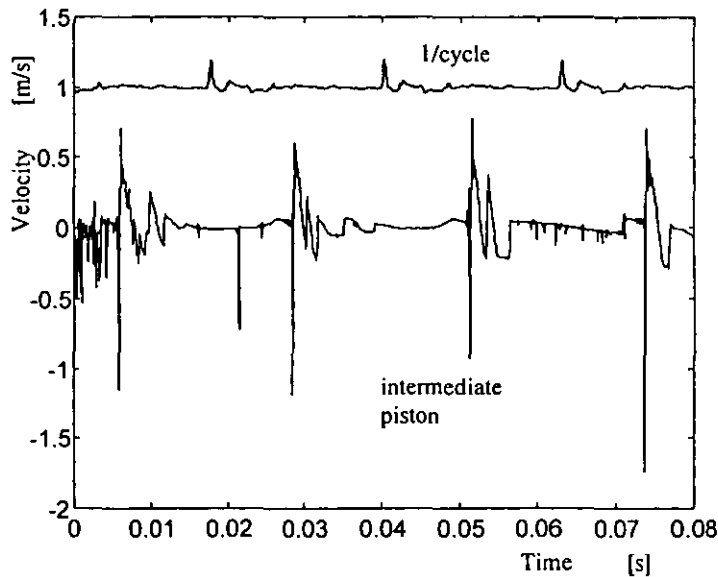
Figure 6.14 Velocity of intermediate piston with 1/cycle signal

The intermediate piston behaviour is shown in Figure 6.14. The behaviour is periodic but exhibits some variability. As the piston approaches bottom dead centre, the intermediate piston is accelerated downwards due to impact with the striker. Immediately afterwards it is accelerated upwards due to impact with the drill bit (the intermediate piston rests on the drill bit when the rig is stationary). After these two impacts, the intermediate piston experiences some reverses in

direction suggesting that impacts are occurring with the buffer or the drill bit, or both.

The behaviour of the drill bit is similar to that of the intermediate piston (Figure 6.15). The bit is driven downwards by the impact with the intermediate piston, and then upwards by impact with the damper. Variability is again observed between cycles and it is likely that some rattling is occurring.
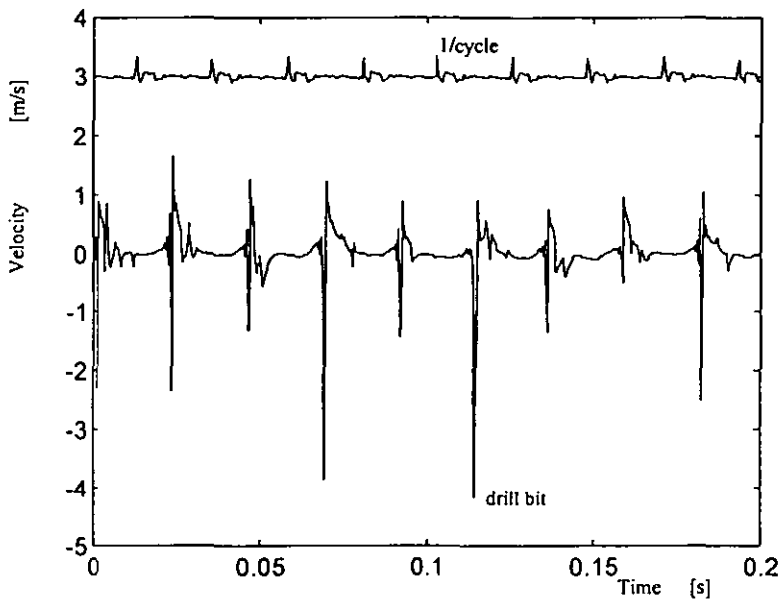
Figure 6.15 Velocity of the drill bit with 1/cycle signal

6.4 Determination of rig mechanical parameters

The mechanical parameters of the hammer drill test rig were determined to provide realistic inputs to the simulation models. Some, such as mass, are easily determined but others, particularly those modelled as springs and dampers, are more difficult to obtain.

The masses measured were:

Striker	0.14kg
Intermediate piston	0.28kg
Drill bit	0.43kg
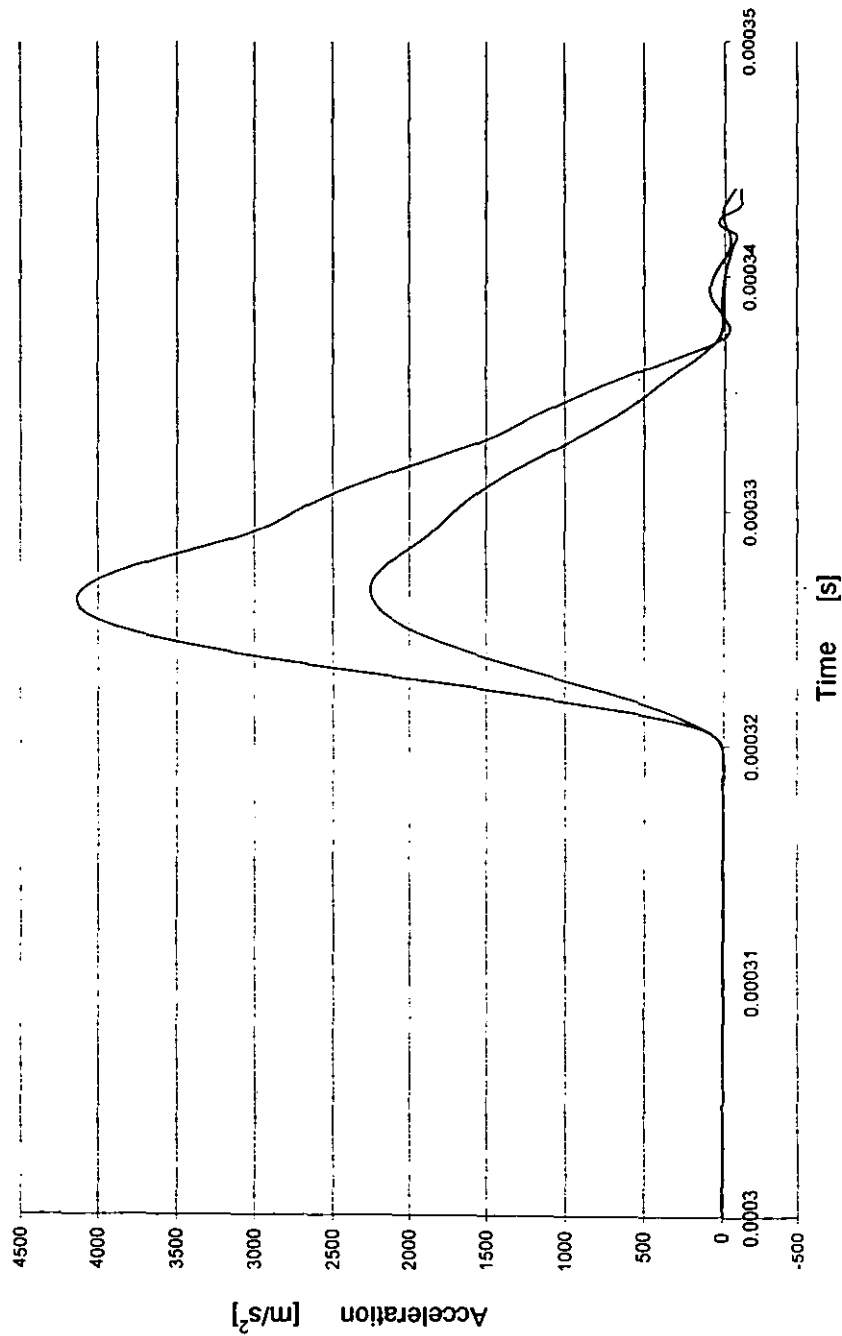
Fig 6.16 Two acceleration time traces from the drill bit/damper interaction experiments

To obtain the spring rates and damping coefficients, for example those describing the interaction between the drill bit and the damper, a technique explained in Babitsky and Veprik [1998] was used.

The drill bit was dropped onto the damper and its acceleration measured by means of a Bruel & Kjaer Type 4374 accelerometer glued to the opposite end of the drill bit from the impacting end. The data were filtered by a low pass filter set to 30kHz in the charge amplifier, to avoid picking up the accelerometer's natural frequency. Two graphs from these tests are shown in Figure 6.16 . They were plotted using Excel. From this data the time from start to end of the pulse, and the time from start of pulse to peak acceleration, were found. These are designated ϑ and α respectively and are related by the following expression [Babitsky and Veprik 1998]:

$$\frac{\alpha}{\vartheta} = \frac{\tan^{-1}\left(\dfrac{2\xi\sqrt{1-\xi^2}}{1-2\xi^2}\right)}{\tan^{-1}\left(\dfrac{(4\xi^2-1)\sqrt{1-\xi^2}}{\xi(3-4\xi^2)}\right)}$$

where ξ is the critical damping factor for the spring-damper model.

The equation was solved to find the critical damping factor in Excel. This was done by varying the value of ξ in small steps to achieve the closest result to the actual value of the time ratio.

	ϑ (s)	α(s)	ξ	f(Hz)
Run 1	6.64×10^{-6}	18.0×10^{-6}	0.181	25000
Run 2	6.25×10^{-6}	18.0×10^{-6}	0.207	24600

In the above table f is the natural frequency of the spring-damper model which can be calculated from the critical damping factor by the relationship $\xi = c/2m\omega_n = c/4\pi m f$ where c is the damping coefficient and $\omega_n = \sqrt{k/m}$ where k is the stiffness and m is the mass.

The equation of motion for the spring and damper system being impacted is given by [Babitsky and Veprik 1998]:

$$x(t) = Ae^{-ht} \sin \Omega t$$

where $A = V/\Omega$, $\Omega^2 = k/m - c^2/4m^2$, $h = c/2m$ and x is the displacement and V is the unknown initial velocity.

Using Excel, the initial velocity can be found by calculating the acceleration by a simple difference technique (calculating the displacements over a range of time values, then subtracting the adjacent displacements and dividing by the time step, and similarly to obtain the accelerations). The calculated accelerations were compared with the experimental results. Excel was also used to find the smallest sum of squared differences between them, thus identifying the best value of V. The resulting acceleration is shown in Figure 6.17 together with the experimental result for one run and a filtered version of the calculated acceleration (filtered using Matlab). The lack of correlation in shape between the calculated and experimental result suggests that the spring-damper model for the interaction between the drill bit and the damper requires improvement. It is likely that the model will require the addition of nonlinear stiffness where the stiffness depends on direction [Fu and Paul 1970, Lundberg 1973b] or the addition of dry friction [Neilson et al 1995] .
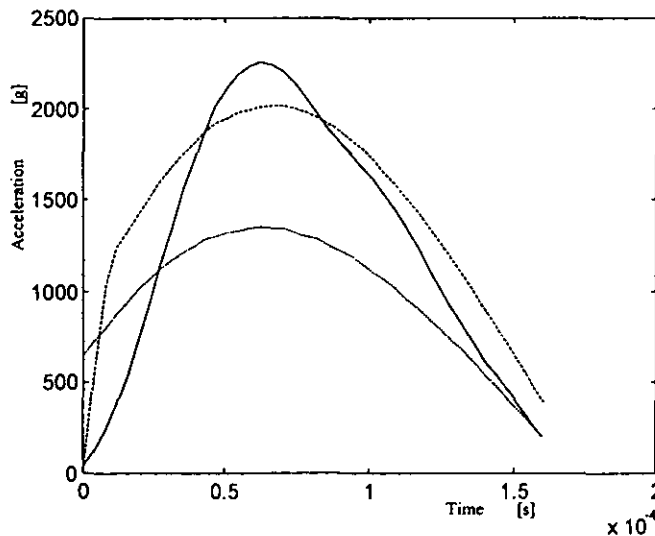
Figure 6.17 Acceleration measure for checking model: solid line – experimental data, dashed line – data calculated from model using Excel (filtered and x1.5), dotted line – data calculated from model using Excel (unfiltered).

6.5 Discussion

This study has demonstrated that it is possible to take measurements from an experimental rig based on an actual hammer drill. This rig can now be used to improve the simulation models. This type of rig can be used during hammer drill development.

Several points need to be considered in future experiments. A thorough comparison between the behaviour of the original drill and the experimental rig is required, and between the behaviour of the damper and concrete. With the laser vibrometer, the angle of 30° was chosen for convenience. Ideally an investigation of other angles and distances between the vibrometer and target should be carried out to select the optimum measurement conditions. In a similar way optimum frequency ranges for both the vibrometer and the analyser should be obtained. However, the vibration of the floor may need to be considered when operating the vibrometer in its upper frequency. It was found that when certain pieces of equipment were operated either in the room below or in the surrounding area, the vibrometer output was of poor quality especially when set to the highest frequency range. Using the correct frequency range is important to ensure that the impact behaviour is captured with sufficient detail.

An approximate calculation can be carried out to determine the likely frequency range of the response to the impulses [Meier-Dörnberg 1969]. The approximate acceleration spectrum for an impulse is shown in Figure 6.18 . The frequency f_1 can be calculated from maximum acceleration divided by maximum velocity, while the frequency f_2 is equal to the maximum jerk divided by the maximum acceleration. For a section of the striker's motion in Figure 6.19 (showing the point where the striker strikes the intermediate piston), the maximum velocity is 7.5m/s and by simple differencing the maximum acceleration is found to be 150000m/s^2 with a maximum jerk of 6.9x10^{9}m/s^3 . Using these values, f_1 is then 20kHz and f_2 is 46kHz. Both of these values are within the range of the analyser and the vibrometer. This process should be repeated to check the values of velocity,

acceleration and jerk and to make sure that the most appropriate settings are chosen.
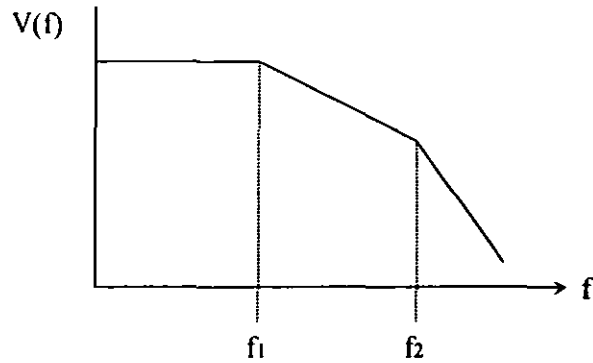
Figure 6.18 Approximate acceleration spectrum of a response to an impulse
[Halliwell et al 1999]
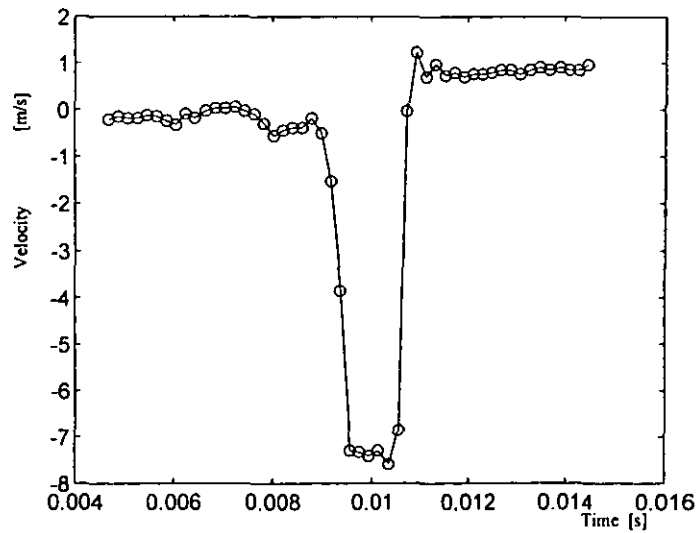
Figure 6.19 Closeup of striker behaviour

Other measurements can also be carried out, including measurement of the pressure of the air between the piston and striker, and a method of detecting impacts with the buffer (perhaps by using a strain gauge). An optical means of measuring the displacement of the moving parts and outer tube, would be useful. Noise generation could also be studied.

The other system parameters, such as the buffer stiffness, will also have to be determined for full comparison with the models. Methods like those described in section 6.4 could be used. Comparative measurement of the moving parts by using two vibrometers would aid model improvement.

7 CONCLUSION

There have been several previous studies of vibro-impact devices. Much of the early work was aimed at obtaining a better understanding of the simpler practical devices. However, in recent years the emphasis has increasingly turned to aspects of machine behaviour, such as chaos, which are generally of theoretical interest only and do not assist in the design process.

Percussion machines are complex vibro-impact devices and this has led to a general lack of reliable theoretical tools to assist the design process. With the growing awareness of vibration induced injury there is a now a need for a more rational design methodology for these machines.

The hammer drill is a percussion machine that is known to cause injury. The current study focussed on the impact unit of an electrically powered hammer drill. As the impact unit is complex, it was initially simplified to a two degree of freedom system with impact excitation.

If a vibro-impact device requires a numerical solution due to its complexity, it is important to first obtain an analytical solution to a simplified version of the device. This allows a reliable numerical model to be developed to which complexity can then be added, thus minimising the likelihood of errors.

The periodic Green's function method was the analytical method selected for this study, since it was developed specifically for systems with discontinuities. The equations of motion were solved for the initial two degree of freedom system for both sinusoidal and impulse excitation cases, without recourse to numerical methods. This is the first purely analytical solution that has been obtained for such a two degree of freedom system with impact excitation. Two solutions to the equation of motion were found but a stability analysis showed that only one was stable. As a check the solution was simplified to a single degree of freedom system without damping, thus producing the frequency response of an impact oscillator.

From this analytical solution, a good understanding of the behaviour of the basic two degree of freedom vibro-impact system was obtained. The frequency response indicated two resonances. One was a grazing resonance at a frequency slightly

greater than the natural frequency of the excited system. The other resonance was at approximately twice the natural frequency of the excited system and showed clapping behaviour. Previous studies of similar devices have seldom considered the frequency response and had generally studied only the lower of the two resonances. An antiresonance was identified where the system behaved like a vibration absorber and this operating regime is a possible area for the development of improved hammer drill designs. The responses obtained for the sinusoidal and impulse excitation cases were similar. This similarity was due to the underlying structure of the backbone curve. As long as the excitation term is small in comparison with the backbone term the differences in response between the two types of excitation will be small.

The numerical method selected for this study was based on the widely used Simulink package. The starting point for the numerical modelling was the two degree of freedom model that was studied using the periodic Green's function method. However it was found that the use of compliance in the impact surfaces was essential, to avoid the accumulation of integration errors due to infinite acceleration at impact. This particular problem with the classical impact equations has seldom been mentioned in previous vibro-impact studies. The compliance was applied in such a way so as to avoid physically impossible reaction force directions in the compliance. The results obtained were in good agreement with the results from the periodic Green's function method for both sinusoidal and impulse excitation. The Simulink models had the advantage that the excitation frequency could be swept both up and down. The models had similar behaviour to the two mass experimental rig where one resonance that would occur in the up sweep would be completely omitted during a down sweep.

More complex models could be rapidly created in Simulink. However the understanding previously obtained from the periodic Green's function analysis was of great assistance in avoiding erroneous results. Sources of error included the integration time step size, the length of time taken for a frequency sweep and incorrect formulation of the compliance. A slow sweep was found to be essential to allow transients to die away. It was found that added complexity was readily

achieved by making one mass a loose mass. The loose mass model showed the same two resonances and overall behaviour as the original model. However, there was a reduction in resonant frequency due to the altered natural frequency.

A two mass experimental rig was developed to support the initial two degree of freedom model. The experimental results were in general agreement with the analytical and numerical results. Precise comparison with the analytical and numerical results was not possible due to variability in the magnitude of the excitation. A slow sweep was required to allow the transients to die away. Two resonances were observed, a grazing resonance and a clapping resonance. The clapping resonance was found to occur only on the up sweep. By varying the frequency of excitation a more complete understanding of the impact pattern and the motion of the masses was obtained.

The first experimental rig to be based on an actual hammer drill was also developed. This hammer drill rig is intended to support the development of more complex models that may be required for some stages of hammer drill development, for example the loose mass model. The tests carried out demonstrated that it was possible to measure the velocities of the internal parts using a laser vibrometer. By varying the hammer drill speed a general understanding of its behaviour was obtained. The hammer drill showed periodic behaviour with the same period as the excitation but with some variation from cycle to cycle, particularly for the drill bit. It is possible that there may be some chatter between parts, especially between the intermediate piston and the drill bit.

Further research can be carried out to improve the analytical and numerical models by including additional features to obtain good agreement between the model predictions and measurements taken from an actual hammer drill (for example, the hammer drill rig developed in this study). The effect of nonlinear springs, dry friction and stress waves should be evaluated for possible inclusion in the impact unit model. It is also necessary to identify the most suitable impact models for the various impact surfaces, both within the drill and between the drill and the material being worked on. Sources of vibration outside the impact unit, particularly the excitation pressure pulse, also require investigation before a comprehensive design

methodology can be developed. The experimental hammer drill rig developed here is well suited to development work on commercial hammer drills. Additional parameters can be measured including displacement, air pressure within the tube, buffer forces and the effect of varying speed. The rig could also be used to investigate design modifications such as variation of mass or changes to the excitation method.

APPENDIX

This appendix contains the Matlab programs written to support the studies described in this thesis.

A.1 Programs for experimental studies

These programs require data files from the analyser without the header information removed.

A.1.1 timeav.m

This program was used to calculate the time between pulses for the impact pattern experiment in section 5.1.1.

```
% read in data and calculate average time between pulses
% ask for filename containing data
nname=input('filename ','s');
% open file, read data, close file
cd c:\sally\mdata
fid=fopen(nname);
s=fscanf(fid,'%e');
fclose(fid);
cd c:\sally
n=size(s);
% input max frequency set on the analyser
freq=input('max frequency ');
% calculate time between samples based on analyser's sampling frequency
delt=1/(2.56*freq);
% set up vector with times for each sample
tt=delt:delt:delt*n;
% set up initial values of variable 'slope' to detect positive peaks
j=0;
if (s(1)>0)&(s(1)<s(2))
        slope=1;
else
        slope=0;
end
% run through data picking the positive peaks and storing their values
% and times, reset 'slope' as appropriate
for i=1:n-1
        if s(i)>0
                if (s(i)>s(i+1))&(slope==1)
                        slope=0;
                        j=j+1;
                        pt(j)=tt(i);
                        p(j)=s(i);
                elseif (s(i)<s(i+1))&(slope==0)
                        slope=1;
                end
        else
                slope=0;
        end
```

```
end
% 'maxp' is number of positive peaks
maxp=j;
% preparation for removing the spurious peaks
% by finding the first big peak
if p(2)>4*p(1)
        x=2;
elseif p(3)>4*p(1)
        x=3;
else
        x=1;
end
peak(1)=p(x);
peakt(1)=pt(x);
% now cycle through the peaks and list the times of the big ones
k=1;
for i=x+1:maxp
        if 4*p(i)<p(x)
                p(i)=0;
        else
                k=k+1;
                peakt(k)=pt(i);
        end
end
% 'maxpeak' is final number of peaks of interest
maxpeak=k
diffa=0;
for i=1:maxpeak-1
% find the time step between each peak
        diff(i)=peakt(i+1)-peakt(i);
% sum the time steps
        diffa=diffa+diff(i);
end
% average the time steps
diffav=diffa/(maxpeak-1)
diffreq=1/diffav
```

A.1.2 sineswpf.m

This program calculates excitation frequencies from force spectra files and creates files for analysis in sinesw.m and sinesw3.m. It was used for the work in section 5.1.2.

```
% read in force spectra files and calculate excitation frequencies
% ask for filename
nname=input('filename ','s');
%open, read and close file
cd c:\sally\mdata
fid=fopen(nname);
while fid<2
        nname=input('try again    filename ','s');
        fid=fopen(nname);
end
q=fscanf(fid,'%e');
```

```
% read first piece of data (number of excitation points i.e. half the number of files listed in file)
N=q(1);
% read filenames into matrix
filn=fscanf(fid,'%s',[11,2*N]);
fclose(fid);
% second and third pieces of data in file are no of lines and analyser baseband frequency
L=q(2);
f=q(3);
filn=filn';
% calculate frequency step and provide frequency array
fd=f/L;
xf=0:fd:f;
% open each force file (first N filenames) and extract frequency of peak
for i=1:N
        fid=fopen(filn(i,:));
        z=fscanf(fid,'%e');
        fclose(fid);
        x(i)=xf(find(z==max(z)));
end
x=x';
prepare data for storing in file formatted for sinesw.m
A([1:3],1)=q;
A([4:N+3],1)=x;
A=A';
filnf=filn([1:N],:);
filnf=filnf';
filnr=filn([N+1:2*N],:);
filnr=filnr';
fname=input('new filename for force files ','s');
rname=input('new filename for response files ','s');
% write force data to a file (number of files, no of lines, baseband frequency, list of excitation
% frequencies and list of filenames for data)
fid=fopen(fname,'w');
fprintf(fid,'%7.4f\n',A);
fprintf(fid,filnf);
fclose(fid);
% repeat for response data
fid=fopen(rname,'w');
fprintf(fid,'%7.4f\n',A);
fprintf(fid,filnr);
fclose(fid); cd \sally;
```

A.1.3 sinesw.m

This program reads a file (created by sineswpf.m) containing list of filenames for the data and plots a waterfall plot.

```
% read in spectra files and produce a waterfall plot
% ask for filename
nname=input('filename ','s');
% open, read and close file
cd c:\sally\mdata
fid=fopen(nname);
q=fscanf(fid,'%e');
```

```
% read first piece of data no of files
N=q(1);
% read filenames into matrix
filn=fscanf(fid,'%s',[11,N]);
fclose(fid);
% calculate frequency step and provide frequncy array from data given in the file
L=q(2);
f=q(3);
fd=f/L;
x=0:fd:f;
% make array from list of excitation frequencies
yf=q(4:N+3);
filn=filn';
% open each file and extract data, create array containing the relevant excitation frequency
% and update the overall matrices
for i=1:N
        fid=fopen(filn(i,:));
        z=fscanf(fid,'%e');
        fclose(fid);
        y=linspace(yf(i),yf(i),L+1);
        Z(:,i)=z;
        X(:,i)=x';
        Y(:,i)=y';
end
cd c:\sally
% plot data as a waterfall plot
plot3(X,Y,Z)
view(-5,60)
% X contains the frequency range of the spectra
% Y contains the frequencies used to excite the structure
% Z contains the magnitudes of the spectra
```

A.1.4 sinesw3.m

This program calculates the frequency response of the system by taking the maximum response which occurs close to the excitation frequency. The files required are listed in a file created by sineswpf.m.

```
% read in spectra files and produce a plot of max points
% ask for filename
nname=input('filename ','s');
% open file containing list of filenames of spectra files
cd c:\sally\mdata
fid=fopen(nname);
while fid<2
        nname=input('try again    filename ','s');
        fid=fopen(nname);
end
q=fscanf(fid,'%e');
% read in first piece of data number of files
N=q(1);
% read in filenames as an array
filn=fscanf(fid,'%s',[11,N])';
fclose(fid);
```

```
% create array of frequencies from no of lines and baseband frequency
L=q(2);
f=q(3);
fd=f/L;
xf=0:fd:f;
% create array from list of excitation frequencies
yf=q(4:N+3);
% create an array of 0's
p=linspace(0,0,L+1)';
% find max and min values of excitation frequecies
ymax=max(yf);
ymin=min(yf);
% open each file
for i=1:N
        fid=fopen(filn(i,:));
        z=fscanf(fid,'%e');
        fclose(fid);
        % zero the array parts that have frequencies outside the excitation range
        z(xf<ymin & xf>ymax)=p(xf<ymin & xf>ymax);
        % zero the array parts which are not within 3 frequency steps of the
        % relevant excitation frequency
        A=xf<(yf(i)-3*fd);
        B=xf>(yf(i)+3*fd);
        if yf(i)==ymax
                z(A)=p(A);
        elseif yf(i)==ymin
                z(B)=p(B);
        else
                z(A|B)=p(A|B);
        end
        % find the max value of the response
        y(i)=max(z); x(i)=yf(i);
end
cd c:\sally
plot(x,y)
```

A.2 Programs used to generate graphs for section 3.6

A.2.1 jidnew.m

This program calculates the displacement responses to impulse excitation and plots them against frequency ratio.

```
% displacement against frequency - impact excitation
m1=0.125;
m2=0.094;
k1=135;
k2=128;
c2=0.1;
R=0.7;
delta=0.001;
F=0.009;
Omega1=sqrt(k1/m1);
Omega2=sqrt(k2/m2);
```

```
b2=c2/(2*m2);
lambda2=sqrt(Omega2^2-b2^2);
M1=m1*m2/(m1+m2);
M=M1*(1+R);
fr=0.7501:0.02:2.996;
G=linspace(0,0,length(fr));
omega=fr*Omega1;
T=2*pi./omega;
B2=exp(-b2*T);
r=1-cos(Omega1*T);
A1=1./(m1*Omega1*2*r);
A2=1./(m2*lambda2*(1+B2.^2-2*B2.*cos(lambda2*T)));
chi1(1,:)=A1.*sin(Omega1*T);
chi2(1,:)=A2.*B2.*sin(lambda2*T);
C=chi1(1,:)+chi2(1,:);
dchi1=-1/(2*M1);
dchi2=-1/(2*M1);
D=dchi1+dchi2;
q1=(1/M+D)/Omega1;
q2=q1.^2+C.^2;
q3a=2*r*F^2.*A1.^2-delta^2;
q3b=abs(q3a);
E=q3b<1e-6;
q3a(E)=G(E);
q4=2*r*F^2.*A1.^2.*C.^2+q1.^2.*q3a;
q5=sqrt(q4);
q6=-C*delta./q2+q5./q2;
J=q6;
Q=q6<0;
J(Q)=G(Q);
sphi=(delta+J.*C)*m1*Omega1*2.*r./(2*F)-J.*q1.*sin(Omega1*T)./(2*r*F.*A1);
L=sphi<0;
phi=asin(sphi);
tphi=pi-phi;
tphi(L)=2*pi-asin(abs(sphi(L)));
phi(L)=asin(abs(sphi(L)))+pi;
tau=phi/omega;
ttau=tphi/omega;
t(1,:)=linspace(0,0,length(fr));
cc1=F*A1.*(sin(Omega1*tau)+sin(Omega1*(T-tau)));
cc2=F*A1.*(sin(Omega1*ttau)+sin(Omega1*(T-ttau)));
xx1=cc1-J.*chi1(1,:);
xx2=cc2-J.*chi1(1,:);
x2(1,:)=J.*chi2(1,:)+delta;
d1=abs(xx1-x2(1,:));
d2=abs(xx2-x2(1,:));
x1(1,:)=xx1;
chit(1,:)=cc1/F;
N=d1>d2;
chit(1,N)=cc2(N);
x1(1,N)=xx2(N);
tau(N)=ttau(N);
for i=2:101
        t(i,:)=(i-1)*T/100;
        if t(i,1)+tau<=T
        chit(i,:)=A1.*(sin(Omega1*(t(i,:)+tau))+sin(Omega1*(T-t(i,:)-tau)));
```

```
          else
          chit(i,:)=A1.*(sin(Omega1*(t(i,:)+tau-T))+sin(Omega1*(2*T-t(i,:)-tau)));
          end
          chi1(i,:)=A1.*(sin(Omega1*t(i,:))+sin(Omega1*(T-t(i,:))));
          chi2(i,:)=A2.*exp(-b2*t(i,:)).*(sin(lambda2*t(i,:))+B2.*sin(lambda2*(T-t(i,:))));
          x1(i,:)=F*chit(i,:)-J.*chi1(i,:);
          x2(i,:)=J.*chi2(i,:)+delta;
end
px1=max(max(x1),abs(min(x1)));
px2=max(max(x2),abs(min(x2)));
plot(fr,px1,'w-',fr,px2,'w:')
```

A.2.2 jidtw.m

This program calculates displacements at one frequency under impulse excitation
and plots them against time.

```
% displacement against time - impact excitation
m1=0.125;
m2=0.094;
k1=135;
k2=128;
c2=0.1;
R=0.7;
delta=0.001;
F=0.005;
fr=1.501;
%fr=2.1301
Omega1=sqrt(k1/m1);
Omega2=sqrt(k2/m2);
b2=c2/(2*m2);
lambda2=sqrt(Omega2^2-b2^2);
M1=m1*m2/(m1+m2);
M=M1*(1+R);
omega=fr*Omega1;
T=2*pi/omega;
B2=exp(-b2*T);
r=1-cos(Omega1*T);
A1=1/(m1*Omega1*2*r);
A2=1/(m2*lambda2*(1+B2^2-2*B2*cos(lambda2*T)));
chi1(1)=A1*sin(Omega1*T);
chi2(1)=A2*B2*sin(lambda2*T);
C=chi1(1)+chi2(1);
dchi1=-1/(2*m1);
dchi2=-1/(2*m2);
D=dchi1+dchi2;
q1=(1/M+D)/Omega1;
q2=q1^2+C^2;
q3a=2*r*F^2*A1^2-delta^2;
q4=2*r*F^2*A1^2*C^2+q1^2*q3a;
q5=sqrt(q4);
J=-C*delta/q2+q5/q2;
sphi=(delta+J*C)*m1*Omega1*2*r/(2*F)-J*q1*sin(Omega1*T)/(2*r*F*A1);
if sphi>=0;
```

```
        phi=asin(sphi);
        tphi=pi-phi;
else
        tphi=2*pi-asin(abs(sphi));
        phi=asin(abs(sphi))+pi;
end
tau=phi/omega;
ttau=tphi/omega;
t(1)=0;
cc1=F*A1*(sin(Omega1*tau)+sin(Omega1*(T-tau)));
cc2=F*A1*(sin(Omega1*ttau)+sin(Omega1*(T-ttau)));
xx1=cc1-J*chi1(1);
xx2=cc2-J*chi1(1);
x2(1)=J*chi2(1)+delta;
x2T=J*A2*B2*sin(lambda2*T)+delta;
d1=abs(xx1-x2(1));
d2=abs(xx2-x2(1));
if d1<d2
        x1(1)=xx1;
        chit(1)=cc1/F;
else
        chit(1)=cc2/F;
        x1(1)=xx2;
        phi=tphi;
        tau=ttau;
end
for i=2:101
        t(i)=(i-1)*T/100;
        if t(i)+tau<=T
        chit(i)=A1*(sin(Omega1*(t(i)+tau))+sin(Omega1*(T-t(i)-tau)));
        else
        chit(i)=A1*(sin(Omega1*(t(i)+tau-T))+sin(Omega1*(2*T-t(i)-tau)));
        end
        chi1(i)=A1*(sin(Omega1*t(i))+sin(Omega1*(T-t(i))));
        chi2(i)=A2*exp(-b2*t(i))*(sin(lambda2*t(i))+B2*sin(lambda2*(T-t(i))));
        x1(i)=F*chit(i)-J.*chi1(i);
        x2(i)=J.*chi2(i)+delta;
end
plot(t,x1,'w-',t,x2,'w:')
```

A.2.3 jinew.m

This program calculates the response of impulse J to impulse excitation and plots it against frequency ratio.

```
% impulse against frequency - impact excitation
m1=0.125;
m2=0.094;
k1=135;
k2=128;
c2=0.1;
R=0.5;
delta=0.001;
F=0.009;
```

```
Omega1=sqrt(k1/m1);
Omega2=sqrt(k2/m2);
b2=c2/(2*m2);
lambda2=sqrt(Omega2^2-b2^2);
M1=m1*m2/(m1+m2);
M=M1*(1+R);
fr=0.7501:0.02:2.996;
G=linspace(0,0,length(fr));
omega=fr*Omega1;
T=2*pi./omega;
B2=exp(-b2*T);
r=1-cos(Omega1*T);
A1=1./(m1*Omega1*2*r);
A2=1./(m2*lambda2*(1+B2.^2-2*B2.*cos(lambda2*T)));
chi1=A1.*sin(Omega1*T);
chi2=A2.*B2.*sin(lambda2*T);
C=chi1+chi2;
dchi1=-1/(2*M1);
dchi2=-1/(2*M1);
D=dchi1+dchi2;
q1=(1/M+D)/Omega1;
q2=q1.^2+C.^2;
q3a=2*r*F^2.*A1.^2-delta^2;
q3b=abs(q3a);
E=q3b<1e-6;
q3a(E)=G(E);
q4=2*r*F^2.*A1.^2.*C.^2+q1.^2.*q3a;
q5=sqrt(q4);
q6=-C*delta./q2+q5./q2;
J=q6;
Q=q6<0;
J(Q)=G(Q);
plot(fr,J)
```

A.2.4 jsdnew.m

This program calculates the displacement responses to sinusoidal excitation and plots them against frequency ratio.

```
% displacement against frequency - sinusoidal excitation
m1=0.125;
m2=0.094;
k1=135;
k2=128;
c1=0.1;
c2=0.1;
R=0.7;
delta=0.001;
F=0.5;
Omega1=sqrt(k1/m1);
Omega2=sqrt(k2/m2);
b1=c1/(2*m1);
b2=c2/(2*m2);
lambda1=sqrt(Omega1^2-b1^2);
```

```
lambda2=sqrt(Omega2^2-b2^2);
M1=m1*m2/(m1+m2);
M=M1*(1+R);
f1=[0.75:0.01:0.91];
f2=[1.03];
f3=[1.041:0.01:1.1];
f4=[1.2:0.01:2.9];
fr=[f1 f2 f3 f4];
%fr=0.7501:0.01:2.996;
omega=fr*lambda1;
T=2*pi./omega;
G=linspace(0,0,length(fr));
Fs=F./sqrt((k1-m1*omega.^2).^2+(c1*omega).^2);
B1=exp(-b1*T);
B2=exp(-b2*T);
A1=1./(m1*lambda1*(1+B1.^2-2*B1.*cos(lambda1*T)));
A2=1./(m2*lambda2*(1+B2.^2-2*B2.*cos(lambda2*T)));
chi1(1,:)=A1.*B1.*sin(lambda1*T);
chi2(1,:)=A2.*B2.*sin(lambda2*T);
C=chi1(1,:)+chi2(1,:);
if (c1==0&c2==0)
        dchi1=-1/(2*(1+R)*M);
        dchi2=-1/(2*(1+R)*M);
else
        dchi1=A1.*B1.*((-b1*sin(lambda1*T)+lambda1*cos(lambda1*T))-B1*lambda1);
        dchi2=A2.*B2.*((-b2*sin(lambda2*T)+lambda2*cos(lambda2*T))-B2*lambda2);
end
D=dchi1+dchi2;
qx=(1/M1+D).^2./omega.^2;
qq=qx+C.^2;
q1=-delta*C./qq;
q2=Fs.*C./qq;
q3a=Fs.^2-delta^2;
q3b=abs(q3a);
q3a(find(q3b<1e-6))=G(find(q3b<1e-6));
q3=qx.*q3a;
q4=Fs.^2.*C.^2;
q4a=q4+q3;
q5=sqrt(q4a)./qq;
q6=q1+q5;
J=q6;
J(find(q6<0))=G(find(q6<0));
sphi=-J.*(1/M+D).*sqrt(c1^2+(m1^2*(Omega1^2-omega.^2).^2./omega.^2))/F;
E=sphi<0;
phi=asin(sphi);
tphi=pi-asin(sphi);
phi(E)=asin(abs(sphi(E)))+pi;
tphi(E)=2*pi-asin(abs(sphi(E)));
t(1,:)=linspace(0,0,length(fr));
cc1=Fs.*cos(phi);
cc2=Fs.*cos(tphi);
j1=J.*chi1(1,:);
xx1=cc1-j1;
xx2=cc2-j1;
x2(1,:)=J.*chi2(1,:)+delta;
d1=abs(xx1-x2(1,:));
```

```
d2=abs(xx2-x2(1,:));
x1(1,:)=xx1;
L=d1>d2;
x1(1,L)=xx2(L);
phi(L)=tphi(L);
for i=1:100
        t(i+1,:)=i*T/100;
        chi1(i+1,:)=A1.*exp(-b1*t(i+1,:)).*(sin(lambda1*t(i+1,:))+B1.*sin(lambda1*(T-t(i+1,:))));
        chi2(i+1,:)=A2.*exp(-b2*t(i+1,:)).*(sin(lambda2*t(i+1,:))+B2.*sin(lambda2*(T-t(i+1,:))));
        x1(i+1,:)=Fs.*cos(omega.*t(i+1,:)+phi)-J.*chi1(i+1,:);
        x2(i+1,:)=J.*chi2(i+1,:)+delta;
end
px1=abs(max(max(x1),abs(min(x1))));
px2=max(max(x2),abs(min(x2)));
plot(fr,px1,'w-',fr,px2,'w:')
```

A.2.5 jsdtw.m

This program calculates displacements at one frequency under sinusoidal excitation and plots them against time.

```
% displacement against time - sinusoidal excitation
m1=0.125;
m2=0.094;
k1=135;
k2=128;
c1=0.1;
c2=0.1;
R=0.7;
delta=0.001;
F=0.007;
fr=1.0501;
%fr=2.131
Omega1=sqrt(k1/m1);
Omega2=sqrt(k2/m2);
b1=c1/(2*m1);
b2=c2/(2*m2);
lambda1=sqrt(Omega1^2-b1^2);
lambda2=sqrt(Omega2^2-b2^2);
M1=m1*m2/(m1+m2);
M=M1*(1+R);
omega=fr*lambda1;
T=2*pi/omega;
Fs=F/sqrt((k1-m1*omega^2)^2+(c1*omega)^2);
B1=exp(-b1*T);
B2=exp(-b2*T);
A1=1/(m1*lambda1*(1+B1^2-2*B1*cos(lambda1*T)));
A2=1/(m2*lambda2*(1+B2^2-2*B2*cos(lambda2*T)));
chi1(1)=A1*B1*sin(lambda1*T);
chi2(1)=A2*B2*sin(lambda2*T);
C=chi1(1)+chi2(1);
if(c1==0&c2==0)
dchi1=-1/(2*M1);
dchi2=-1/(2*M1);
```

```
else
dchi1=A1*B1*((-b1*sin(lambda1*T)+lambda1*cos(lambda1*T))-B1*lambda1);
dchi2=A2*B2*((-b2*sin(lambda2*T)+lambda2*cos(lambda2*T))-B2*lambda2);
end
D=dchi1+dchi2;
qx=(1/M+D)^2/omega^2;
qq=qx+C^2;
q1=-delta*C/qq;
q2=Fs*C/qq;
q3a=Fs^2-delta^2;
if abs(q3a)<1e-6
        q3a=0;
end
q3=qx*q3a;
q4=Fs^2*C^2;
q4a=q4+q3;
q5=sqrt(q4a)/qq;
q6=q1+q5;
if q6<0
        J=0;
else
        J=q6;
end
sphi=-J*(1/M+D)*sqrt(c1^2+(m1^2*(Omega1^2-omega^2)^2/omega^2))/F;
if sphi<0
        phi=asin(abs(sphi))+pi;
        tphi=2*pi-asin(abs(sphi));
else
        phi=asin(sphi);
        tphi=pi-asin(sphi);
end
t(1)=0;
cc1=Fs*cos(phi);
cc2=Fs*cos(tphi);
j1=J.*chi1(1);
xx1=cc1-j1;
xx2=cc2-j1;
x2(1)=J*chi2(1)+delta;
d1=abs(xx1-x2(1));
d2=abs(xx2-x2(1));
if d1<d2
        x1(1)=xx1;
else
        x1(1)=xx2;
        phi=tphi;
end
for i=1:100
        t(i+1)=i*T/100;
        chi1(i+1)=A1*exp(-b1*t(i+1))*(sin(lambda1*t(i+1))+B1*sin(lambda1*(T-t(i+1))));
        chi2(i+1)=A2*exp(-b2*t(i+1))*(sin(lambda2*t(i+1))+B2*sin(lambda2*(T-t(i+1))));
        x1(i+1)=Fs*cos(omega*t(i+1)+phi)-J*chi1(i+1);
        x2(i+1)=J*chi2(i+1)+delta;
end
plot(t,x1,'w-',t,x2,'w:')
```

A.2.6 jsnew.m

This program calculates the response of impulse *J* to sinusoidal excitation and plots it against frequency ratio.

```
% impulse against frequency - sinusoidal excitation
m1=0.125;
m2=0.094;
k1=135;
k2=128;
c1=0.1;
c2=0.1;
R=0.7;
delta=0.001;
F=0.5;
Omega1=sqrt(k1/m1);
Omega2=sqrt(k2/m2);
b1=c1/(2*m1);
b2=c2/(2*m2);
lambda1=sqrt(Omega1^2-b1^2);
lambda2=sqrt(Omega2^2-b2^2);
M1=m1*m2/(m1+m2);
M=M1*(1+R);
f1=[0.75:0.01:0.9];
f2=[1.03];
f3=[1.041:0.01:1.1];
f4=[1.2:0.01:2.9];
fr=[f1 f2 f3 f4];
%fr=0.7501:0.02:2.996;
omega=fr*lambda1;
T=2*pi./omega;
G=linspace(0,0,length(fr));
if F==0
        Fs=G;
else
        fd=sqrt((k1-m1*omega.^2).^2+(c1*omega).^2);
        Fs=F./fd;
end
B1=exp(-b1*T);
B2=exp(-b2*T);
A1=1./(m1*lambda1*(1+B1.^2-2*B1.*cos(lambda1*T)));
A2=1./(m2*lambda2*(1+B2.^2-2*B2.*cos(lambda2*T)));
chi1=A1.*B1.*sin(lambda1*T);
chi2=A2.*B2.*sin(lambda2*T);
C=chi1+chi2;
if(c1==0&c2==0)
dchi1=-1/(2*M1);
dchi2=-1/(2*M1);
else
dchi1=A1.*B1.*(-b1*sin(lambda1*T)+lambda1*cos(lambda1*T)-B1*lambda1);
dchi2=A2.*B2.*(-b2*sin(lambda2*T)+lambda2*cos(lambda2*T)-B2*lambda2);
end
D=dchi1+dchi2;
qx=(1/M+D).^2./omega.^2;
```

```
qq=qx+C.^2;
q1=-delta*C./qq;
if F==0
        q2=G;
else
        q2=Fs.*C./qq;
end
q3a=Fs.^2-delta^2;
q3b=abs(q3a);
q3a(find(q3b<1e-6))=G(find(q3b<1e-6));
q3=qx.*q3a;
q4=Fs.^2.*C.^2;
q4a=q4+q3;
q5=sqrt(q4a)./qq;
q6=q1+q5;
J=q6;
J(find(q6<0))=G(find(q6<0));
plot(fr,J)
```

REFERENCES

MATLAB User's Guide; The MathWorks Inc, Natick, Mass.; 1992.

MATLAB Reference Guide; The MathWorks Inc, Natick, Mass.; 1992.

MATLAB Release Notes Version 4.2; The MathWorks Inc, Natick, Mass.; 1994

SIMULINK User's Guide; The MathWorks Inc, Natick, Mass.; 1992.

SIMULINK Release Notes Version 1.3; The MathWorks Inc, Natick, Mass.; 1994.

British Standard BS EN 28662-3:1995 (ISO 8662-3:1992)
Hand-held portable power tools - Measurement of vibrations at the handle. Part 3
Rock drills and rotary hammers.

Andronov, A.A.; 1945; L I Mandelshtam and the theory of nonlinear vibrations;
Izvestiya Academy of Sciences of the USSR, Physics series Vol 9 No 1-2. (in
Russian)

V K Astashev and V I Babitsky; 1988; Dynamics of a resonant machine; in
Dymanics and control of machines, ed G Kreinin; Mashinostroenie, Moscow;
p168-209. (in Russian)

J Awrejcewicz, K Tomczak and C-H Lamarque; 1996; Multibody vibro-impact
dynamics; EUROMECH - 2nd European Nonlinear Oscillation Conference,
Prague, Sept 9-13; Vol 2 p9-12.

V I Babitsky; 1998; Theory of Vibroimpact Systems; Springer Verlag, Berlin;
(revised English translation of Russian edition, published by Nauka, 1978).

V Babitsky; 1992; Some applications of autoresonant strongly nonlinear vibratory
systems; Machine Vibration, 1:110-119.

V I Babitsky and M Z Kolovsky; 1967; Investigation of vibrations of a linear system with stops with exact and approximate methods; Mashinovedenie No4. (in Russian)

V I Babitsky and M Z Kolovsky (with V L Krupenin); 1995; Mechanical Influences and Methods of Vibroprotection; in Vibrations in Engineering, Vol 6: Protection from Vibration and Impact; ed K V Frolov; Mashinostroenie, Moscow 1995. (in Russian)

V I Babitsky, A S Kovaleva and B L Krupenin; 1982; Investigation of quasi-conservative vibroimpact systems by the method of averaging; Mekhanika Tverdogo Tela No1 p41-49. (in Russian)

V I Babitsky and V L Krupenin; 1985; Vibrations in Strongly Nonlinear Systems; Nauka, Moscow. (in Russian)

V I Babitsky and A M Veprik; 1998; Universal bumpered vibration isolator for severe environment; Journal of Sound and Vibration, 218(2):269-292.

C N Bapat; 1982; A Study of Vibroimpact Systems; PhD Thesis; University of Manitoba, Canada.

C N Bapat and C Bapat; 1988; Impact-pair under periodic excitation; Journal of Sound and Vibration, 120(1):53-61.

C N Bapat, N Popplewell and K McLachlan; 1983; Stable periodic motions of an impact pair; Journal of Sound and Vibration, 87(1):19-40.

C N Bapat and S Sankar; 1985; Single unit impact damper in free and forced vibration; Journal of Sound and Vibration, 99(1):85-94.

R Beccu; 1996; Transmission of elastic stress wave energy through joints and bends in percussive rock drilling systems; Doctoral thesis; Uppsala University.

G W Blankenship and A Kahraman; 1995; Steady state forced response of a mechanical ocillator with combined parametric excitation and clearance type non-linearity; Journal of Sound and Vibration, 185(5):743-765.

L Borg; 1977; Optical stress wave measurement in hammer drilling rods; Review of Scientific Instruments, 48(12):1583-1584.

C Budd, F Dux and A Cliffe; 1995; The effect of frequency and clearance variations on single degree of freedom impact oscillators; Journal of Sound and Vibration, 184(3):475-502.

C Cempel; 1974; The multi-unit impact damper: equivalent continuous force approach; Journal of Sound and Vibration, 34(2):199-209.

C Cempel; 1978; Detection of clearances in machine kinematic pairs by a coherence method; Journal of Sound and Vibration, 60(3):411-416.

S Chatterjee, A K Mallik and A Ghosh; 1995; On impact dampers for non-linear vibrating systems; Journal of Sound and Vibration, 187(3):403-420.

S Chatterjee, A K Mallik and A Ghosh; 1996; Periodic response of piecewise non-linear oscillators under harmonic excitation; J Sound and Vibration, 191(1):129-144.

R J Comparin and R Singh; 1989; Non-linear frequency response characteristics of an impact pair; Journal of Sound and Vibration, 134(2):259-290.

P A Cook; 1986; Nonlinear Dynamical Systems; Prentice Hall, London.

T O Dalrymple; 1989; Numerical solutions to vibroimpact via an initial value problem formulation; Journal of Sound and Vibration, 132(1):19-32.

J P Den Hartog; 1956; Mechanical Vibrations, 4th Ed; Dover Publications, New York.

J P Den Hartog; 1961; Mechanics; Dover Publications, New York.

L H Donnell; 1930; Longitudinal wave transmission and impact; Transactions of ASME, 52:153-167.

J F Doyle; 1989; Wave Propagation in Structures; Springer Verlag; New York.

S Dubowsky and F Freudenstein; 1971; Dynamic analysis of mechanical systems with clearances, Part 1: Formation of dynamic model; Journal of Engineering for Industry, Trans ASME, 93:305-309.

S Dubowsky and F Freudenstein; 1971; Dynamic analysis of mechanical systems with clearances, Part 2: Dynamic response; Journal of Engineering for Industry, Trans ASME, 93:310-316.

D M Egle; 1967; An investigation of an impact vibration absorber; Journal of Engineering for Industry, Trans ASME, 89:653-661.

D M Egle; 1967; discussion on 'On the stability of the impact damper' by Masri & Caughey (1966); Journal of Applied Mechanics, Transactions of ASME, 34:253.

D J Ewins; 1984; Modal Testing: Theory and Practice; Research Studies Press; Taunton.

W Fang and J A Wickert; 1994; Response of a periodically driven impact oscillator; Journal of Sound and Vibration, 170(3):397-409.

A V Frolov, D N Eshutkin and Y M Smirnov; 1990; Motion conditions of impact-action hydraulic machines; Soviet Mining Science, 25(6):520-528, (translation of Fiziko-Tekhnicheskie Problemy Razrabotki Poleznykh Iskopaemykh, No.6, p23-31, 1989).

C C Fu; 1969; Dynamic stability of an impact system connected with rock drilling; Journal of Applied Mechanics (Transactions of ASME), 36:743-749.

C C Fu and B Paul; 1968; Stability of motion of impact tools; International Journal of Solids and Structures, 4:897-905.

C C Fu and B Paul; 1969; Dynamic stability of a vibrating hammer; Journal of Engineering for Industry, Trans ASME, 91:1175-1179.

C C Fu and B Paul; 1970; Energy transfer through chains of impacting rods; International Journal for Numerical Methods in Engineering, 2:363-385.

T Fujita and S Hattori; 1980; Periodic vibration and impact characteristics of a nonlinear system with collision; Bulletin of the JSME, 23:409-418.

L E Galhoud, S F Masri and J C Anderson; 1981; Transfer function of a class of nonlinear multidegree of freedom oscillators; Journal of Applied Mechanics, Transactions of ASME, 54:215-225.

G Gemne, R Lundström and J-E Hansson; 1993; Disorders induced by work with hand-held vibrating tools; Arbete och Hälsa 1993:6; Arbets Miljö Institutet (National Institute of Occupational Health); Sweden.

G M L Gladwell and W M Mansour; 1971; The analysis of some intermittent contact devices; Journal of Sound and Vibration, 15(4):495-507.

C Glocker and F Pfeiffer; 1992; Dynamical systems with unilateral contacts; Nonlinear Dynamics, 3:245-259.

W Goldsmith; 1960; Impact - The theory and physical behaviour of colliding solids; Edward Arnold; London.

M J Griffin; 1990; Handbook of Human Vibration; Academic Press; London.

C Grubin; 1956; On the theory of the acceleration damper; Journal of Applied Mechanics, Trans ASME, 23:373-378.

I Gutman; 1968; Industrial Uses of Mechanical Vibrations; Business Books, London.

N A Halliwell; 1993; Laser Vibrometry; Chap 6 of Optical Methods in Engineering Metrology; ed D C Williams; Chapman and Hall, London.

N A Halliwell, S A Kember and S J Rothberg; 1999; Laser vibrometry for impact measurements; in Dynamics of Vibro-Impact Systems; ed V I Babitsky; Springer, Berlin; p279-288.

C Hayashi; 1964; Non-Linear Oscillations in Physical Systems; Princeton University Press, Princeton NJ.

R C Hilborn; 1994; Chaos and Nonlinear Dynamics; Oxford University Press, New York.

J B Hunt; 1979; Dynamic Vibration Absorbers; Mechanical Engineering Press; London.

K H Hunt and F R E Crossley; 1975; Coefficient of restituition interpreted in vibriompact; Journal of Applied Mechanics, Transactions of ASME, 42:440-445.

K L Johnson; 1985; Contact Mechanics; Cambridge University Press; Cambridge.

W Johnson; 1976; 'Simple' linear impact; International Journal of Mechanical Engineering Education, 4:167-181.

H G Kaper; 1961; The behaviour of a mass-spring system provided with a discontinuous dynamic vibration absorber; Applied Scientific Research, Section A, 10:369-383.

M Kato, M Dazai and H Takase; 1976; Study on impact damper having a spring supported additional mass; Bulletin of the JSME, 19:103-109.

S A Kember and V I Babitsky; 1999; Dynamics of an impact unit for percussion machines; in Dynamics of Vibro-Impact Systems, ed V I Babitsky; Springer, Berlin.

S A Kember and V I Babitsky; 1999; Excitation of vibro-impact systems by periodic impulses; Journal of Sound and Vibration, 227(2):427-447.

T W B Kibble; 1985; Classical Mechanics; 3rd Ed; Longman; Harlow.

A E Kobrinskii; 1969; Dynamics of Mechanisms with Elastic Connections and Impact Systems; Iliffe Books; London. (translation of Mekhanizmy s uprugimi zvyazyami, Nauka, Moscow, 1964)

MZ Kolovsky; 1966; Nonlinear theory of vibroprotection systems; Nauka, Moscow. (in Russian)

H Kolsky; 1963; Stress Waves in Solids; Dover Publications; New York.

H M Lankarani and P E Nikravesh; 1994; Continuous contact force models for impact analysis in multibody systems; Nonlinear Dynamics, 5:193-207.

C H Lee and K P Byrne; 1987; Impact statistics for a simple random rattling system; Journal of Sound and Vibration, 119(3):529-543.

P Lieber and D P Jensen; 1945; An acceleration damper: development, design and some applications; Transactions of ASME, 67(7):523-530.

M J Lighthill; 1964; Introduction to Fourier Analysis and Generalised Functions; Cambridge University Press, Cambridge.

S Q Lin and C N Bapat; 1992; Estimation of clearances and impact forces using vibroimpact response: sinusoidal excitation; Journal of Sound and Vibration, 157(3):485-513.

S Q Lin and C N Bapat; 1993; Estimation of clearances and impact forces using vibroimpact response: random excitation; Journal of Sound and Vibration, 163(3):407-421.

B Lundberg; 1973; Energy transfer in percussive rock destruction - I Comparison of percussive methods; International Journal of Rock Mechanics and Mining Sciences and Geomechanical Abstracts, 10:381-399.

B Lundberg; 1973; Energy transfer in percussive rock destruction - II Supplement on hammer drilling; International Journal of Rock Mechanics and Mining Sciences and Geomechanical Abstracts, 10:401-419.

B Lundberg; 1982; Microcomputer simulation of stress wave energy transfer to rock in percussive drilling; International Journal of Rock Mechanics and Mining Sciences and Geomechanical Abstracts, 19:229-239.

B Lundberg, J Carlsson and K G Sundin; 1990; Analysis of elastic waves in non-uniform rods from two point strain measurement; Journal of Sound and Vibration, 137(3):483-493.

H Luo and S Hanagud; 1998; On the dynamics of vibration absorbers with motion limiting stops; Trans ASME Journal of Applied Mechanics, 65:223-233.

K G McConnell; 1995; Vibration Testing Theory and Practice; Wiley, New York.

K McGregor; 1967; The Drilling of Rock; CR Books Ltd.

K Magnus; 1965; Vibrations; Blackie; London. (translation of Schwingungen, Teubner, Stuttgart 1961)

N M M Maia and J M M e Silva (Eds); 1997; Theoretical and Experimental Modal Analysis; Research Studies Press, Taunton.

W M Mansour and D R Teixeiro Filho; 1974; Impact dampers with Coulomb friction; Journal of Sound and Vibration, 33(3):247-265.

S F Masri; 1967; discussion on 'An investigation of an impact vibration absorber' by Egle (1967a); Journal of Engineering for Industry, Transactions of ASME, 89:658-660.

S F Masri; 1970; General motion of impact dampers; Journal of the Acoustical Society of America, 47:229-237.

S F Masri and T K Caughey; 1966; On the stability of the impact damper; Journal of Applied Mechanics, Trans ASME, 33:586-592.

S F Masri and A M Ibrahim; 1972; A hybrid electromechanical analogue computer technique for optimising vibration systems; Journal of Engineering for Industry, Trans ASME, 94:381-387.

S F Masri and A M Ibrahim; 1973; Response of the impact damper to stationary random excitation; Journal of the Acoustical Society of America, 53:200-211.

K E Meier-Dörnberg; 1969; Die Beschreibung von Stoßvorgängen durch ihre Zeitfunktionen, Fourier- und Schockspektren; VDI-Berichte, 135:9-14.

L Meirovitch; 1986; Elements of Vibration Analysis; 2nd Ed; McGraw Hill, New York.

L Meirovitch; 1997; Principles and Techniques of Vibrations; Prentice Hall, Upper Saddle River, NJ.

N Minorsky; 1962; Non-Linear Oscillations; Van Nostrand; Princeton NJ.

Y A Mitropolsky and A M Samoilenko; 1985; Forced oscillations of systems with impulse force; International Journal of Non-Linear Mechanics, 20(5/6):419-426.

F C Moon; 1987; Chaotic Vibrations; Wiley, New York.

J Moscinski and Z Ogonowski (Editors); 1995; Advanced Control with MATLAB and Simulink; Ellis Horwood, London.

R F Nagaev and V Y Turkin; 1973; Synchronous regime of work of impact-vibrating jaw crusher; Obogashenie rud., No2. (in Russian)

S Natsiavas; 1993; Dynamics of multiple-degree-of-freedom oscillators with colliding components; Journal of Sound and Vibration, 165(3):439-453.

A H Nayfeh; 1981; Introduction to Perturbation Techniques; Wiley; New York.

R D Neilson, A A Rodger and R G Stevenson; 1995; Development of a computer based model of vibro-impact driving; Machine Vibration, 3:164-175.

M M Nigm and A A Shabana; 1983; Effect of an impact damper on a multi-degree of freedom system; Journal of Sound and Vibration, 89(4):541-557.

N S Nise; 1995; Control Systems Engineering, 2nd Ed; Benjamin Cummings, Redwood City, Ca.

T Nygren; 1995; On Transmission, Reflection and Dissipation of Extensional Wave Energy at a Non-uniform Viscoelastic Junction between Elastic Bars; Licentiate Thesis; Uppsala University, Sweden.

A L Paget; 1937; Vibration in steam turbine buckets and damping by impact; Engineering, 143:305-7.

R Palej and J Niziol; 1986; On a direct method of analysing impacting mechanical system; Journal of Sound and Vibration, 108(2):191-198.

W H Park; 1967; Mass-spring-damper response to repetitive impact; Journal of Engineering for Industry, Transactions of ASME, 89:587-596.

F Peterka and O Szollos; 1996; The stability analysis of a symmetric two degree of freedom system with impacts; EUROMECH - 2nd European Nonlinear Oscillation Conference, Prague, Sept 9-13; Vol 1 p345-8.

F Peterka and O Szollos; 1997; Dynamics of the opposed piledriver; IUTAM Symposium on the Interaction between Dynamics and Control in Advanced Mechanical Systems, ed DH van Campen, p271-8.

N Popplewell, C N Bapat and K McLachlan; 1983; Stable periodic vibroimpacts of an oscillator; Journal of Sound and Vibration, 87(1):41-59.

N Popplewell and S E Semercigil; 1989; Performance of the bean bag impact damper for a sinusoidal external force; Journal of Sound and Vibration, 133(2):193-223.

W H Press, S A Teukolsky, W T Vetterling and B P Flannery; 1992; Numerical Recipes in Fortran, 2nd Ed.; Cambridge University Press, Cambridge.

R B Randall; 1977; Frequency Analysis, 2nd Ed.;Bruel and Kjaer

G F Roach; 1970; Green's Functions – Introductory Theory with Applications; Van Nostrand Reinhold, London.

E N Rosenwasser; 1969; Vibrations of Nonlinear Systems; Nauka, Moscow. (in Russian)

I G Rusakov and A A Kharkevich; 1942; Forced vibrations of a system that is striking a stop; Journal of Technical Physics, No 11-12. (in Russian)

M M Sadek; 1965-6; The behaviour of the impact damper; Proeedings of the Institution of Mechanical Engineers, 180:895-906.

M M Sadek and B Mills; 1967; discussion on 'On the stability of the impact damper' by Masri & Caughey (1966); Journal of Applied Mechanics, Transactions of ASME, 34:253.

S E Semercigil, D Lammers and Z Ying; 1992; A new tuned vibration absorber for wideband excitations; Journal of Sound and Vibration, 156(3):445-459.

S E Semercigil, N Popplewell and R Tyc; 1988; Impact damping of random vibrations; Journal of Sound and Vibration, 122(1):178-184.

M Senator; 1970; Existence and stability of periodic motions of a harmonically forced impacting system; Journal of the Acoustical Society of America, 47:1390-97.

D L Sikarskie and B Paul; 1969; Periodic motions of a two body system subjected to repetitive impact; Journal of Engineering for Industry, Trans ASME, 91:931-938.

V W T Sin and M Wiercigroch; 1999; A symmetrically piecewise linear oscillator: design and measurement; Proceedings of the Institution of Mechanical Engineers, 213C:241-249.

J J Stoker; 1950; Nonlinear Vibrations in Mechanical and Electrical Systems; Interscience Publishers, New York.

W T Thomson; 1993; Theory of Vibration with Applications; 4th Ed; Chapman and Hall; London.

S P Timoshenko and J N Goodier; 1982; Theory of Elasticity; 3rd Ed; McGraw Hill.

G R Tomlinson and J Lam; 1984; Frequency response characteristics of structures with single and multiple clearance-type non-linearity; Journal of Sound and Vibration; 96(1):111-125.

M A Veluswami and F R E Crossley; 1975; Multiple impacts of a ball between two plates, Part 1: Some experimental observations; Journal of Engineering for Industry, Trans ASME, 97:820-827.

M A Veluswami, F R E Crossley and G Horvay; 1975; Multiple impacts of a ball between two plates, Part 2: Mathematical modelling; Journal of Engineering for Industry, Trans ASME, 97:828-835.

A M Veprik and B L Krupenin; 1985; On the solution of a system maintaining distributed impacting elements; Mashinvedenie 6:9-14. (in Russian)

G B Warburton; 1957; discussion on 'On the theory of the acceleration damper' by C Grubin (1956); Journal of Applied Mechanics, Trans ASME, 24:322-324.

G S Whiston;1983; An analytical model of two dimensional impact/sliding response to harmonic excitation; Journal of Sound and Vibration, 86(4):557-562.

L A Wood and K P Byrne; 1981; Analysis of a random repeated impact process; Journal of Sound and Vibration, 78(3):329-345.

L A Wood and K P Byrne; 1982; Experimental investigation of a random repeated impact process; Journal of Sound and Vibration, 85(1):53-69.

C M Wu and B Lundberg; 1994; Efficiency of percussive drilling of rock with a bent drill rod; International Journal of Impact Engineering, 15(6):735-747.

K Yasuda and M Toyoda; 1978; The damping effect of an impact damper; Bulletin of the JSME, 21:424-430.

A A Zevin; 1976; Optimal regime in vibration-impact systems having one degree of freedom; Izvestiya AN USSR, Mekhanika Tverdogo Tela, 11(2):35-41 (English translation in Mechanics of Solids p28-33).

V F Zhuralyov and DM Klimov; 1988; Applied Methods in the Theory of Oscillations; Nauka, Moscow. (in Russian)